From grains to tracks: high-resolution sedimentology of track-bearing Stormberg strata, southern Africa

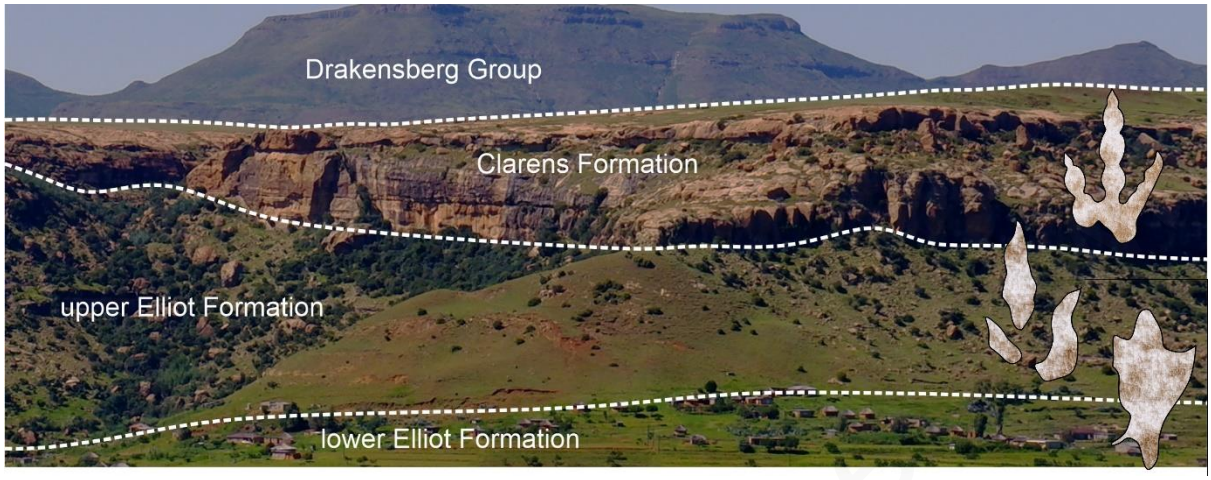

By

Loyce Mpangala

Supervisor: Dr Miengah Abrahams
Co-supervisor: Prof Emese M. Bordy

Dissertation presented for the degree of Master of Science in Geology in the Department of Geological Sciences

Department of Geological Sciences

University of Cape Town

June 2023

Declaration

1. I acknowledge that plagiarism is wrong. Plagiarism is using another's work and pretending that it is one's own.

2. I have used the South African Journal of Geology convention for citation and referencing. Each contribution to, and quotation, in this project from the work(s) of other people has been attributed, cited and referenced.

3. This project is my own work.

4. I have not allowed and will not allow anyone to copy my work with the intention of passing it off as their own work.

Signature

Signed by candidate

Loyce Mpangala

Date: 19/06/2023

Acknowledgements

I would like to express my sincere gratitude to my supervisor, Dr Miengah Abrahams, for her exceptional support and guidance throughout this project. I am truly grateful for her dedication, encouragement, enthusiasm, and prompt feedback, especially during the writing process. I would also like to extend my appreciation to my co-supervisor, Prof Emese Bordy, for her continuous support, valuable guidance, swift feedback, and inspiring words of encouragement.

I would like to acknowledge Akhil Rampersadh for his valuable field assistance, as well as Richard Harrison and Kyle Isaacs from the University of the Western Cape for their assistance with thin section preparation. I am also thankful to Howard Head for helping with modal composition analysis and to Dr Kelly Kirsten for reviewing and providing feedback on my final draft. Furthermore, I extend my appreciation to Jonathan Van Rooyen from the XRF preparation lab in the Department of Geological Science at UCT and Megan Welman Purchase from the Faculty of Natural and Agricultural Sciences at the University of the Free State for their help in XRD sample preparation and analysis.

The research component of this project was funded by UCT Research Development Grant [2021] obtained by my supervisor, Dr Miengah Abrahams. I would also like to acknowledge the generous financial support I received for my MSc studies from the following organisations:

- GENUS (DSI-NRF Centre of Excellence in Palaeosciences, UID 86073)
- Palaeontological Scientific Trust (PAST), Johannesburg, South Africa
- UCT General Award

I am deeply grateful to my incredible and selfless family for their unwavering support and constant belief in me, even during times when I doubted myself. A special mention goes to my amazing mother, Edith Esther Mpangala, to whom I dedicate this project. Lastly, I give honour and praise to God, my Father, for seeing me through this journey.

Abstract

Tracks registration is influenced by the dynamic interplay between the pedal anatomy of the trackmaker, its behaviour, and the substrate conditions it interacts with. Differences in substrate conditions, especially those linked to grain size and moisture content, often result in the most dramatic variations in track morphology. In the upper Stormberg Group, main Karoo Basin of southern Africa, diverse trace fossils, primarily comprising Upper Triassic–Lower Jurassic dinosaur tracks, are preserved. Extensive studies have been carried out to document these individual tracksites and to examine the variations between sites and through time, with recent studies suggesting that track abundance and anatomical fidelity increase up-stratigraphy. Despite the well-established understanding of the effects of substrate on track registration and preservation, these past studies have not specifically focused on the substrate conditions, and when substrate conditions were considered, the emphasis was primarily on macro-sedimentary features. Here, we examine the micro-sedimentary features of track-bearing units in the upper Stormberg Group using petrographic techniques, to better understand the palaeosubstrate and its effect on fossil track registration and preservation. The analysis revealed that very fine-grained sands and substrates modified by microbial activity tend to preserve tracks with greater abundance and higher anatomical fidelity. Furthermore, the prevalence of very fine-grained and microbially modified strata, and their associated track trends, increases in younger stratigraphic units. Across the Triassic–Jurassic boundary of southern Africa, there was a proliferation of dinosaur populations, possibly linked to the end–Triassic mass extinction events, which has been credited globally for track abundance increases in the Lower Jurassic. However, our findings suggest that, locally, the observed increase in track abundance (and anatomical fidelity) up-stratigraphy may also be linked to substrate–composition differences, which were ultimately controlled by large-scale changes in the palaeoenvironment from high-energy meandering fluvial to lower-energy aeolian-lacustrine settings in the Late Triassic and Early Jurassic, respectively.

Table of Contents

1. Introduction

The main Karoo Basin (MKB) in southern Africa is globally recognised for its extensive continental successions (i.e., the Karoo Supergroup), which accumulated over ~120 million years from the Late Carboniferous to the Early Jurassic (e.g., Catuneanu et al., 1998, 2005). The basin is renowned for its rich natural resources, fossil heritage, and notable record of mass extinction events such as the end–Permian and end–Triassic events (e.g., Raup and Sepkoksi, 1982; Rubidge, 2009; Soeder and Borglum, 2019). The upper Stormberg Group (i.e., Elliot and Clarens formations) comprises fluvio-lacustrine and aeolian successions in the MKB. These Upper Triassic–Lower Jurassic strata, which recorded the end-Triassic mass extinction events, preserve diverse vertebrate body and trace fossils (e.g., Bordy et al., 2020a). The vertebrate trace fossil record is dominated by dinosaur tracks and trackways, which were originally documented by missionaries from the Paris Evangelical Mission (e.g., Dornan, 1908; Ellenberger and Ellenberger, 1956, 1958, 1960; Ellenberger et al., 1963; Ellenberger, 1970, 1972, 1974), and later revised by numerous authors (e.g., Olsen and Galton, 1984; Ambrose, 2003; Knoll, 2004, 2005; Smith et al., 2009; Abrahams et al., 2017, 2021, 2022, 2023; Bordy et al., 2017, 2020a; McPhee et al., 2017; Sciscio et al., 2017; Rampersadh et al., 2018; Bordy, 2021; Mukaddam et al., 2021) who focused on refining the ichnotaxonomic assignment, palaeodiversity and palaeoecology of the tracks, as well as the macro-sedimentological features of the track-bearing rocks.

Track registration results from the dynamic interaction between the trackmaker's pedal anatomy, its behaviour and the substrate conditions (Padian and Olsen, 1984; Avanzini, 1998; Avanzini et al., 2012). Numerous studies have shown how these factors, either individually or combined, influence the resultant track morphology (e.g., Gatesy et al., 1999; Milan and Bromley, 2006, 2008; Avanzini, 1998; Avanzini et al., 2012), with differences in substrate conditions, specifically linked to grain size and water saturation, often leading to the most dramatic variations in track morphology (e.g., Milan and Bromley, 2006, 2008; Jackson et al., 2010). Consequently, recent studies of ichnosites within the upper Stormberg Group have considered the macro-sedimentology of outcrops and extra-morphological features of specific tracks to gain insights into the palaeosubstrate conditions to better understand the preserved track morphology (e.g., Sciscio et al., 2016; Rampersadh et al., 2018; Abrahams et al., 2020; Bordy, 2021).

However, understanding the geo-mechanical properties of track-bearing substrates can be challenging, as sediment properties are influenced by physical, chemical and biological processes that occur before, during and after track registration (e.g., Avanzini et al., 2012; Carvalho et al., 2013; Razzolini et al., 2014). These processes impact the properties of sediment grains, such as size, shape, composition, sorting, packing, cementation and compaction. Among these processes, microbial activity plays a significant role in the cohesiveness, deformation and erodibility of the sediment (e.g., Carvalho et al., 2013; Dai et al., 2015). Microbial activity is preserved in the geological record as microbially induced sedimentary structures (MISS), which are identified as diverse surface textures on bedding planes (e.g., wrinkle structures, pitted textures, microbial mats; Noffke et al., 2001, 2022). Substrates that are microbially-stabilised have an enhanced track preservation potential as the microbes bind and consolidate the registered tracks, acting as a protective layer, and induce early track lithification by cementing the sediment (e.g., Marty et al., 2009; Carvalho et al., 2013; Dai et al., 2015).

Despite the known influence of substrates on track registration and preservation, the micro-sedimentary properties of the track-bearing strata in the upper Stormberg Group have not been considered to date. Additionally, observations of MISS have been limited to isolated ichnosites within the upper Stormberg Group, without considering their collective presence alongside the tracks throughout the entire Group. This oversight could have significant implications for the ichnotaxonomic assignment, which, in turn, would affect our local understanding of ichnostratigraphy, palaeodiversity, macroevolutionary palaeoecology and palaeoethology in the region.

Aims of research

This study aims to quantify the micro-sedimentary properties of the track-bearing units from the upper Stormberg Group in southern Africa to better understand the influence of palaeosubstrate conditions on fossil track morphology and preservation potential. This was accomplished through the following approaches:

1) Examining the petrographic properties, such as grain size, grain shape, grain composition, of the sedimentary host rocks. This analysis complements the

established macro-sedimentary observations at known ichnosites, providing a deeper understanding of the palaeosubstrate conditions and refining our knowledge of the palaeoenvironmental context.

2) Considering the observations of MISS in conjunction with the tracks throughout the entire upper Stormberg Group, rather than focusing solely on individual tracksites. This contributes to a more holistic understanding of how microbial activity influences track morphology and preservation.

By integrating the clastic sedimentary properties and considering the influence of microbial activity at individual tracksites within the upper Stormberg Group, this study aims to quantitively demonstrate the role of substrate in shaping the observed local track trends up-stratigraphy, from the Upper Triassic to Lower Jurassic.

2. Geological background

2.1 Preamble

The MKB preserves primarily Upper Carboniferous–Lower Jurassic sedimentary and minor igneous rocks that cover about two-thirds of southern Africa's surface (Figure 2.1; Cole, 1992; Johnson et al., 1996, 1997; Catuneanu et al., 1998). During the Late Carboniferous, the southern margin of Gondwana experienced a compressional tectonic regime that resulted in the formation of the ~6000-km-long Pan-Gondwanan fold-thrust belt, and an intracratonic foreland basin system to the north of it (Catuneanu et al., 1998). In southern Africa, the former is preserved as the Cape Fold Belt (CFB; ~1300 km long), whereas the latter is the MKB (Figure 2.1; Johnson et al., 1997; Catuneanu et al., 1998, 2005). The infill of the MKB, the Karoo Supergroup, has a maximum cumulative thickness of ~6 km in the south, and tapers dramatically to the north (Catuneanu et al., 1998; Scheiber-Enslin et al., 2015). The Karoo Supergroup is made up of five primary groups, which are from oldest to youngest: Dwyka, Ecca, Beaufort, Stormberg and Drakensberg (Figure 2.1; Johnson et al., 1996; Catuneanu et al., 1998). Herein, the Dwyka, Ecca and Beaufort groups constitute the lower Karoo within the Karoo Supergroup, while the upper Karoo is made up of the Stormberg and Drakensberg groups. The Karoo groups comprise sedimentary rock successions, except for the Drakensberg Group, which consists of intrusive and extrusive volcanic rocks and subordinate sedimentary interbeds (Johnson et al., 1996; Catuneanu et al., 1998; Bordy et al., 2020b, 2022). The Karoo succession reflects a range of environments, in chronological order, from glacial, deep marine to shallow marine, fluvio-lacustrine, aeolian, to continental volcanic settings (Johnson et al., 1997; Bordy et al., 2004a, 2004b, 2005, 2020b, 2022; Catuneanu et al., 2005; Bordy and Head, 2018; Head and Bordy, 2022).

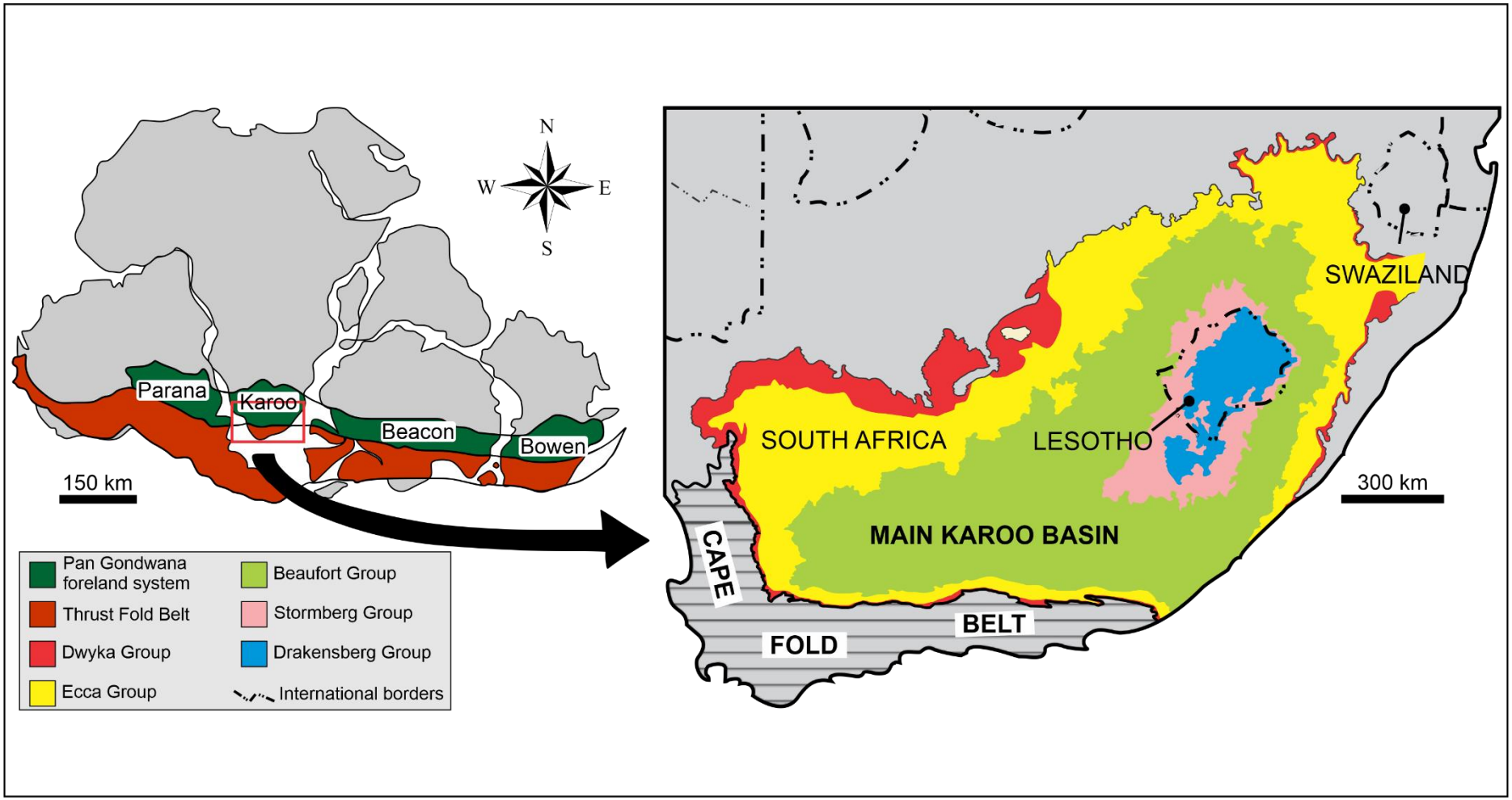

Figure 2.1. Pan-Gondwana foreland system containing the MKB, and the distribution of the Karoo Supergroup across the MKB. Other remnants of the Pan-Gondwana foreland system include the Parana Basin in South America, Beacon Basin in Antarctica and Bowen Basin in Australia. Modified from Catuneanu and Elango (2001).

2.1.1 Tectonic setting of the main Karoo Basin

The MKB is considered to be a retroarc foreland basin that formed as a result of the crustal shortening and lithospheric loading of the CFB following the northward subduction of the palaeo-Pacific plate along the southern margin of Gondwana (Figure 2.2; e.g., Johnson et al., 1997; Catuneanu et al., 1998, 2005). Subsidence was greatest near the CFB orogenic load, resulting in a northward-shallowing asymmetrical basin (Figure 2.2A; Catuneanu et al., 1998). The primary controls on the basin evolution were orogenic loading and unloading events as well as large-scale climatic changes (Figure 2.2B; Catuneanu et al., 1998). During the CFB orogenic loading event, the proximal part (foredeep) underwent surface down-warping, while the distal part of the basin experienced flexural uplift (Figure 2.2B; Catuneanu et al., 1998). The subsidence created accommodation space for sediments to accumulate near the orogen in the foredeep from the earliest Permian to the Middle Triassic (~300–247 Ma), in form of the Dwyka, Ecca, and Beaufort groups (Figures 2.1, 2.2; Catuneanu et al., 1998; Hansma et al., 2016). In contrast, the distal part of the basin subsided during the final stages of basin evolution (i.e., first-order orogenic unloading event of the CFB), creating a foresag into which upper Karoo strata were deposited, chiefly from the erosion of the CFB and lower Karoo strata (Figure 2.2B; Halbich, 1983; Catuneanu et al., 1998; Bordy et al., 2004a). This foresag existed from the Late Triassic onwards (~237–183 Ma), and preserved the Stormberg Group (Figures 2.1, 2.2; Catuneanu et al., 1998; Bordy et al., 2004a). Clastic sedimentation gradually ended around 183 Ma, when the tectonic regime changed from compressional to extensional, heralding the breakup of Gondwana (Duncan et al., 1997; Catuneanu et al., 1998; Bordy et al., 2004a; Muir et al., 2020). It was this time when continental flood basalts extruded and associated sills and dykes intruded, resulting in the Lower Jurassic Drakensberg Group (Figure 2.1; Duncan et al., 1997; Catuneanu et al., 1998; Bordy et al., 2020b, 2022).

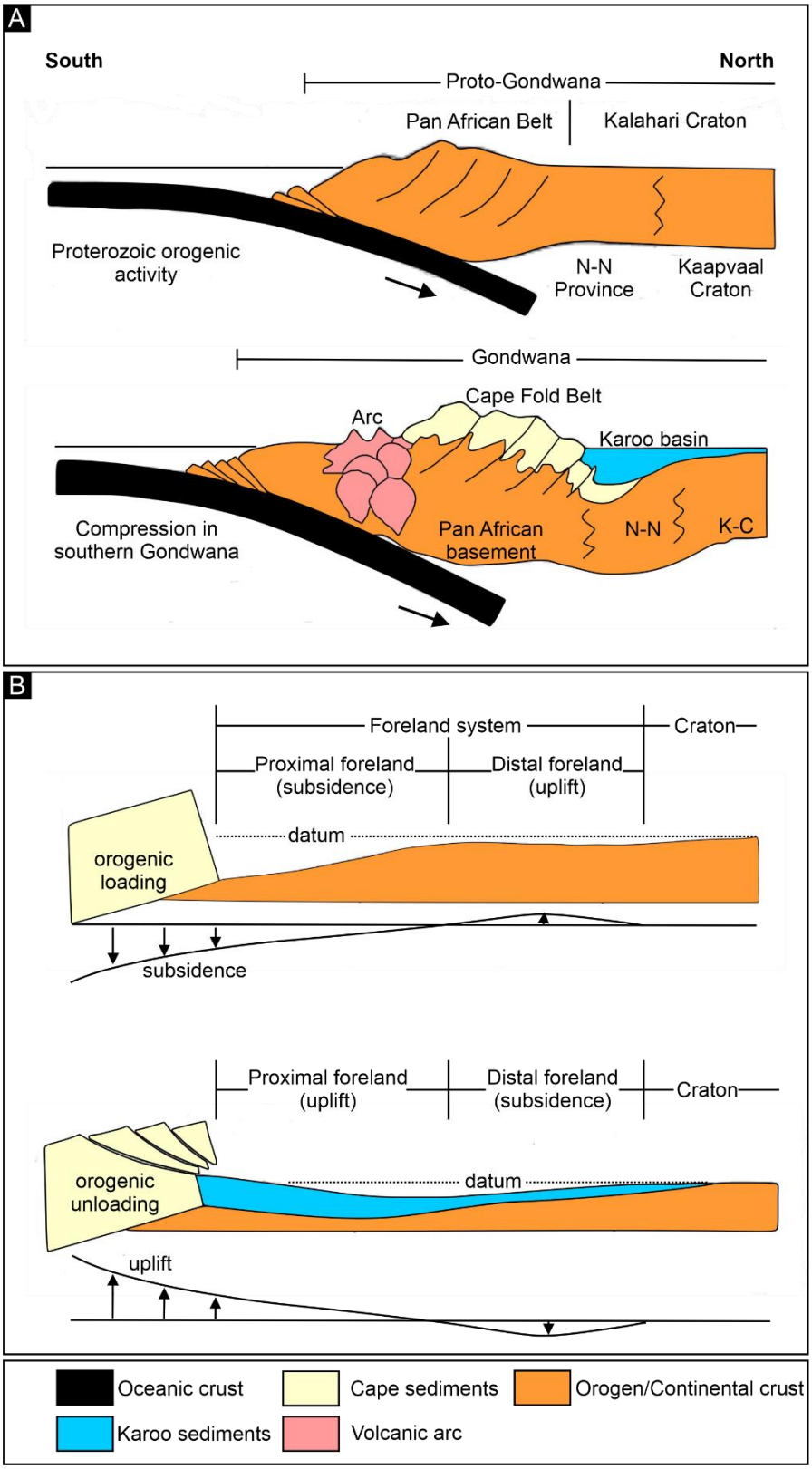

Figure 2.2. Formation and evolution dynamics of the MKB. **A)** The MKB formation resulting from lithospheric loading of the CFB following the northward subduction of the palaeo-Pacific plate beneath Gondwana. **B)** Surface profiles of the flexural foreland system during CFB orogenic loading and unloading events. Sediments accumulate in the subsided proximal part of the orogen (foredeep) during orogenic loading and in the subsided distal section of the basin (foresag) during orogenic unloading. Modified from Catuneanu et al. (1998).

2.1.2 Stratigraphy of the upper Stormberg Group

The Upper Triassic–Lower Jurassic upper Stormberg Group consists of the Elliot and Clarens formations (Johnson et al., 1996, 1997). The Elliot Formation, encompassing the Triassic–Jurassic boundary, is comprised of a series of laterally continuous continental red beds i.e., fluvio-lacustrine sandstones and floodplain mudstones (e.g., Smith et al., 1993; Johnson et al., 1996, 1997; Bordy et al., 2004a, 2004b). This Formation has a relatively sharp contact with the underlying Carnian Molteno Formation, the oldest unit of the Stormberg Group, and a gradational contact with the overlying Clarens Formation (Bordy et al., 2004a, 2004b; Bordy and Eriksson, 2015). The Elliot Formation has a maximum thickness of ~460 m in the south of the MKB, gradually decreasing to <70 m in the north of the basin (Bordy et al., 2004b). Based on architectural differences in sandstone body geometries and mudstone units, as well as sedimentary structures, fossils, colour characteristics, palaeocurrents and provenances, the Elliot Formation is informally subdivided into the lower Elliot Formation (lEF) and upper Elliot Formation (uEF; Table 2.1; Bordy et al., 2004a, 2004b, 2004c, 2020a).

The lEF is characterized by lenticular, multi-storey, asymmetrical channel-shaped sandstone bodies with a maximum lateral extent of 100–150 m and a maximum thickness of 20–25m (Table 2.1; Bordy et al., 2004a, 2004b). These sandstone bodies fine upwards and their bases are marked by mud-pebble conglomerates lags (Bordy et al., 2004b). The sandstones are predominantly fine- to medium-grained and moderately to poorly sorted (Bordy et al., 2004b). The sandstone beds are separated by laterally continuous, light red-purple mudstone units with green and grey mottles that average 20–30 m in thickness (Table 2.1; Bordy et al., 2004b). The mudstones are predominantly massive and very rarely laminated (Bordy et al., 2004b). Sedimentary structures characterizing the lEF are predominantly trough and planar cross-bedding, massive beds, and less common low-angle cross-beds and horizontal lamination (Bordy et al., 2004a, 2004b). The depositional environment is interpreted to be a perennial, moderately meandering fluvial system with palaeocurrents indicating that the major rivers flowed from south to north and from southwest to northeast (Table 2.1; Bordy et al., 2004b). The lEF vertebrate fossil record is typified by sauropodomorphs, diapsids, cynodonts, therapsids, pseudosuchians, temnospondyl amphibians and possible theropods (Table 2.1; see Kitching and Raath, 1984; Knoll, 2004; Abdala et al., 2007; McPhee et al., 2017; Bordy et al., 2020a). Several vertebrate footprints have been preserved, including

Sauropodopus, *Pentasauropus*, *Tetrasauropus*, *Pseudotetrasauropus, Grallator* and *Brachychirotherium* (Table 2.1; see Ellenberger, 1970, 1972, 1974; Kitching and Raath, 1984; Olsen and Galton, 1984; Knoll, 2004; Abdala et al., 2007; Bordy et al., 2017, 2020a; McPhee et al., 2017).

The uEF is characterized by multi-storey, sheet-sandstone bodies with a lateral extent averaging >100 m and a maximum thickness of 5–6 m (Table 2.1; Bordy et al., 2004a, 2004b). Pedogenic conglomerates are common and highly diagnostic within the uEF sandstone units (Bordy et al., 2004b). The sandstones are predominantly very fine- to fine-grained and relatively well sorted (Bordy et al., 2004b). The sandstones beds are separated by laterally continuous, deep red/maroon mudstone units with sporadic grey mottles that average 0.5–10 m in thickness (Table 2.1; Bordy et al., 2004b). The uEF's mudstones are mostly massive, with laminated mudstones being more common than in the lEF (Bordy et al., 2004b). Sedimentary structures that characterize the uEF are primarily massive beds, horizontal laminations, ripple cross laminations and less common trough cross-beds (Bordy et al., 2004b). The depositional environment is interpreted to be an ephemeral, flash flood-dominated fluvial system with palaeocurrents flowing from the south, southwest and west with a small proportion from the north (Table 2.1; Bordy et al., 2004b). In comparison to the lEF, the uEF vertebrate fossil record has a more diverse assemblage, which includes sauropodomorphs, basal ornithischians, theropods, mammaliaformes, cynodonts, crocodylomorphs, temnospondyl amphibians and possible testudinata (Table 2.1; e.g., Kitching and Raath, 1984; Olsen and Galton, 1984; Knoll, 2005; Abdala et al., 2007; McPhee et al., 2017; Bordy et al., 2020a). A variety of vertebrate burrows and footprints have been preserved, the latter of which includes *Trisauropodiscus*, *Kalosauropus*, *Moyenisauropus*, *Episcopopus, Batrachopus*, *Ameghinichnus*, *Kayentapus,* and tridactyl tracks on the *Grallator-Eubrontes*-like plexus (Ellenberger et al., 1963; Ellenberger, 1970, 1972, 1974; Kitching and Raath, 1984; Knoll, 2005; Abdala et al., 2007; Smith et al., 2009; Wilson et al., 2009; Bordy et al., 2016, 2020a; Sciscio et al., 2016, 2017; Abrahams et al., 2017, 2020; McPhee et al., 2017).

Table 2.1. Key sedimentary facies characteristics, interpreted palaeoenvironments, as well as vertebrate body and trace fossils in the upper Stormberg Group (Ellenberger et al., 1970,1972,1974; Kitching and Raath, 1984; Olsen and Galton, 1984; Johnson et al., 1997; Bordy et al., 2004a, 2004b, 2004c, 2020a; Knoll 2004, 2005; Abdala et al., 2007; Smith et al., 2009; McPhee et al., 2017; Bordy and Head, 2018; Mukaddam et al., 2021).

Key features	lEF	uEF	CLAR
Geological time scale	Norian – Rhaetian (~215.0 – 205.5 Ma)	Hettangian – Sinemurian (~199.3 ± 0.3 – 190.8 ± 1.0 Ma)	Sinemurian – Pliensbachian (~190.8 ± 1.0 – 180.0 Ma)
Conglomerate characteristics	Mud-pebble conglomerate	Carbonate nodules conglomerate and bone fragments	n/a
Sandstone body characteristics	Multi-storey, asymmetrical channel-fill, lateral accretion, with unit thicknesses about 20–25 m Lateral extent: max 100–150 m	Multi-storey, tabular, sheet-like bodies with unit thicknesses of about 5–6 m Lateral extent: min 100–150 m	Tabular, sheet-like bodies with notable white, cream and pale-yellow colour Thickness: 90–150m
Sandstone facies characteristics	Grain size: fine- to medium-grained Sedimentary structures: trough and planar cross-beds, massive beds and low-angle cross-beds occurring rarely	Grain size: very fine- to fine-grained Sedimentary structures: massive beds, horizontal lamination, ripple cross lamination with soft sediment deformation structures	Grain size: very fine- to medium grained Sedimentary structures: large-scale cross-bedding, ripple marks, desiccation cracks and calcareous concretions
Mudstone facies characteristics	Light red-purple with green-grey mottles mudstone units with thicknesses of about 20–30 m Limited pedogenic overprinting	Brick red-maroon with sporadic light grey mottles mudstone units of about 0.5–10 m in thickness	Pale green to light green-grey mudstone units with thicknesses of <30 cm
Palaeoenvrionment	Perennial meandering channels	Ephemeral fluvial channels and lakes	Aeolian with ephemeral lakes
Key vertebrate fossils	Sauropodomorphs, cynodonts, diapsida, therapsids, temnospondyl amphibians pseudosuchia and possible theropods	Sauropodomorphs, theropods, cynodonts, basal ornithischians, crocodylomorphs, mammaliaforms, temnospondyly amphibians, and possible testudinata	Crocodylomorphs, freshwater fish, freshwater crustaceans, mammaliaforms, ornithischian, cynodonts and basal sauropodomorph
Trace fossils	*Sauropodopus, Pentasauropus, Tetrasauropus, Grallator and Brachychirotherium*	*Kalosauropus, Moyenisauropus, Episcopopus ventrosus, Batrachopus, Kayentapus and Grallator*	*Kalosauropus, Kayentapus, Episcopopus, Brasilichnium-like tracks and Grallator-Eubrontes*

The Clarens Formation (CLAR) has a conformable upper contact with the Drakensberg Group (Bordy and Head, 2018; Bordy et al., 2020a, 2021). This Formation is distinguished by caves, cliffs and overhangs that form large-scale cross-beds with thicknesses ranging from 90–150 m (Table 2.1; Bordy and Head, 2018). The CLAR is subdivided into three zones: the lower, middle and upper zones (Beukes, 1970; Bordy and Head, 2018; Head and Bordy, 2022). The lower and upper zones are dominated by light red to cream, massive, thickly bedded loess-like siltstones interbedded with silty, very fine-grained sandstones (Bordy and Head, 2018). These zones also contain finely laminated, dark grey to green mudstones, desiccation cracks and calcareous concretions (Bordy and Head, 2018). The lower and upper zones were interpreted to reflect wet depositional conditions of permanent to ephemeral rivers and lakes that coexisted with the aeolian environment (Beukes, 1970; Bordy and Head, 2018; Head and Bordy, 2022). The middle zone consists of white, thickly bedded (up to 10 m), large-scale cross-bedded, fine- to medium-grained sandstones that are better sorted and contain less clayey matrix compared to the other two zones (Bordy and Head, 2018). This zone reflects drier conditions, and the predominance of large-scale crossbedding suggests an aeolian origin (Bordy and Head, 2018). While less fossiliferous than the uEF, the lower CLAR (the base of the cliffs) has been reported to preserve a diverse range of vertebrate fossils including crocodylomorphs, freshwater fish, freshwater crustaceans, mammaliaforms, ornithischian, cynodonts and basal sauropodomorphs (Table 2.1; e.g., Ellenberger, 1970, 1972; Knoll, 2005; Mcphee et al., 2017; Bordy et al., 2020a). Furthermore, diverse trace fossils have also been preserved including *Kalosauropus*, *Kayentapus*, *Episcopopus, Brasilichnium*-like tracks and *Grallator-Eubrontes* like plexus (Dornan, 1908; Ellenberger, 1970, 1972; Olsen and Galton, 1984; Bordy et al., 2020a; Abrahams et al., 2021; Mukaddam et al., 2021).

2.1.3 Southern African dinosaur tracks

The upper Stormberg Group rocks in southern Africa preserve a diverse range of vertebrate trace fossils, predominantly dinosaur tracks (e.g., Ellenberger, 1955, 1970, 1972, 1974; Ellenberger and Ellenberger, 1956; Ellenberger et al., 1963; Ambrose, 2003; Smith et al., 2009; Wilson et al., 2009; Marsicano et al., 2014; Bordy et al., 2016, 2017, 2020a, 2022; Sciscio et al., 2016, 2017; Abrahams et al., 2017, 2020, 2021; Rampersadh et al., 2018; Bordy, 2021). Much of the early knowledge on these dinosaur tracks stems from the pioneering work of missionaries who extensively documented many ichnosites in Lesotho from the 1950s to 1970s (e.g., Ellenberger, 1955, 1970, 1972, 1974; Ellenberger and Ellenberger, 1956, 1958, 1960; Ellenberger et al., 1963). The majority of the discovered dinosaur tracks (Table 2.1) have been assigned to the ichnogenera: *Kayentapus*, *Grallator*, *Anchisauripus*, and *Eubrontes* (i.e., the K-GAE plexus; Hitchcock, 1836, 1856; Lull, 1904; Olsen, 1980). These ichnogenera are considered to have evolved along a morphological continuum, in which the elongation and mesaxony decrease, and digit thickness increases with track size (e.g., Olsen et al., 1998). *Grallator* is the ichnogenus assigned to the smallest tracks on the spectrum (track length (TL) of < 15 cm), whereas *Anchisauripus* tracks are medium-sized with a TL ranging between 15–25 cm (Olsen et al., 1998). *Eubrontes* tracks are large (TL > 25 cm), and *Kayentapus* are relatively larger (TL > 35 cm) and are more gracile (Olsen et al., 1998; Lockley et al., 2011). It is widely assumed that all tracks assigned to the K-GAE plexus were registered by various theropod trackmakers (Olsen et al., 1998; Li et al., 2006).

2.2 Track registration and preservation

The registration and preservation of tracks in the geological record is influenced by a variety of environmental factors, including sedimentation processes (e.g., Carvalho et al., 2013; Razzolini et al., 2014; Carvalho and Leonardi, 2021). There are optimal environmental factors for track registration (see section 2.2.1), and the potential for track preservation is higher in environments with low and cyclic rates of sedimentation (e.g., Razzolini et al., 2014; Carvalho and Leonardi, 2021). Consequently, the majority of fossil tracks in the geological record are associated with depositional environments characterized by episodic sedimentation of fine-grained sediments in semi-arid palaeoenvironments (e.g., Carvalho, 2000; Carvalho et al., 2013; Paik et al., 2017; Xing et al., 2019; Carvalho and Leonardi, 2021).

2.2.1 Controls on tracks registration

During track registration, the resulting track morphology is influenced by the dynamic interaction of the trackmaker's pedal anatomy, locomotion and the substrate over which the animal is moving (Padian and Olsen, 1984; Avanzini, 1998; Milan and Bromley, 2006, 2008; Avanzini et al., 2012). For example, the track morphology of a running tridactyl trackmaker differs significantly from that of a strolling pentadactyl trackmaker. Furthermore, the locomotion of the trackmaker (e.g., running vs walking) affects its foot movement sequence in interaction with the substrate, which, among other factors, influences which digit of the pedal anatomy is most deeply impressed (Avanzini, 1998). The most dramatic changes in track morphology are mainly attributed to varying substrate conditions, specifically linked to water saturation and grain size (i.e., functionally tridactyl hind track impressions are tridactyl in less saturated substrates vs tetradactyl in saturated substrates; Figure 2.3; e.g., Gatesy et al., 1999; Milan and Bromley, 2008; Jackson et al., 2010; Bordy, 2021; Mancuso et al., 2022). The degree to which a track morphology reflects the trackmaker's pedal anatomy is termed anatomical fidelity or morphological preservation grade and can range from 0 to 3 (Table 2.2; Belvedere and Farlow, 2016; Gatesy and Falkingham, 2017; Marchetti et al., 2019).

Dry sediments (i.e., with 0% moisture), irrespective of grain size, are less likely to retain tracks due to the lack of cohesion between the grains, whereas relatively firm substrates with low- to moderate moisture content (i.e., 10–20%) are more likely to register tracks that accurately reflect the tracemakers anatomy (Figure 2.3; e.g., Gatesy et al., 1999; Milan and Bromley, 2008; Jackson et al., 2010; Mancuso et al., 2022). Super-saturated substrates (i.e., ~30%) cause track deformation and are typically associated with sediment collapse features and expulsion rims as the trackmaker's foot sinks and is withdrawn from the substrate (Figure 2.3; e.g., Gatesy et al., 1999; Milan and Bromley, 2006, 2008; Jackson et al., 2010; Mancuso et al., 2022). Saturated substrates show explicit grain size effects on track morphology, with finer grains deforming easily from impulsive liquefaction attributed to their low permeability and coarser grains deforming less due to their higher permeability (e.g., Jackson et al., 2010). Generally, tracks registered in coarser grained, sand-dominated substrates register less anatomical detail than finer grained sandy or clay-rich substrates, mainly due to the lack of cohesive properties in the substrate (Jackson et al., 2010).

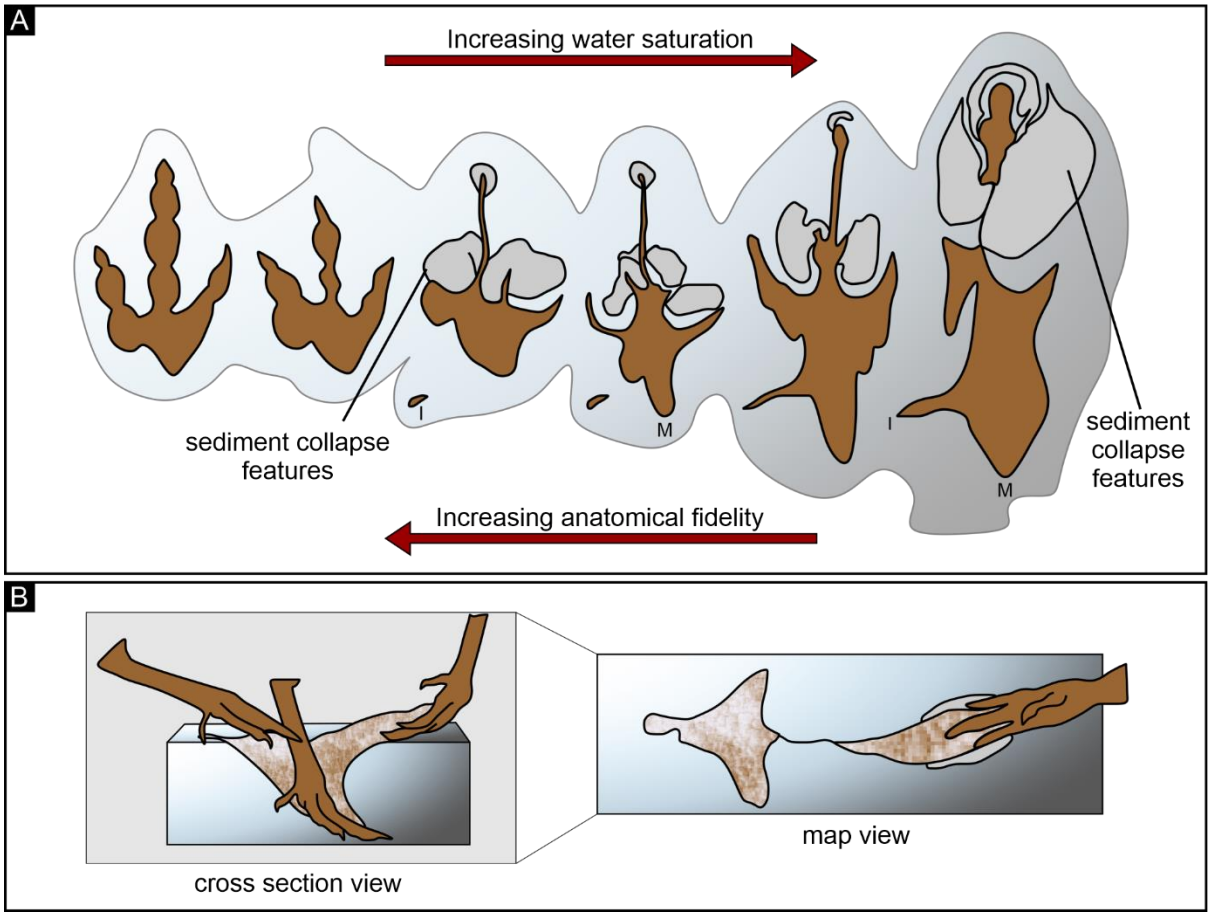

Figure 2.3. Range of track morphologies resulting from varying substrate conditions linked to increasing water saturation. **A)** Anatomical fidelity of the track impression decreases with increasing water saturation of the substrate. Track digit I (I) and the metatarsal (M) interact with saturated substrates, and sediment collapse features are commonly associated with the track impressions. **B)** Track deformation caused by the downward and forward sinking of the trackmaker's foot in a super-saturated substrate. Modified from Gatesy et al. (1999).

Table 2.2. Preservation grade criteria of tracks of a specific grade as defined by Belvedere and Farlow (2016) and Marchetti et al. (2019).

Preservation grade	Description Belvedere and Farlow (2016)	Additional decription Marchetti et al. (2019)	Additional details Marchetti et al. (2019)	
0	No visible morphological details	Digit impressions and palm/sole unrecognisable; track completely distorted; track walls may not be defined; possible preservation of secondary features like tail impressions and drag marks; significant directional deformation of the anatomical related morphology; superimposition or erosion	p	Partial preservation (e.g., missing digits)
			c	Morphology cut (e.g., superimposition)
			w	Anomolous width (e.g., very broad digits)
			f	Flattened footprint
			a	Anomolous morpholgy (multi-directional deformation)
			m	Anomolous morpholgy (mono-directional deformation)
1	Faint or distorted digit impressions that are recognizable; claw marks are recognizable; general outline is observed	Incomplete; claw marks and digital pads may be missing; undefined tracks walls; may be preserved with secondary features such as tail and drag impressions; considerable directional deformation of anatomy related morphology; lots of superimposition/erosion	s	Skin/scale impressions
			d	Drag marks
			b	Digit tip bifurcations
2	Digit impressions are fairly clear and sharp, for the most part; claw marks and some digital pads are observed	Palm/sole present and nearly complete if taxonomically relevant; track walls are reasonably defined; secondary features such as tail impressions, digit drags etc may be preserved; low occurrence of directional deformation of anatomy related morphology		
3	All digit impressions are sharp and clear; well-defined digit walls, claw impressions and digital pads preserved	Palm/sole present if taxonomically relevant; secondary features such as tail impressions, digit skin impressions may be preserved; absence of superimposition or erosion; no directional deformation of anatomy related morphology		

2.2.2 The role of microbially induced sedimentary structures (MISS)

MISS are primary sedimentary structures formed from the interaction between microbes and sediment (Noffke et al., 2001, 2022). Both biotic and abiotic processes can produce identical surface textures, making it difficult to distinguish MISS in the geological record, however, by examining the textures and providing detailed descriptions, MISS can be identified with a credible degree of certainty (Davies et al., 2016). Microbes in the substrate have been linked to aiding track registration, lithification and preservation by producing extracellular polymeric substances that act as adhesive organic coatings on sedimentary grains, forming biofilms (e.g., Noffke et al., 2001, 2022). These biofilms continue to grow in favourable ecological conditions, forming thick organic layers that can cover large surfaces and are expressed as diverse surface textures (Figure 2.4; Noffke et al., 2001, 2022).

Substrates that are microbially-stabilized are more cohesive, deform more elastically, and register track impressions with higher anatomical fidelity (Figure 2.4; e.g., Marty et al., 2009; Carmona et al., 2011; Dai et al., 2015). Furthermore, microbially-stabilized substrates promote early track consolidation and preservation by forming protective layers that reduce the erodibility of the underlying registered tracks (Figure 2.4; e.g., Marty et al., 2009; Carvalho et al., 2013; Dai et al., 2015). When the microbes decompose, they precipitate carbonates, inducing early lithification and cementing the substrate, further enhancing the track preservation potential (e.g., Schieber, 2007; Carvalho et al., 2013). Tracks can also act as stagnant pools of water where biofilms can grow and produce a cover on the track, binding and stabilizing the sediment in which the track formed, thus enhancing early track lithification and preservation (e.g., Sciscio et al., 2016).

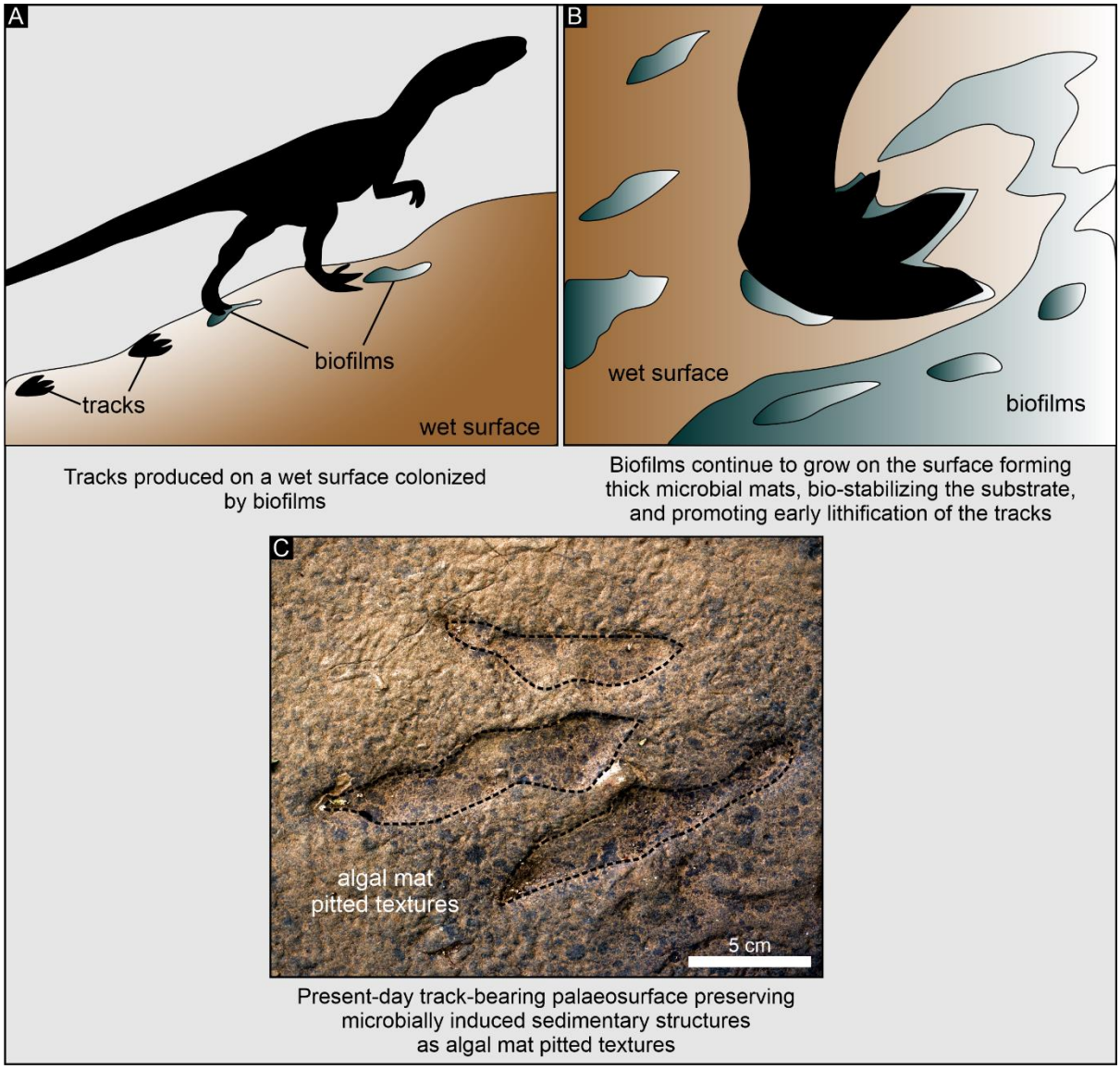

Figure 2.4. A model depicting how MISS can aid in track registration, lithification and preservation. Modified from Sciscio et al. (2016).

3. Methods

3.1 Fieldwork

Fieldwork was carried out in Lesotho and South Africa to collect rock samples from ten previously identified and described track-bearing sites (Figure 3.1; Table 3.1; see Ellenberger, 1955, 1970, 1972, 1974; Ellenberger and Ellenberger, 1956; Ellenberger et al., 1963; Ambrose, 2003; Sciscio et al., 2016, 2017; Bordy et al., 2017; Rampersadh and Bordy, 2019; Abrahams et al., 2022). For ichnosites that have not had their detailed sedimentology assessed, macroscopic observations of the host rocks were described according to the protocol of Miall (1996) to aid the sedimentary facies characterization. This entailed documenting the lithology, geometry (bed shape, thickness, lateral continuity), grain size and sedimentary structures preserved. The outcrops of the host rocks were photographed using a Fujifilm X_T200 camera. From the ten selected ichnosites (Figure 3.1; Table 3.1), eighteen sandstone samples (seven from the lEF, six from uEF and four from the CLAR) were collected for petrographic analysis i.e., assessment of grain size distribution, textural characteristics and grain composition. The samples were collected from the track-bearing strata on which the tracks are preserved, within a meter of the ichnosite. This approach was used to ensure that the samples accurately represent the ancient substrate on which the tracks were registered. For the Qalo ichnosite, where the tracks are preserved as epireliefs beneath a cave overhang, a sample was collected from the sedimentary unit directly underlying the track-bearing surface. Multiple samples were collected at sites where the track-bearing surface was very large (e.g., Maphutseng) or where preserved macro-sedimentary features indicated that substrate saturation varied significantly (e.g., Phuthiatsana; see Table 3.1).

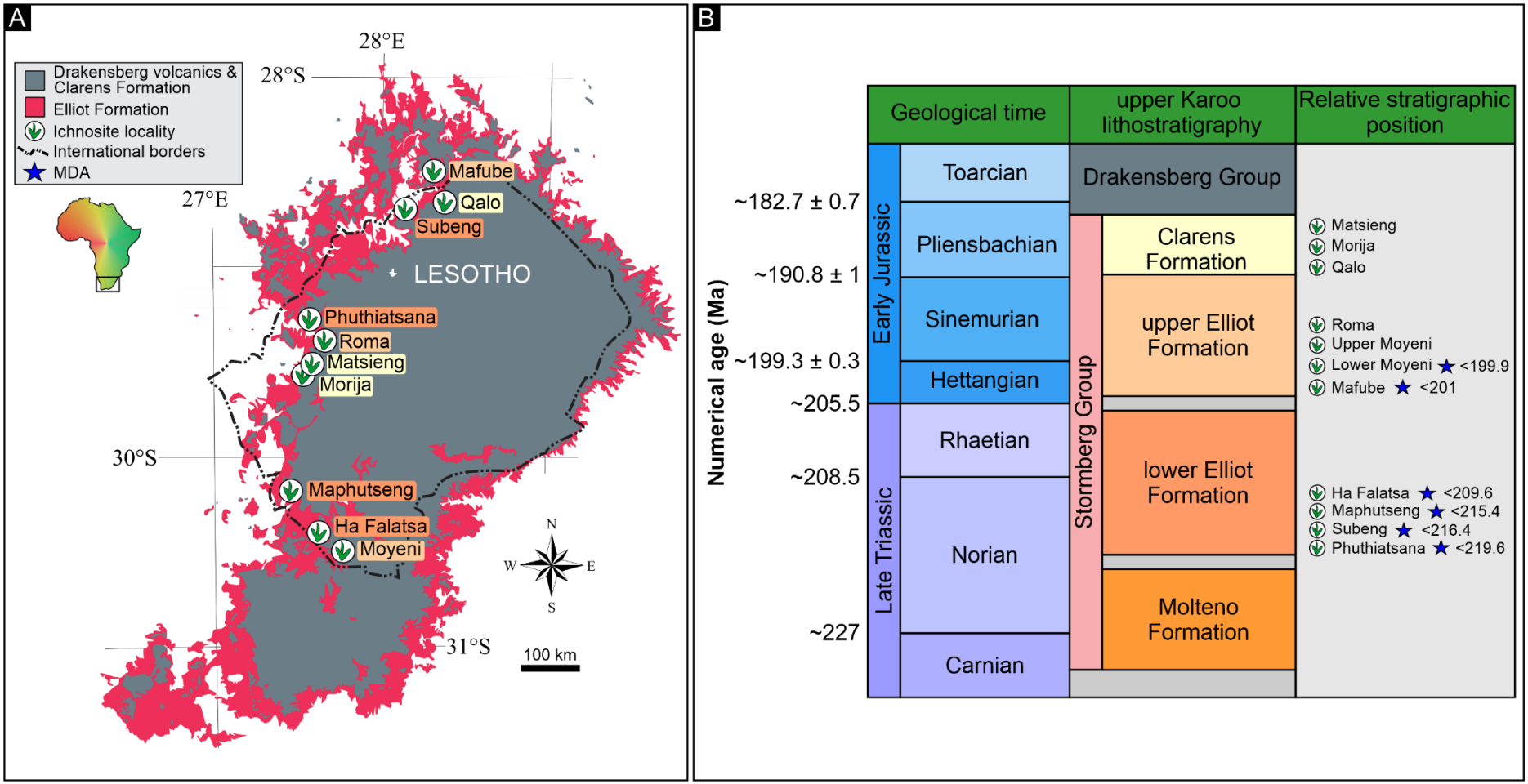

Figure 3.1. Ichnosites overview**. A)** Sampling locations of ichnosites in the upper Stormberg Group of western Lesotho. **B)** Chronostratigraphy of the upper Stormberg Group (Bordy et al., 2020a). Geological time scale based on the International Chronostratigraphic Chart, v2022. Abbreviations: MDA – maximum depositional ages; Ma – millions of years; light grey = stratigraphic gaps.

Table 3.1. Location, stratigraphic position and relevant literature of each sampled ichnosite considered in this study (see Figure 3.1).

Section	Ichnosite	Stratigraphy	GPS co-ordinates	Samples collected	Literature
4.1.1.1	Ha Falatsa	lEF	30°21′57.43″S, 27°34′19.18″E	1	Ellenberger (1970, 1972)
4.1.1.2	Maphutseng	lEF	30°12′44.98″S, 27°28′52.39″E	2	Ellenberger and Ellenberger (1956, 1960); Bordy et al. (2015)
4.1.1.3	Subeng	lEF	28°49′23.53″S, 28°4′29.82″E	1	Ellenberger (1955); Bordy et al. (2017)
4.1.1.4	Phuthiatsana	lEF	29°21′30.02″S, 27°36′35.61″E	3	Ellenberger et al. (1963); Sciscio et al. (in review)
4.1.2.1	Mafube	uEF	28°40′0.04″S, 28°16′54.13″E	1	Sciscio et al. (2016)
4.1.2.2	Moyeni site 1: Lower Moyeni	uEF	30°24′09.5″S, 27°42′07.1″E	1	Ellenberger et al. (1963); Smith et al. (2009)
	Moyeni site 2: Upper Moyeni	uEF	30°23′42.49″S, 27°41′34.66″E	1	Abrahams et al. (2020)
4.1.2.3	Roma site 1: Matobo	uEF	29°27′08.57″S, 27°42′08.51″E	1	Ambrose (2003); Sciscio et al. (2017)
	Roma site 2: Mokhosi	uEF	29°27′17.63″S, 27°42′16.25″E	1	Ambrose (2003); Abrahams et al. (2023)
	Roma site 3: Tlapana	uEF	29°27′09.03″S, 27°42′04.01″E	2	Ambrose (2003)
4.1.3.1	Matsieng	CLAR	29°36′53.5″S, 27°33′57.43″E	2	Ellenberger (1970, 1972)
4.1.3.2	Morija	CLAR	29°37′58.02″S, 27°30′47.51″E	1	Dornan (1908); Ellenberger (1970, 1972)
4.1.3.3	Qalo	CLAR	28°42′17.46″S, 28°20′12.53″E	1	Dornan (1908); Ellenberger (1970, 1972)

3.2 Petrographic analysis

3.2.1 Sample preparation

Eighteen sandstone samples were cut into standard thin sections measuring 45 mm long, 25 mm wide and 30 µm thick at the University of the Western Cape. The thin sections were prepared as follows (Figure 3.2): 8–10 cm pieces of rock were cut from their respective primary rock sample using a Buehler abrasive cutter and sectioning saw to make parallel slabs. These slabs were then dried in an oven at 80 °C for 15 minutes. To smooth out the surface, one side of each slab was rubbed against a 400-grit glass in circular motions with silicon carbide powder and water, followed by rubbing on a 600-grit glass. The slabs were once again dried in the oven for 15 minutes at 80 °C. Because sandstone samples are soft, they needed to be impregnated before they can be gritted. Impregnation involves removing moisture from a porous substance and gluing it to a component (in this case, liquid resin epoxy) to make it firm enough for handling, cutting and grinding without damaging the sample. The smoothed side of the lapped slabs was coated with resin and then dried in the oven at 70 °C for 10 minutes. The surface resin was removed by rubbing the dried impregnated slabs in circular motions on a 400-grit glass in circular motions with silicon carbide powder and water. A glass slide was then glued to the lapped face of the slab using resin, and the slab was cut to ~50 µm using a discoplan-TS. Further thickness reduction to 30 µm was achieved by rubbing the thin sections on a 600-grit glass in circular motions with silicon carbide powder and water. The first-order interference colours of quartz grains were observed using a Leica transmitted light microscope since quartz is the most common and abundant mineral in rocks and serves as a reference for thickness reduction to 30 µm. After drying for 10 minutes at 40 °C in the oven, the thin sections were covered with glass coverslips, labelled, ready for petrographic analysis.

3.2.2 Petrography

The thin sections were subjected to textural, grain size distribution, and modal composition analyses (see Appendices A, B). For textural analysis, visual comparison charts were utilised to assess grain roundness, sphericity, sorting, grain packing, and grain contacts, providing semi-quantitative visual estimates (Figure 3.3; Appendix B; Taylor, 1950; Powers, 1953; Jerram 2001; Boggs Jr, 2009). The grain roundness scale, for example, comprises six roundness classes: very angular, angular, sub-angular, sub-rounded, rounded, and well-

rounded (Powers, 1953), while a grain sorting descriptions range from very well sorted, well sorted, moderately sorted, poorly sorted to very poorly sorted (Folk, 1968).

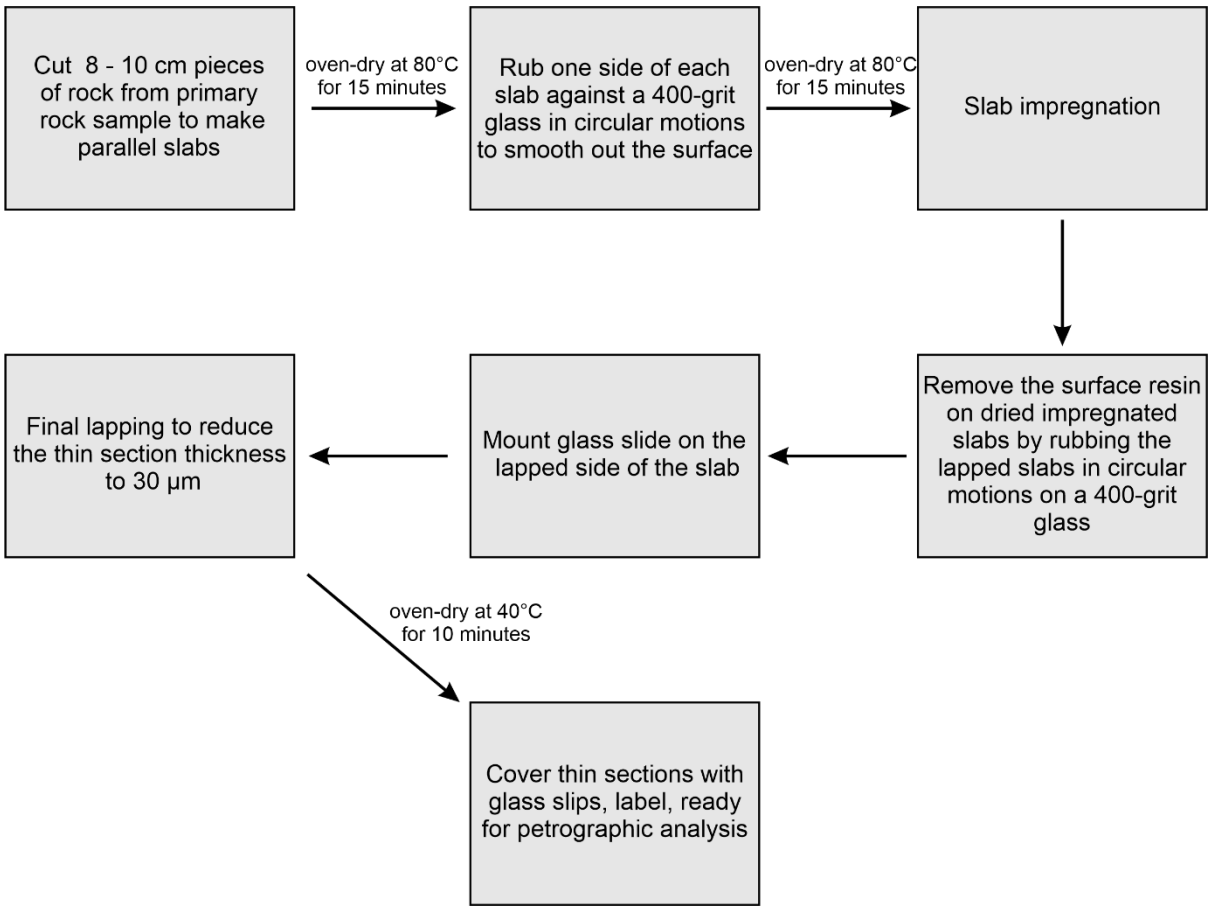

Figure 3.2. Flow chart depicting the key steps followed in thin section preparation.

To estimate the mean grain size, the long axes of 100 grains were measured per thin section using a Leica transmitted light microscope. This number of grains is deemed sufficient to provide a mean grain size value with 90% certainty within 10–13 % of the true value for moderately to well-sorted sandstones (Johnson, 1994). The Udden–Wentworth grain size scale for sediments (Figure 3.3) was utilised to determine the grain size classes of the measured grains, and the frequencies were computed for grain size distribution analysis. The Udden–Wentworth scale is divided into four major grain size categories: clay, silt, sand, and gravel, with grain sizes ranging from <0.063 mm to >64 mm, which are further subdivided.

For modal composition analysis, a minimum of 300 grains were assessed per sample using the Gazzi-Dickinson point counting method, conducted using a Nikon transmitted light microscope and a point counter (Appendix A; Dickinson, 1979, 1985; Ingersoll et al., 1984). A two-spaced counting grid was employed to traverse the thin section, ensuring complete coverage of the entire slide, and only the mineral grain under the cross hairs was counted to avoid duplicate counting. The framework minerals of the sandstones were categorized into monocrystalline quartz (Qm), polycrystalline quartz (Qp), plagioclase (Pf), alkali-feldspar (Kf), lithic fragments (L), mica (Mi), matrix and cement (Appendices A, B). Accessory minerals such as rutile, zircon and opaque minerals were noted but not included in the modal composition analysis due to their trace amounts. Scaled photomicrographs of the identified minerals were captured using the built-in Axiocam camera mounted on a viewing Zeiss petrographic microscope for further examination.

3.3 X-ray diffraction (XRD)

For XRD analysis, the rock samples were initially crushed to chip sizes (1–3 mm in diameter) using a jaw crusher and then milled into a fine powder (<10 µm) using a rotary mill at the University of Cape Town. The analysis was conducted at the University of Free State using a PANanalytical-Empyrical diffractometer equipped with a Cu K-alpha X-ray tube. Mineralogical identification was performed using the HighScore software, which detects diffraction patterns and mineral phases (Appendix C).

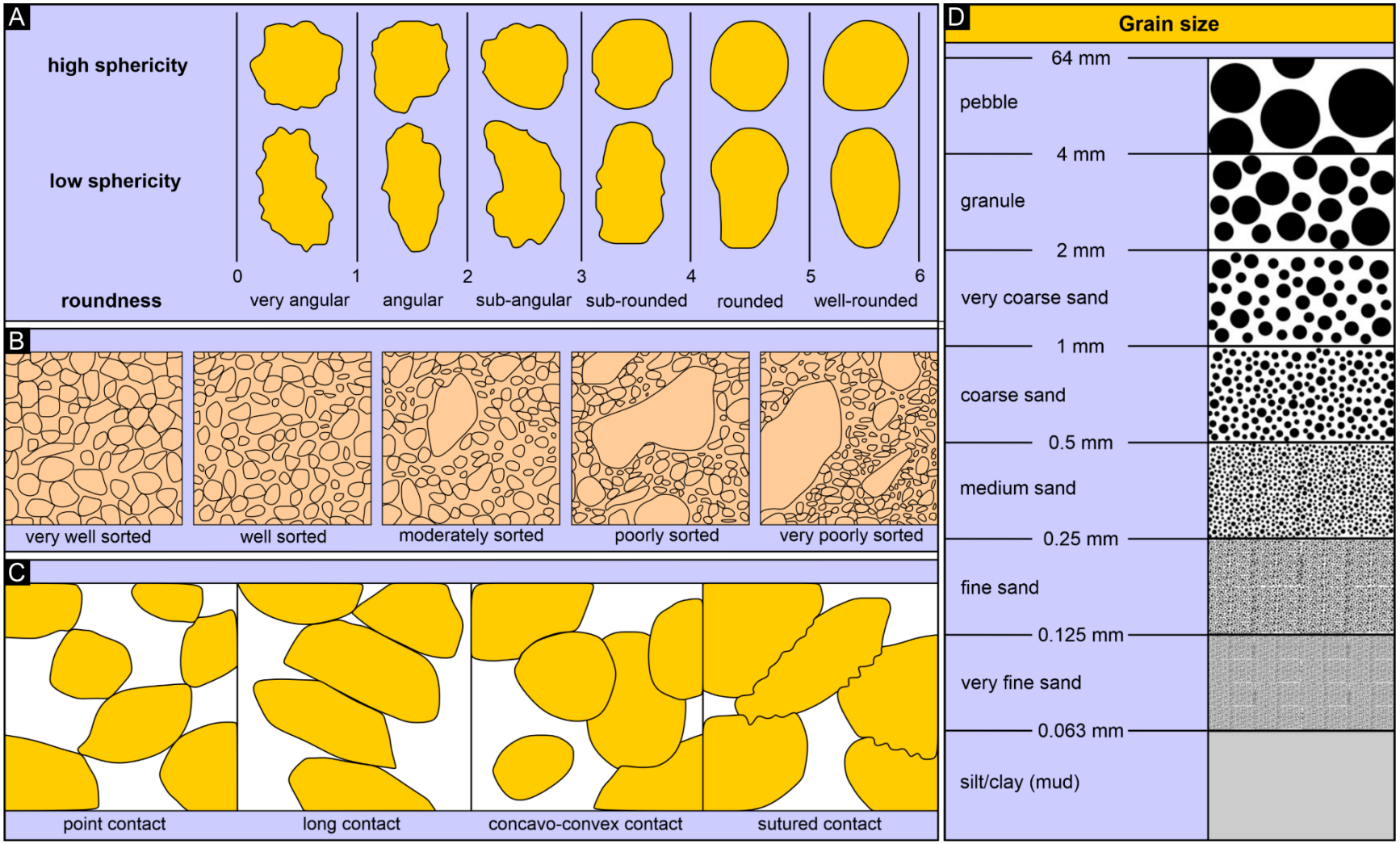

Figure 3.3. Comparison charts for semi-quantitative visual estimations and grain size distribution. **A)** Roundness and sphericity scale (after Powers, 1953). **B)** Degree of sorting (after Jerram, 2001). **C)** Grain contacts (after Taylor, 1950). **D)** Grain size classification scheme in millimetre (mm) scale (after Wentworth, 1922).

4. Results

4.1 Ichnosites

The ichnosites considered herein are described in stratigraphic order from the lEF to the uEF, and finally to the CLAR (Figure 3.1; Table 3.1). Within each stratigraphic unit, the ichnosites are listed in alphabetical order. For most of these ichnosites, previous authors have conducted macro-sedimentological analyses and provided detailed descriptions of vertebrate tracks (see Table 3.1). However, the Mokhosi ichnosite is an exception as the macro- and micro-sedimentary features were obtained during this MSc study and have been recently published (see Abrahams et al., 2023).

4.1.1 Lower Elliot Formation ichnosites

4.1.1.1 Ha Falatsa

The Ha Falatsa ichnosite, measuring about 650 by 20 m in size, was first described by Ellenberger (1970, 1972). The ichnosite consists of multiple track-bearing palaeosurfaces that preserve ripple marks, desiccation cracks and soft sediment deformation structures expressed as wavy laminations (Abrahams, 2020). Tridactyl, tetradactyl and pentadactyl tracks and trackways are preserved at the ichnosite (Ellenberger 1970, 1972). The anatomical fidelity of the tracks ranges between 0 and 2, with the tracks lacking anatomical detail, and in some cases, being incomplete.

Petrography

The Ha Falatsa track-bearing sandstone predominantly comprises medium sand (60%), with the majority of the grains ranging between 0.35–0.45 mm (Figure 4.1A). The sandstone also has a significant coarse sand component (35%) with an average grain size of ~0.6 mm, as well as a minor fine sand component (4%; Figure 4.1A). The sand grains are moderately sorted, subangular to subrounded and have low sphericity, with the coarse sands generally being more subangular than the medium sands, which are more subrounded (Figure 4.1B; Appendix B). The sand grains are closely packed and have both concavo-convex and long grain contacts. Based on the modal composition analysis, the sandstone is composed mainly of

monocrystalline quartz (60.3%), polycrystalline quartz (25.6%), lithic fragments (13.3%) and a trace amount of feldspar and mica (Figure 4.1B). These findings are consistent with the results of the XRD analysis, which indicated the presence of quartz (82%), plagioclase feldspar (7%) and kaolinite (7%; Appendix C). The quartz grains generally have a coarser size compared to other types of grains (e.g., 0.66 mm monocrystalline quartz vs 0.35 mm lithic fragment grain; Appendix A). Moreover, the quartz grains exhibit secondary overgrowths around their original detrital grain boundaries (Figure 4.1B). Accessory minerals present in the sandstone include opaque minerals, rutile and zircon inclusions within quartz grains (Appendix B).

4.1.1.2 Maphutseng

The Maphutseng ichnosite was first documented by Ellenberger and Ellenberger (1956, 1960) and subsequently revised by other authors (e.g., Ellenberger, 1970, 1972; Knoll, 2004; Bordy et al., 2015; Sciscio et al., in review). The ichnosite comprises two surfaces, a northern and southern surface (Maphutseng A and B, respectively), which are both ripple-marked and desiccated. The northern surface is larger in size and preserves tridactyl tracks as epireliefs, whereas the southern surface preserves both tetradactyl and tridactyl tracks as hyporeliefs. The anatomical fidelity of the tracks on both surfaces varies between 0 and 3, with the northern surface (i.e., Maphutseng A) preserving a greater number of tracks compared to the southern surface (i.e., Maphutseng B).

Petrography: Maphutseng A

The Maphutseng A sandstone mainly consists of medium sand (75%), with the majority of grains ranging between 0.32–0.45 mm, and a subordinate fine sand component (25%; Figure 4.2A). The sand grains are moderately sorted, subangular to subrounded and have low sphericity, with the medium sands generally being more subangular than fine sands, which are more subrounded (Figure 4.2B; Appendix B). The sand grains are closely packed and have mostly concavo-convex and long grain contacts. Based on the modal composition analysis, the sandstone comprises monocrystalline quartz (66.6%), polycrystalline quartz (11.6%), lithic fragments (13.6%), plagioclase feldspar (4.6%), alkali feldspar (1.6%) and mica (1.6%; Figure 4.2B). The composition is comparable to the findings of the XRD analysis, which indicated the presence of quartz (80%), plagioclase feldspar (7%), alkali feldspar (5%) and mica (8%;

Appendix C). The quartz and feldspar grains have similar grain sizes of ~0.4 mm and are generally larger than the other grains which have grain sizes of ~0.3 mm. Minor amounts of mica are present in the sandstone and occur as random elongated flakes. Accessory minerals in the sandstone include rutile, opaque minerals and zircon inclusions within quartz grains (Appendix B).

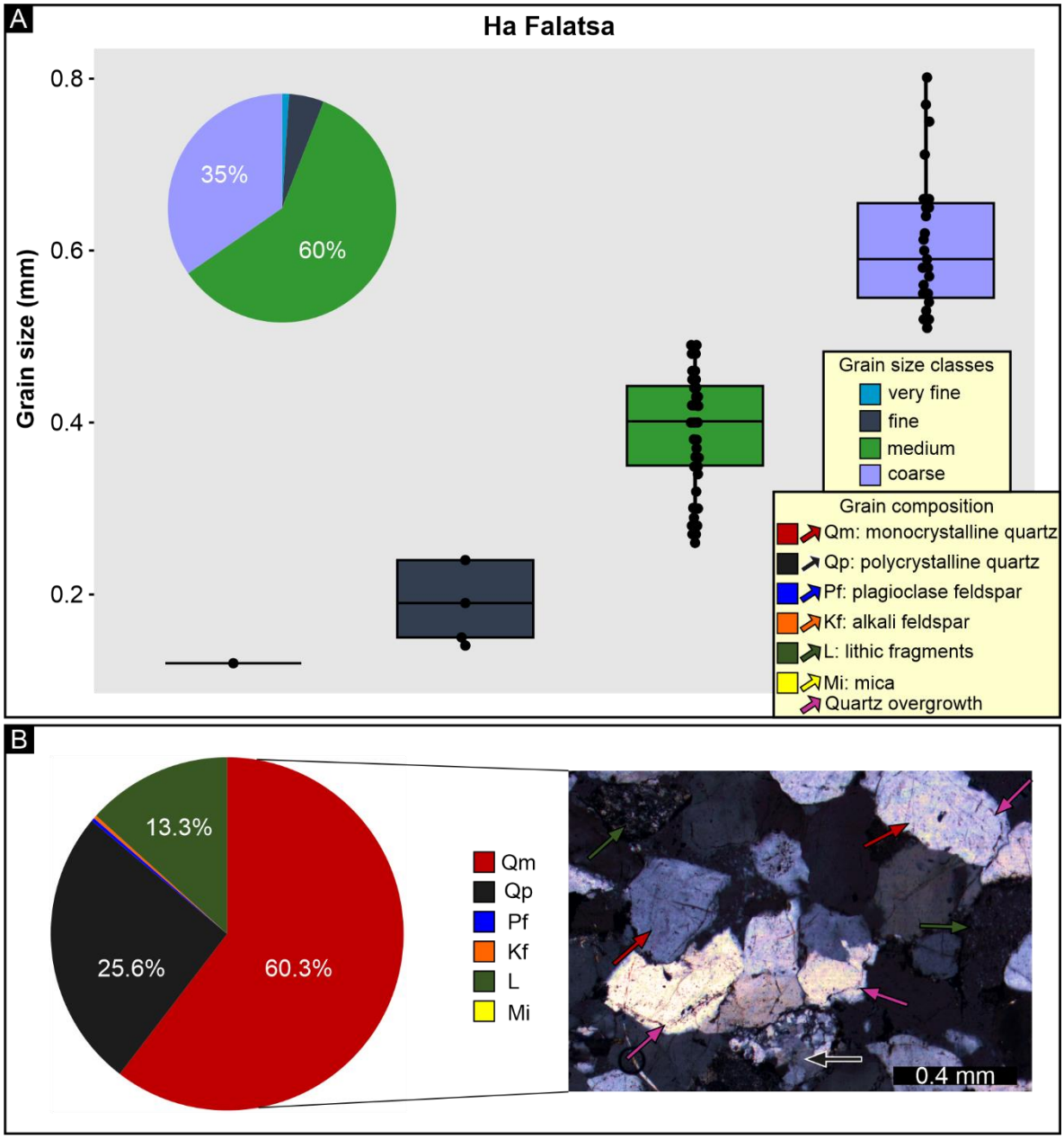

Figure 4.1. Petrographic properties of Ha Falatsa ichnosite sandstone. **A)** Grain size distribution. **B)** Modal composition and photomicrograph of the sandstone under cross-polarized light showing moderately sorted, sub-angular to subrounded grains of monocrystalline quartz, polycrystalline quartz, lithic fragments and evidence for quartz overgrowths.

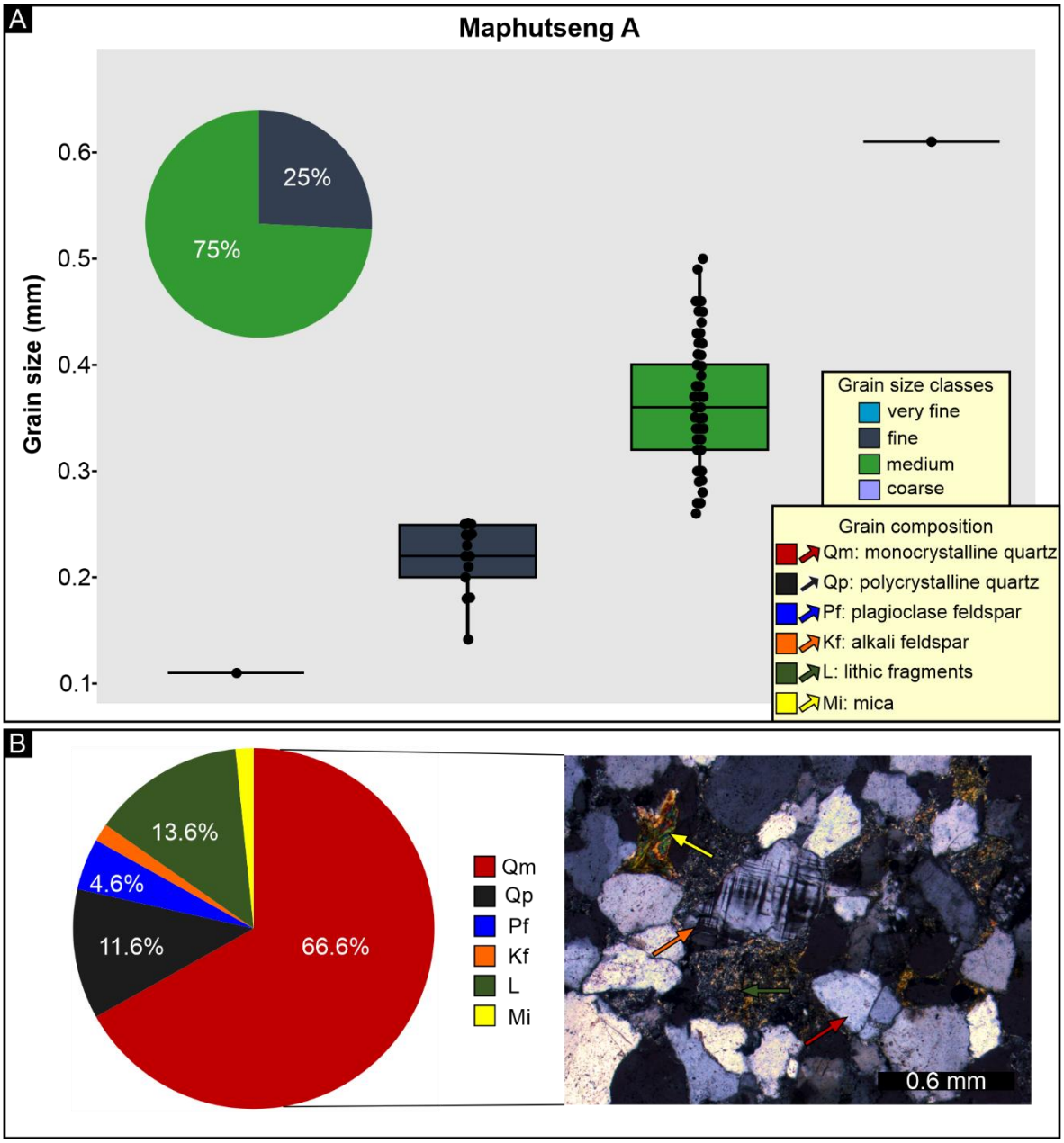

Figure 4.2. Petrographic properties of Maphutseng A sandstone. **A)** Grain size distribution. **B)** Modal composition and photomicrograph of the sandstone under cross-polarized light showing moderately sorted, sub-angular to subrounded grains of monocrystalline quartz, alkali feldspar, lithic fragments and mica.

Petrography: Maphutseng B

The Maphutseng B sandstone predominantly comprises medium sand (81%), with a dominant grain size distribution ranging from 0.26–0.43 mm, and a subordinate fine sand component (16%; Figure 4.3A). The sand grains are moderately sorted, subangular, with low sphericity, close packing and both concavo-convex and long grain contacts (Figure 4.3B; Appendix B). Based on the modal composition analysis, the sandstone consists of monocrystalline quartz (64.6%), polycrystalline quartz (17.6%), lithic fragments (13%), plagioclase feldspar (2%) and

mica (2%; Figure 4.3B; Appendix B). The composition is similar to the results of the XRD analysis, which indicated the presence of quartz (76%), plagioclase feldspar (10%) and mica (10%) and kaolinite (4%; Appendix C). The quartz and feldspar grains have comparable sizes, averaging ~0.35 mm, and are typically larger than the other grain types which average ~0.28 mm in size. Minor amounts of mica are present in the sandstone, occurring as small random fragments. Accessory minerals in the sandstone include rutile, opaque minerals, and zircon inclusions in quartz grains (Appendix B).

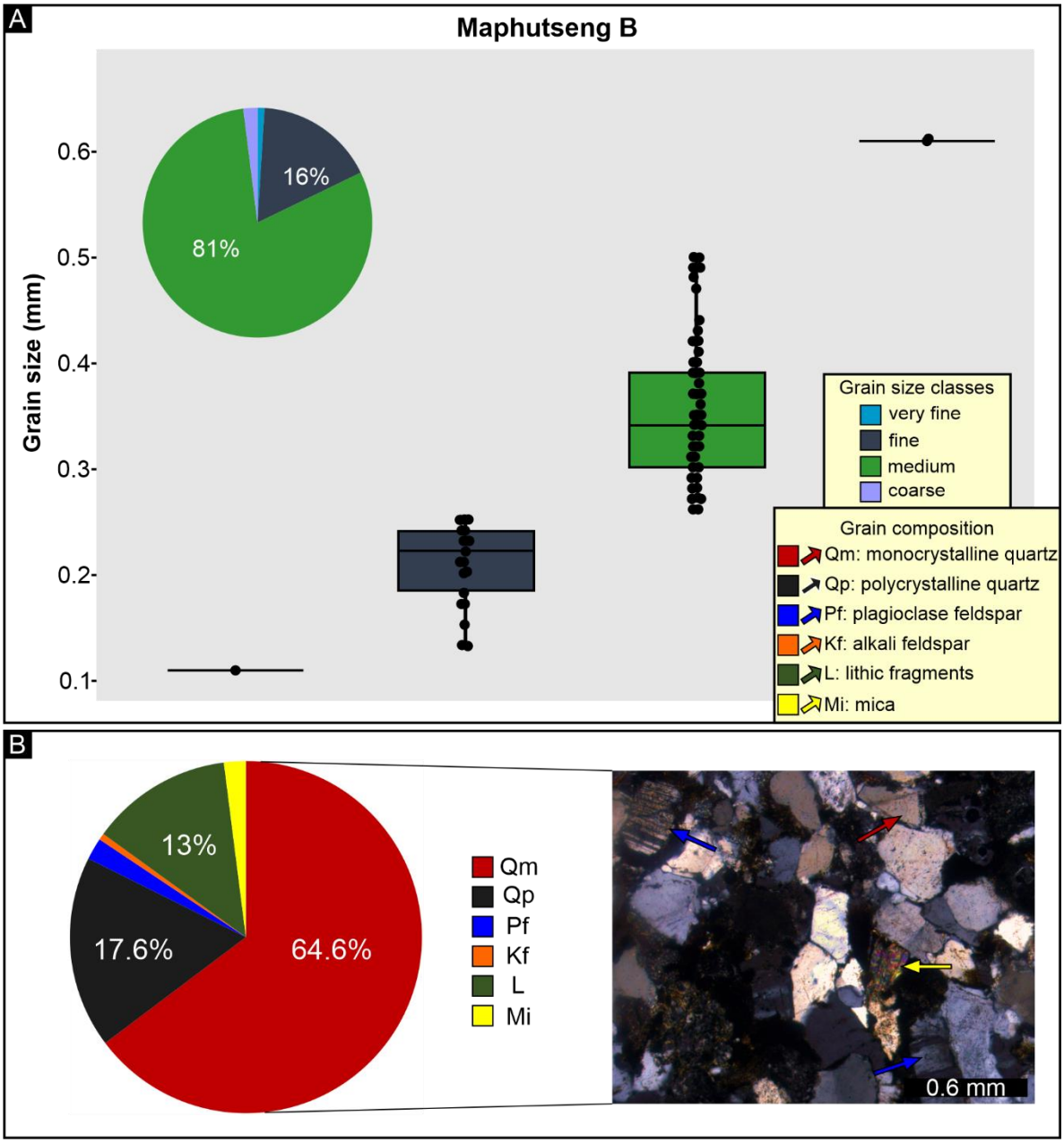

Figure 4.3. Petrographic properties of Maphutseng B sandstone. **A)** Grain size distribution. **B)** Modal composition distribution and photomicrograph of the sandstone under cross-polarized light showing sub-angular grains of monocrystalline quartz, plagioclase feldspar and mica.

Synthesis of the Maphutseng track-bearing sandstones

The two track-bearing sandstones at Maphutseng have very similar petrographic properties. Both sandstones primarily consist of medium sand, with Maphutseng B having a slightly higher proportion of medium sands than Maphutseng A (81% vs 75%, respectively). On average, the dominant grain size distribution range is slightly smaller in Maphutseng A compared to Maphutseng B (0.32–0.45 mm vs 0.26–0.43 mm, respectively). Both sandstones exhibit moderate sorting, low sphericity, and have similar grain packing and contacts. However, unlike Maphutseng B, Maphutseng A contains some subrounded grains. The compositions of the sandstones are generally similar based on both modal composition and XRD analysis findings. Moreover, the sandstones preserve tracks with comparable anatomical fidelity grades, ranging from 0–3. The greater track abundance in Maphutseng A compared to Maphutseng B may be attributed to its relatively larger surface area.

4.1.1.3 Subeng

The Subeng ichnosite was first reported by Ellenberger (1955) and has subsequently been described by numerous authors (e.g., Ellenberger, 1970, 1972; Ellenberger and Ellenberger, 1958; Bordy et al., 2017). The track-bearing palaeosurface is ripple-marked and desiccated and preserves numerous tridactyl, tetradactyl and pentadactyl tracks and trackways (Bordy et al., 2017). The anatomical fidelity of the tracks preserved is variable, ranging between 0 and 2 (Bordy et al., 2017).

Petrography

The Subeng track-bearing sandstone comprises fine sand (57%) with the majority of the grains ranging between 0.17–0.23 mm (Figure 4.4A). The sandstone also has a significant medium sand component (42%) with the majority of the grains ranging between 0.28–0.34 mm (Figure 4.4A). The sand grains are moderately sorted, subangular to subrounded and have low sphericity, with medium sands generally being more subangular than fine sands, which are more subrounded (Figure 4.4B; Appendix B). The sand grains are moderately packed and have both concavo-convex and long grain contacts. Based on the modal composition analysis, the sandstone comprises monocrystalline quartz (57.3%), polycrystalline quartz (16.3%), lithic fragments (12.6%), plagioclase feldspar (7.3%), alkali feldspar (1.6%) and mica (4.6%; Figure 4.4B). The composition is comparable to the XRD analysis, which indicated the presence of

quartz (76%), plagioclase feldspar (9%), mica (11%) and kaolinite (4%; Appendix C). A minor amount of mica is present in the sandstone and occurs as bent elongated flakes (Figure 4.4B). Accessory minerals in the sandstone include rutile, opaque minerals and zircon inclusions in quartz grains (Appendix B).

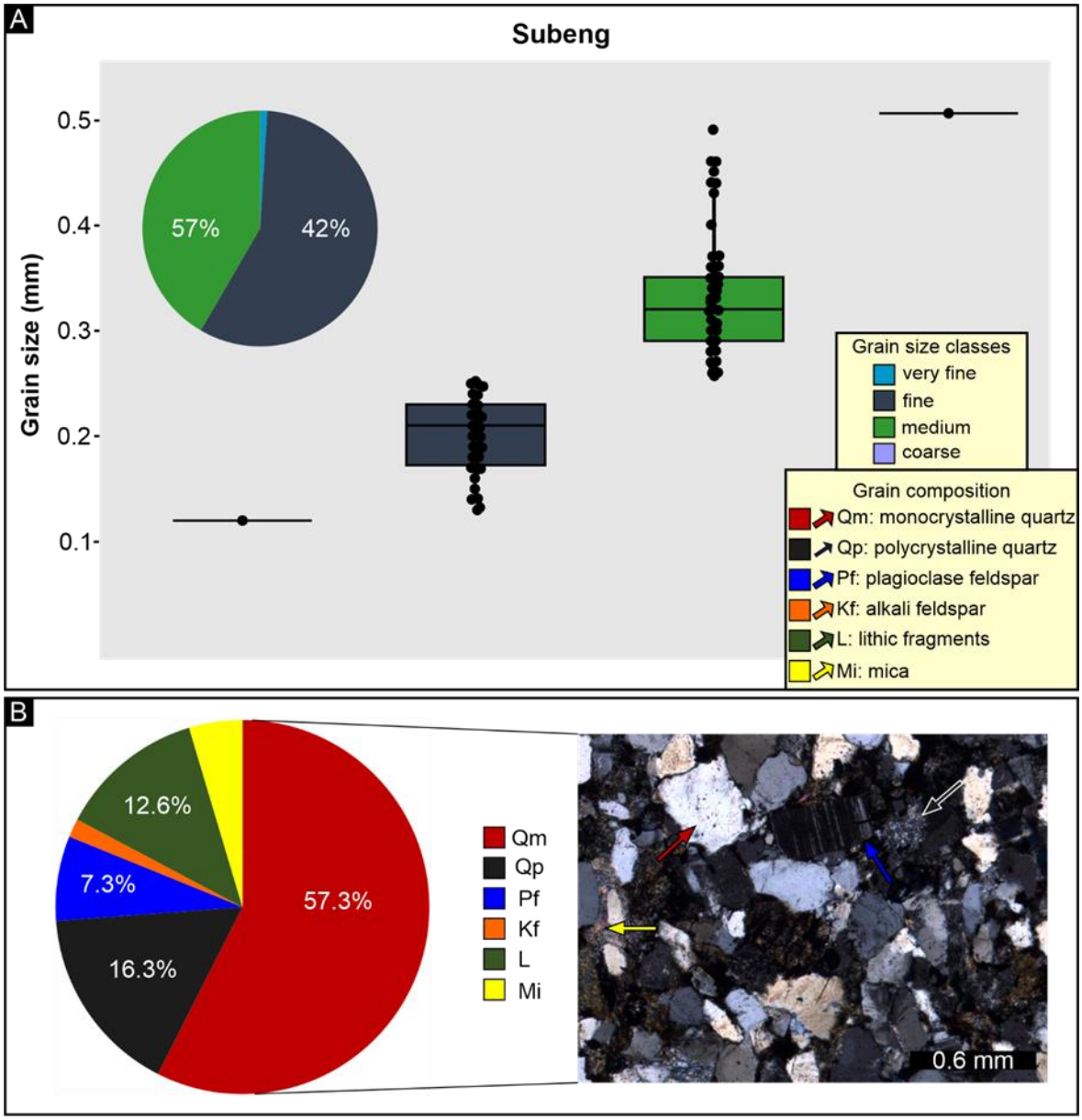

Figure 4.4. Petrographic properties of Subeng ichnosite sandstone. **A)** Grain size distribution. **B)** Modal composition and photomicrograph of the sandstone under cross-polarized light showing moderately, sub-angular to sub-rounded grains of monocrystalline quartz, polycrystalline quartz, plagioclase feldspar and mica.

4.1.1.4 Phuthiatsana

The Phuthiatsana ichnosite, measuring about 80 by 7 m in size, was first documented by Ellenberger et al. (1963) and subsequently revised by other authors (e.g., Ellenberger, 1970, 1972; Sciscio et al., in review). The ichnosite preserves ripple marks, desiccation cracks and tridactyl, tetradactyl and pentadactyl tracks and trackways (Sciscio et al., in review). Notably, the tetradactyl tracks preserve expulsion rims and soft sediment deformation structures, while the tridactyl tracks preserve claw marks and digital pad impressions, suggesting variations in the substrate conditions. The overall anatomical fidelity of the tracks ranges between 1 and 3. Three sandstone samples were collected from the ichnosite: two from the southern side of the surface (Phuthiatsana A and Phuthiatsana B, respectively), and one about 6 m to the north (Phuthiatsana C).

Petrography: Phuthiatsana A

The Phuthiatsana A sandstone predominantly comprises fine sand (64%) with the majority of grains ranging in size between 0.15–0.23 mm (Figure 4.5A). The sandstone also contains a significant component of very fine sand (35%; Figure 4.5A). The sand grains are moderately sorted and subangular, with low sphericity, moderate packing and concavo-convex and long grain contacts (Figure 4.5B; Appendix B). Based on the modal composition analysis, the sandstone comprises monocrystalline quartz (85.3%), polycrystalline quartz (3.6%), lithic fragments (4%), plagioclase feldspar (1.6%) and mica (5.3%; Figure 4.5B). This composition is consistent with the XRD analysis, which indicated the presence of quartz (83%), plagioclase feldspar (10%) and kaolinite (7%; Appendix C). The quartz grains are generally larger compared to other types of grains (~0.18 mm vs <0.15 mm). Minor amounts of mica are present in the sandstone and occur as random small fragments or elongated flakes. Accessory minerals in the sandstone include rutile and opaque minerals (Appendix B).

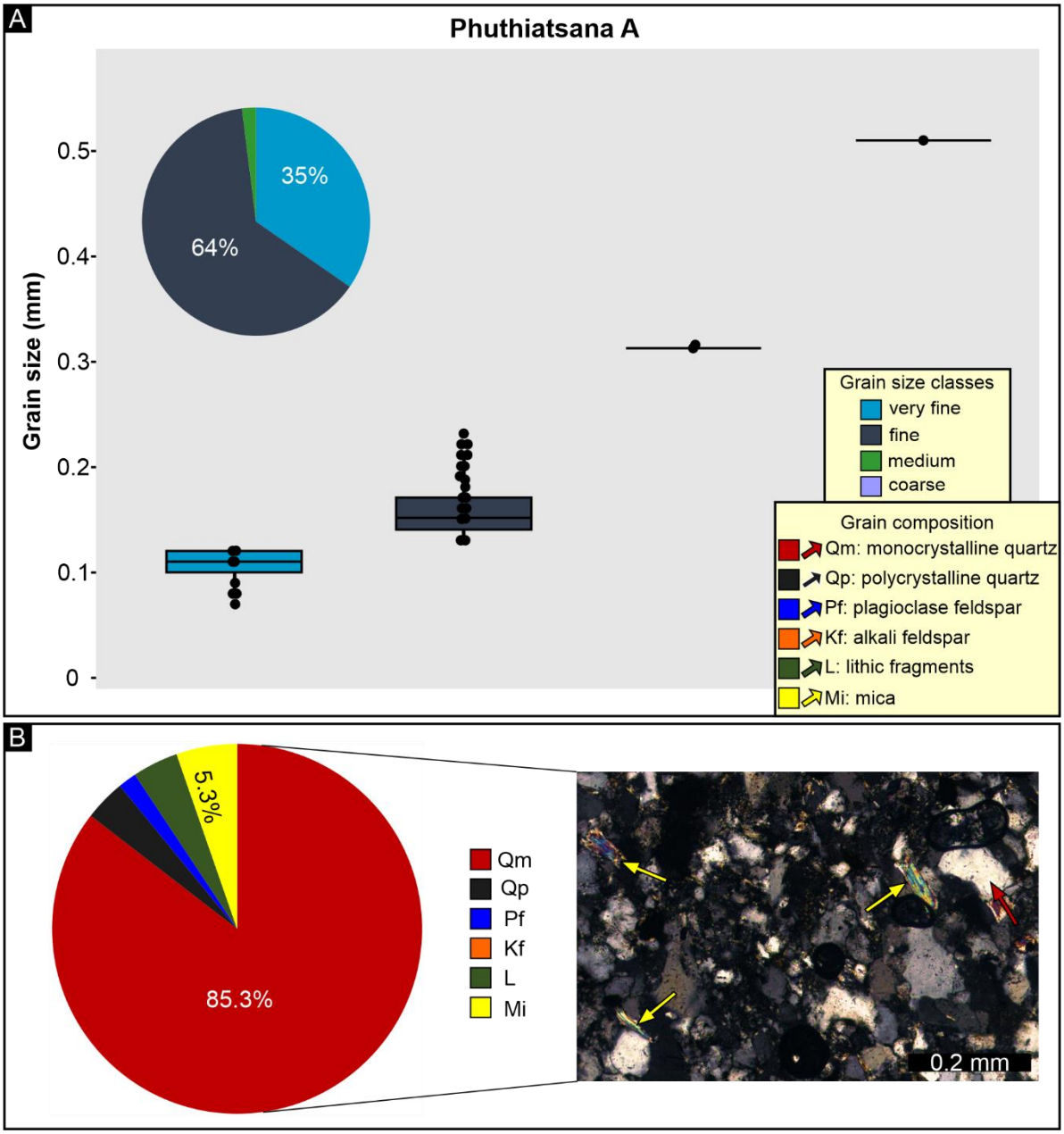

Figure 4.5. Petrographic properties of Phuthiatsana A sandstone. **A)** Grain size distribution. **B)** Modal composition and photomicrograph of the sandstone under cross-polarized light showing sub-angular monocrystalline quartz grains and small fragments of mica.

Petrography: Phuthiatsana B

The Phuthiatsana B sandstone mainly comprises very fine sand (63%) with the majority of the grains ranging between 0.08–0.12 mm (Figure 4.6A). The sandstone also has a significant fine sand component (37%; Figure 4.6A). The sand grains are moderately sorted and subangular, with low sphericity, moderate packing and concavo-convex and long grain contacts. (Figure 4.6B; Appendix B). Based on the modal composition analysis, the sandstone is mainly composed of monocrystalline quartz (90.3%), lithic fragments (1.6%), plagioclase feldspar

(3%) and mica (4.3%; Figure 4.6B). This composition is similar to the results of the XRD analysis, which indicated the presence of quartz (87%), plagioclase feldspar (9%) and kaolinite (4%; Appendix C). Minor amounts of mica are present in the sandstone and occur as random small fragments or elongated flakes. Accessory minerals in the sandstone include rutile and opaque minerals (Appendix B).

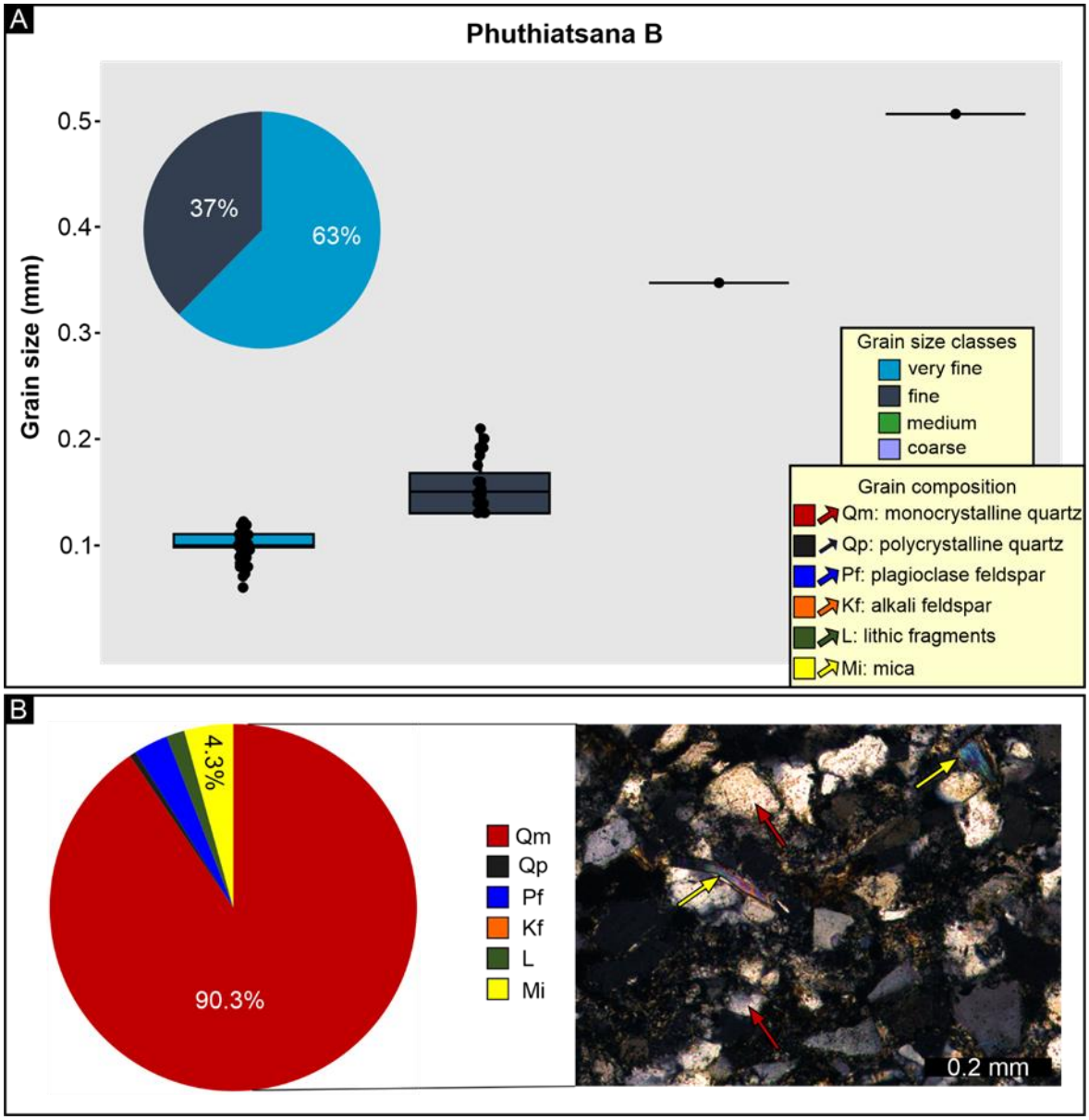

Figure 4.6. Petrographic properties of Phuthiatsana B sandstone. **A)** Grain size distribution. **B)** Modal composition and photomicrograph of the sandstone under cross-polarized light showing sub-angular grains of monocrystalline quartz and mica.

Petrography: Phuthiatsana C

The Phuthiatsana C sandstone comprises fine sand (53%) with majority of the grains ranging between 0.13–0.16 mm, as well as very fine sand (47%) with grains averaging ~0.1 mm (Figure 4.7A). The sand grains are moderately sorted, subangular, with low sphericity, moderate packing and concavo-convex and long grain contacts. (Figure 4.7B; Appendix B). Based on the modal composition analysis, the sandstone comprises of monocrystalline quartz (86.6%), polycrystalline quartz (2%), lithic fragments (2.6%), plagioclase feldspar (4.6%) and mica (4%; Figure 4.7B). These composition findings are comparable to the results obtained from the XRD analysis, which indicated the presence of quartz (84%), plagioclase feldspar (10%) and kaolinite (6%; Appendix C). Minor amounts of mica are present in the sandstone, occurring as random small fragments. Accessory minerals in the sandstone include rutile and opaque minerals (Appendix B).

Synthesis of the Phuthiatsana track-bearing sandstone

The petrographic properties of the three track-bearing Phuthiatsana sandstones have similar petrographic properties. The sandstones are characterized primarily by very fine and fine sands with slightly varying proportions. Phuthiatsana A and Phuthiatsana C have a higher proportion of fine sands than Phuthiatsana B (64% and 53% vs 37%, respectively). Phuthiatsana A has a slightly larger dominant grain size distribution than Phuthiatsana C (0.15–0.23 mm vs 0.13–0.16 mm). The three sandstones exhibit similar sorting, roundness, grain packing, and contacts. Their compositions, as determined by modal composition and XRD analysis, are generally comparable. Interestingly, the Phuthiatsana surface preserves strong evidence of tracks registered under different moisture conditions (i.e., tetradactyl tracks with soft sediment deformation structures, expulsion rims vs tridactyl tracks with claw marks, digital pad impressions). These distinct tracks and extra-morphological features are present despite the absence of significant differences in grain size.

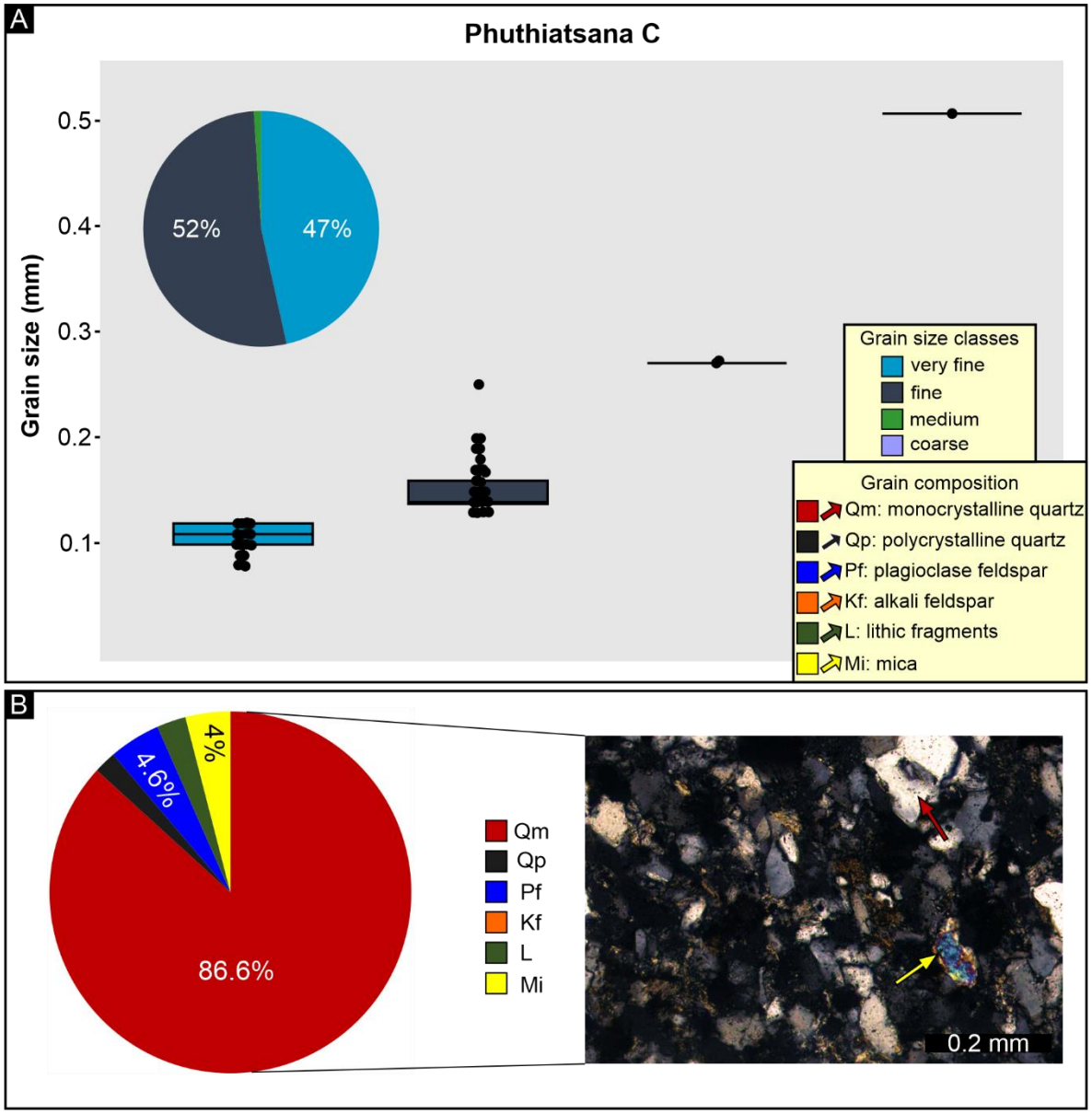

Figure 4.7. Petrographic properties of Phuthiatsana C sandstone. **A)** Grain size distribution. **B)** Grain composition distribution and photomicrograph of the sandstone under cross-polarized light showing sub-angular monocrystalline quartz grains and small fragment of mica.

4.1.1.5 Synthesis of the lEF ichnosites

The track-bearing sandstones from the lEF ichnosites have a wide variation in grain size (Figure 4.1–4.7). The sand grains range from 0.08–0.6 mm, with medium and fine sand classes being the most prevalent (0.15–0.4 mm). The sand grains generally have moderate sorting, similar sphericity, packing and grain contacts, however, the sandstones from Ha Falatsa, Maphutseng A and Subeng ichnosites have more subrounded grains than Maphutseng B and Phuthiatsana sandstones. The composition of the lEF track-bearing sandstones composition varies slightly among the ichnosites, as observed through modal composition and XRD

analyses. On average, according to the XRD findings, quartz accounts a large proportion of the detrital grains (~81%) followed by plagioclase feldspar (~9%), kaolinite (~5%) and mica (~3%).

A slight correlation was observed between grain size, anatomical fidelity and track abundance within the lEF ichnosites. Ichnosites with a larger proportion of very fine to fine sands tend to have slightly more constrained and higher anatomical fidelity grades (e.g., Phuthiatsana with tracks ranging 1–3 vs Maphutseng with tracks ranging 0–3). Furthermore, ichnosites with finer grains tend to have relatively greater track abundance compared to those with coarser grains (e.g., Phuthiatsana with >65 tracks vs Maphutseng with >38 tracks). Moreover, Phuthiatsana is the only lEF ichnosite that preserves tracks associated with sediment collapse features and expulsion rims, indicating a saturated palaeosubstrate. Despite the high water content, it remarkably preserves tracks with relatively higher anatomical fidelity and a significant abundance of tracks commonly found in fine-grained sediments.

4.1.2 Upper Elliot Formation ichnosites

4.1.2.1 Mafube

The Mafube ichnosite was first documented by Sciscio et al. (2016). The palaeosurface, which preserves over 80 tracks, is ripple-marked and desiccated (Sciscio et al., 2016). A noticeable variation in substrate conditions is observed along the surface, from north to south: the tracks in the northern section display more anatomical details, whereas those in the southern section are less anatomically distinct and accompanied by expulsion rims and soft sediment deformation features, suggesting increasingly moist substrate conditions (Sciscio et al., 2016). Unlike the northern surface, the southern surface preserves pervasive MISS expressed as pitted textures (Sciscio et al., 2016). These pitted textures are observed within the tracks, indicating that microbial activity post-dates track registration. The substrate variation at the Mafube corresponds to higher track abundance and lower anatomical fidelity grades on the southern surface.

Petrography

The Mafube sandstone, sampled near the north surface, predominantly comprises very fine sand (67%) with majority of the grains ranging between 0.08–0.12 mm, and a significant fine sand component (33%) with grains averaging ~0.15 mm (Figure 4.8A). The grains are moderately to well sorted, subangular to subrounded, with low sphericity, moderate packing and concavo-convex grain contacts (Figure 4.8B; Appendix B). Based on the modal composition analysis, the sandstone comprises monocrystalline quartz (84%), polycrystalline quartz (1%), lithic fragments (8%) and plagioclase feldspar (7%; Figure 4.8B). The XRD analysis findings indicate the presence of quartz (69%), plagioclase feldspar (26%) and alkali feldspar (5%; Appendix C). Accessory minerals in the sandstone include opaque minerals and zircon inclusions in quartz grains (Appendix B).

4.1.2.2 Moyeni

The town of Moyeni preserves two well-documented dinosaur track-bearing surfaces preserved in the uEF (i.e., Lower Moyeni and Upper Moyeni). The discovery of the Lower Moyeni site is highly attributed to Paul Ellenberger, who provided detailed ichnological accounts of the sites in earlier studies (see Ellenberger et al., 1963; Ellenberger, 1970, 1974) which have subsequently been updated with modern ichnological techniques (e.g., Smith et al., 2009; Wilson et al., 2009; Marsicano et al., 2014; Bordy et al., 2023). In contrast, the Upper Moyeni site was initially discovered by locals and later formally documented by Abrahams et al. (2020).

Lower Moyeni

The Lower Moyeni track-bearing surface is ripple-marked, desiccated, and preserves patches of MISS expressed as pitted, algal mat surface textures. In addition to the vertebrate tracks, the surface also preserves numerous invertebrate traces (Smith et al., 2009). The majority of the invertebrate traces are found on the slightly lower slopes of the surface, while the pitted algal mat textures are preserved on the flat portion of the surface. About 200 tridactyl, tetradactyl and pentadactyl tracks have been preserved, with a higher track abundance and anatomical fidelity observed on the algal mat surface. The tracks destroy the pitted algal mat texture, indicating that microbial activity pre-dates the registration of the tracks. Overall, the tracks have anatomical fidelity grades ranging between 2 and 3, capturing anatomical

features such as claw marks, digital pad impressions and unique anatomical features such as digit drag marks, resting traces, tail impressions and belly drag marks (see Smith et al., 2009; Wilson et al., 2009; Marsicano et al., 2014; Bordy et al., 2023).

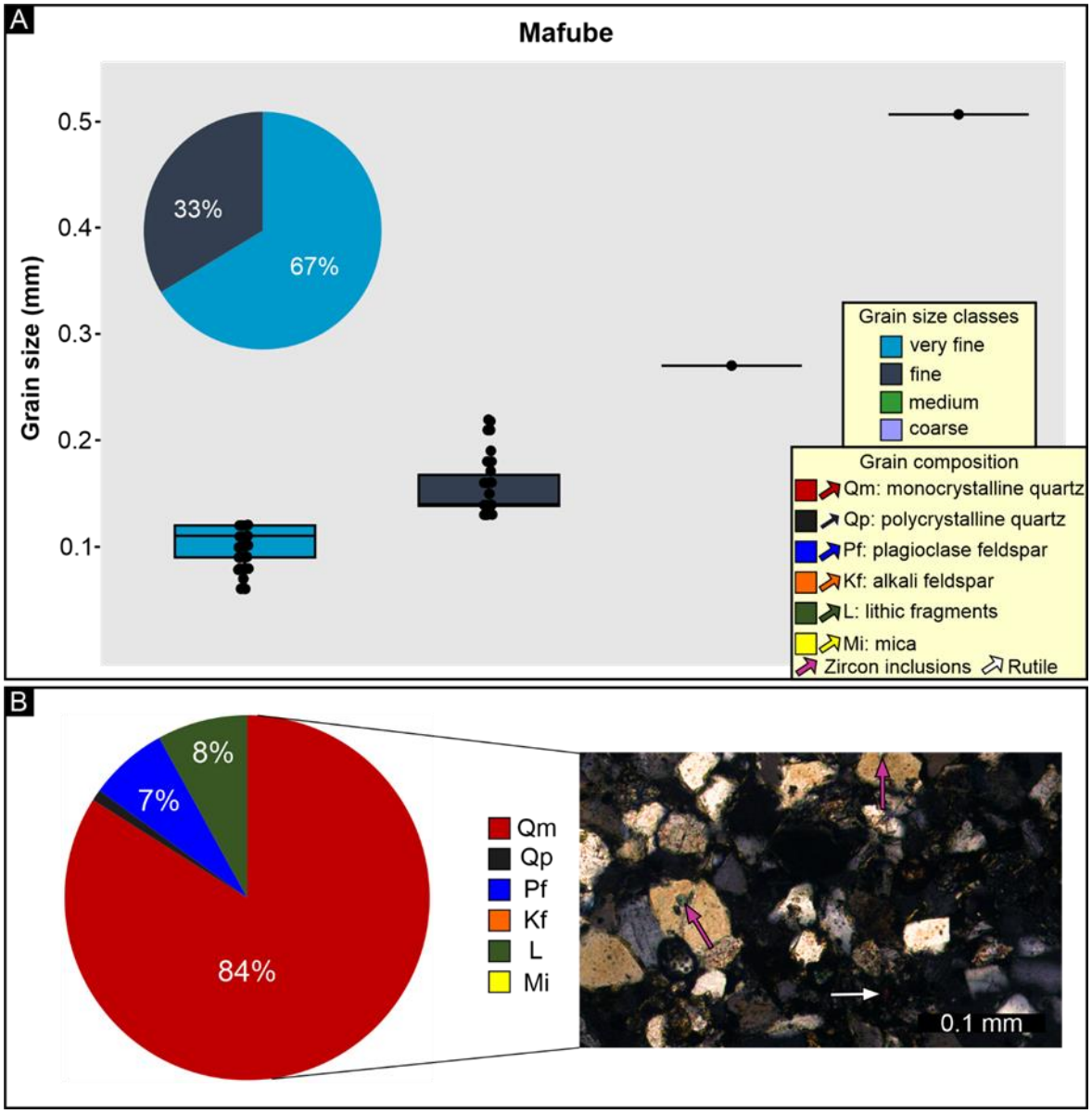

Figure 4.8. Petrographic properties of the Mafube ichnosite sandstone. **A)** Grain size distribution. **B)** Modal composition and photomicrograph of the sandstone under cross-polarized light showing zircon inclusions in quartz grains and a rutile grain.

Petrography

The Lower Moyeni sandstone mainly comprises fine sand (79%), with majority of the grains ranging between 0.14–0.2 mm (Figure 4.9A). The sandstone also has a subordinate very fine sand component (18%) and a minor medium sand component (3%; Figure 4.9A). The sand

grains are moderately to well sorted, subangular to subrounded and have low sphericity, with the fine sands generally being more subangular than the very fine sands, which are more subrounded (Figure 4.9B; Appendix B). The grains are moderately packed and mostly have concavo-convex grain contacts. Based on the modal composition analysis, the sandstone comprises of monocrystalline quartz (71.6%), lithic fragments (19%), plagioclase feldspar (4%), alkali feldspar (2%) and mica (3%; Figure 4.9B). The findings are comparable to the XRD analysis which indicate the presence of quartz (73%), plagioclase feldspar (10%), alkali feldspar (8%) and mica (9%; Appendix C). The quartz grains tend to be larger in size compared to other grain types (~0.16 mm vs 0.12 mm). Minor amounts of mica are present and occur as random small fragments, and accessory minerals in the sandstone include rutile and opaque minerals (Appendix B).

Upper Moyeni

The Upper Moyeni ichnosite is located ~65 m above the Lower Moyeni and was formally documented by Abrahams et al. (2020). The track-bearing palaeosurface is ripple-marked, desiccated, and preserves over 50 tridactyl tracks with anatomical fidelity ranging between 1 and 3. The palaeosurface shows strong evidence for varying substrate conditions, as indicated by the variation in preservation and anatomical details of the tracks (e.g., shallow vs deep impressions, complete vs incomplete tracks; Abrahams et al., 2020). The presence of incomplete and deep track impressions accompanied by expulsion rims and sediment collapse features suggests heavily saturated substrate conditions (e.g., Gatesy et al., 1999).

Petrography: Upper Moyeni

The Upper Moyeni sandstone comprises very fine sand (55%) with majority of the grains ranging between 0.08–0.12 mm (Figure 4.10A). The sandstone also has a significant fine sand component (45%) with grains ranging between 0.13–0.18 mm (Figure 4.10A). The sand grains are moderately to well sorted, subangular to subrounded, with low sphericity, moderate packing and concavo-convex grain contacts (Figure 4.10B; Appendix B). Based on the modal composition analysis, the sandstone comprises monocrystalline quartz (76%), lithic fragments (14%), plagioclase feldspar (7.3%) and mica (2%; Figure 4.10B). The findings are comparable to the XRD analysis findings which indicated the presence of quartz (70%), plagioclase feldspar

(15%), alkali feldspar (8%) and mica (7%; Appendix C). Accessory minerals in the sandstone include rutile, opaque minerals and zircon inclusions in quartz grains (Appendix B).

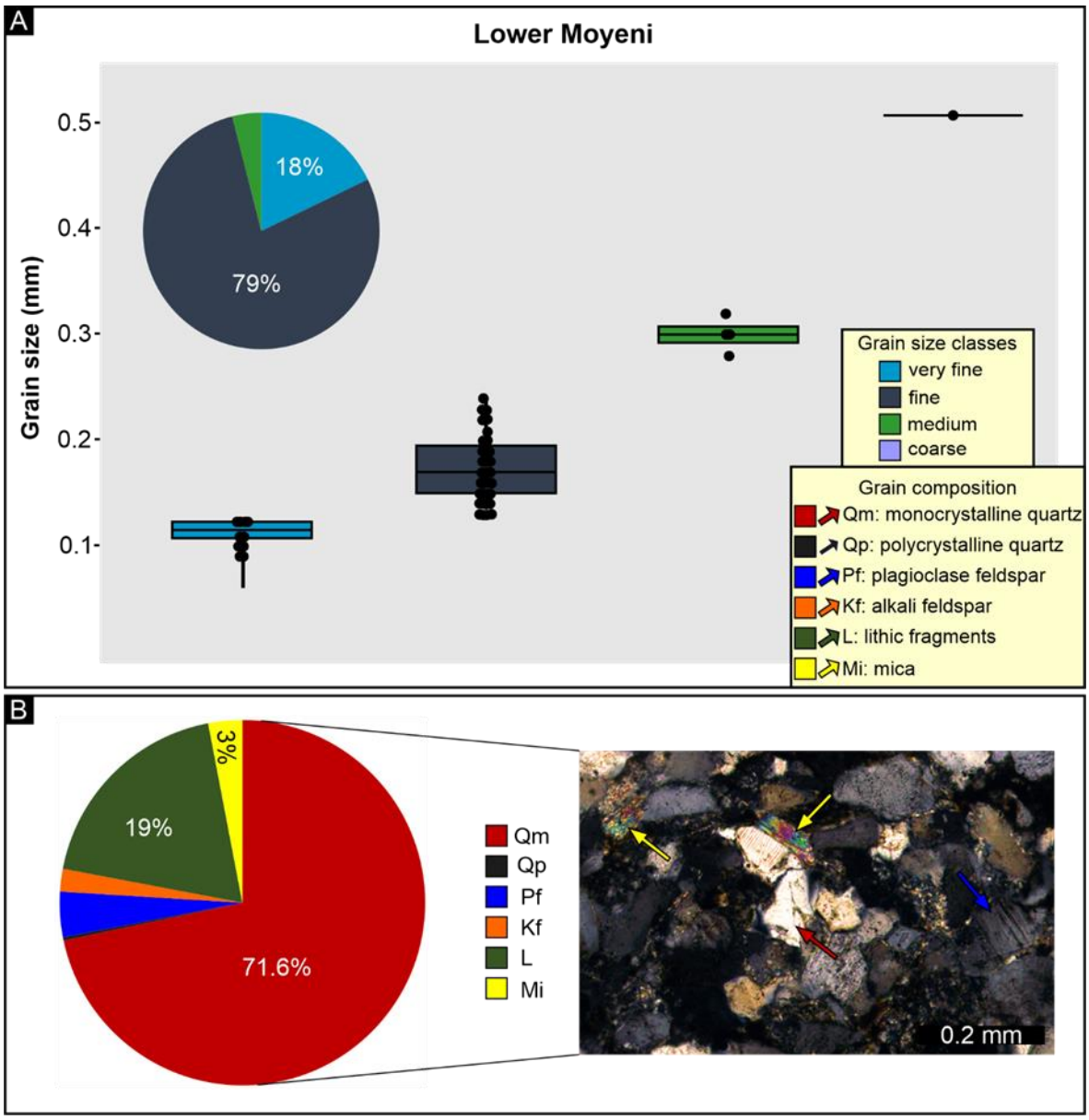

Figure 4.9. Petrographic properties of Lower Moyeni ichnosite sandstone. **A)** Grain size distribution. **B)** Modal composition and photomicrograph of the sandstone under cross-polarized light showing sub-angular to subrounded grains of monocrystalline quartz, plagioclase feldspar and mica.

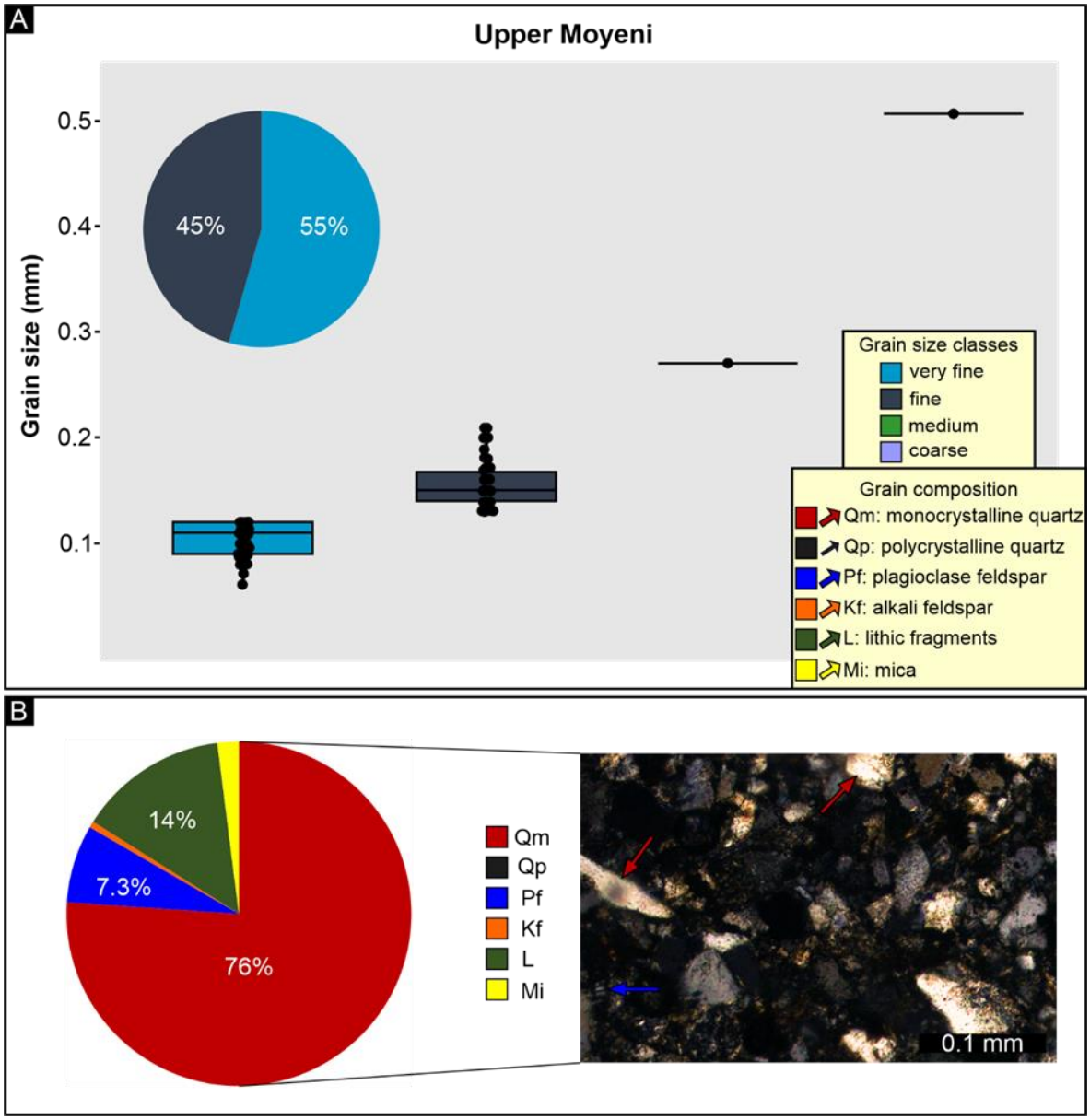

Figure 4.10. Petrographic properties of the Upper Moyeni ichnosite sandstone. **A)** Grain size distribution. **B)** Modal composition and photomicrograph of the sandstone under cross-polarized light showing sub-angular to subrounded grains of monocrystalline quartz and plagioclase feldspar.

4.1.2.3 Roma

There are multiple dinosaur tracksites located in or near the Roma Valley area, which were discovered and initially described by Ambrose (2003). Here, we will focus on three ichnosites that exclusively preserve tridactyl tracks on a single hillside (in alphabetical order: Matobo, Mokhosi and Tlapana). The Mokhosi and Tlapana ichnosites are ~400 m apart on the same stratigraphic bed, while the Matobo ichnosite is situated ~65 m above them (see the Mokhosi site overview).

The host rocks at the Roma ichnosites are part of a large-scale upward-fining succession of clastic sedimentary rocks with a thickness of ~160 m (Sciscio et al., 2017). The clastic host rocks are classified into two major facies associations (coarse- and fine-grained, respectively), based on their shared sedimentology properties of lithology, geometry, grain size characteristics and sedimentary structures (see Sciscio et al., 2017). The coarse-grained facies is characterized by laterally continuous, tabular, multi-storey, massive, very fine- to fine-grained sandstone successions that are either with or without clasts of pedogenic carbonate nodules conglomerates (e.g., Sciscio et al., 2017). The sandstone beds are often horizontal and/or ripple-cross laminated up-surface, with ripple marks towards the track-bearing surface. The fine-grained facies are characterized by sheet-like, massive and laminated, deep red-maroon mudstones, with rootlets, desiccation cracks and in situ carbonate nodules (e.g., Sciscio et al., 2017). They are interbedded with the coarse-grained facies either between single sandstone storey packages (<50 cm thick) or multi-storey sandstone packages (up to 10 m thick; e.g., Sciscio et al., 2017).

Matobo

The Matobo ichnosite was originally described by Ambrose (2003) and later revised by Sciscio et al. (2017). The track-bearing palaeosurface is ripple-marked, desiccated and preserves about 20 tridactyl tracks in varying anatomical fidelity grades between 1 and 2. The depths of the preserved tracks varies significantly, with some tracks being shallow while others are deeply imprinted. The deep impressions could potentially indicate heavily saturated substrate conditions (e.g., Gatesy et al., 1999).

Petrography

The Matobo track-bearing sandstone predominantly comprises very fine sand (76%), with majority of the grains ranging between 0.09–0.12 mm (Figure 4.11A). The sandstone also has a subordinate fine sand component (24%) with an average grain size of ~0.16 (Figure 4.11A). The sand grains are moderately to well sorted, subangular to subrounded, with low sphericity, moderate packing and concavo-convex grain contacts (Figure 4.11B; Appendix B). Based on the modal composition analysis, the sandstone comprises monocrystalline quartz (77%), lithic fragments (12.6%), plagioclase feldspar (7%), alkali feldspar (2.3%) and trace amount of mica (Figure 4.11B). These findings are comparable to the XRD analysis, which indicated the

presence of quartz (72%), plagioclase feldspar (16%), alkali feldspar (8%) and mica (11%; Appendix C). The quartz grains exhibit both high sphericity and low sphericity, unlike the other types of grains present in the sandstone. Accessory minerals present in the sandstone are opaque minerals (Appendix B).

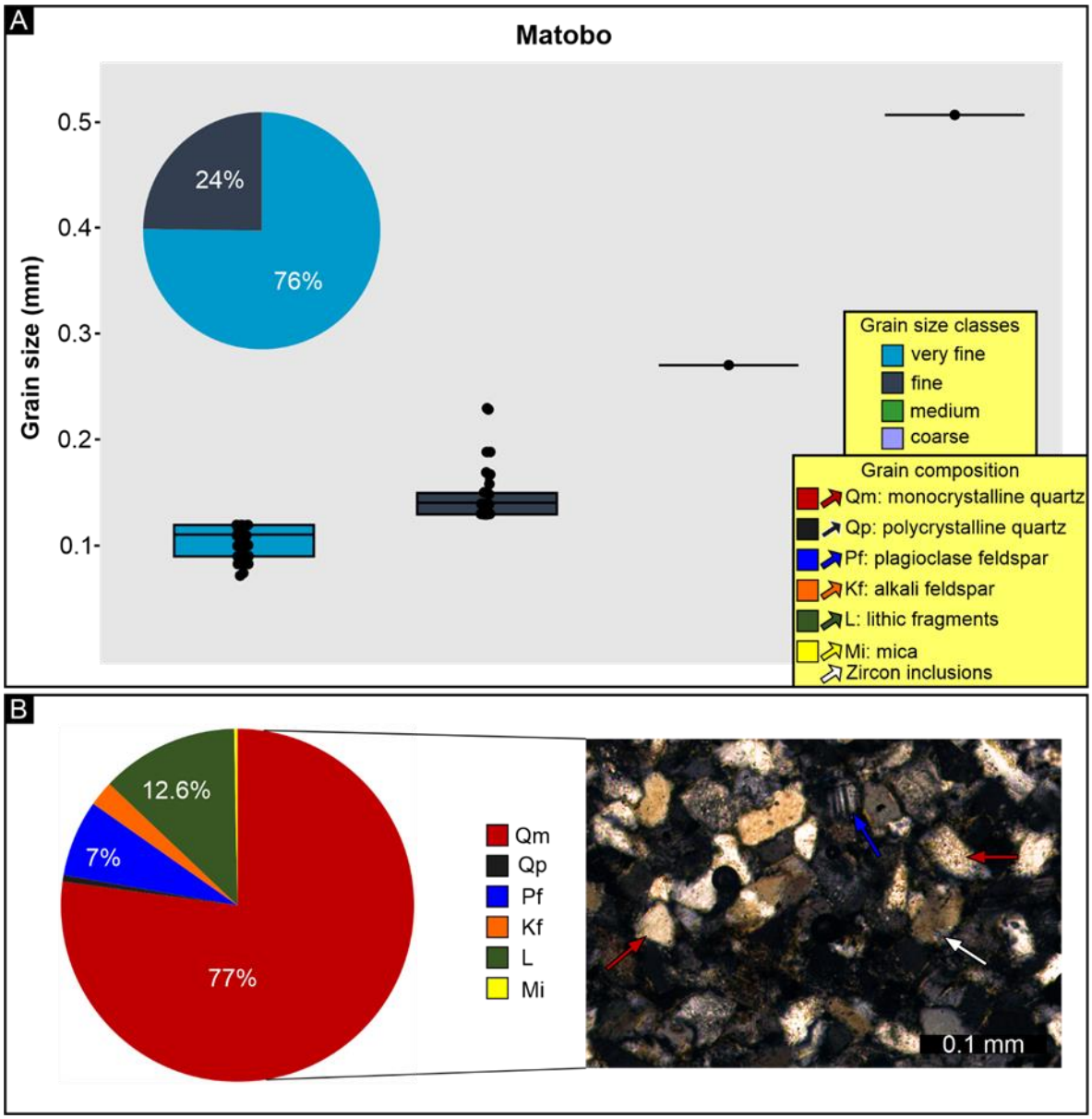

Figure 4.11. Petrographic properties of Matobo ichnosite sandstone. **A)** Grain size distribution. **B)** Modal composition and photomicrograph of the sandstone under cross-polarized light showing subangular to subrounded grains of monocrystalline quartz, plagioclase feldspar and zircon inclusions in quartz.

Mokhosi

The macro- and micro-sedimentary features of the Mokhosi ichnosite, situated ~83 m below the uEF-Clarens stratigraphic contact (Figure 4.12A), were obtained during this MSc study and have been recently published (see Abrahams et al., 2023). The host rocks form laterally continuous, tabular, multi-storey packages of medium sandstone beds that range in thickness between 25–40 cm (Figures 4.12B, 4.12C; Abrahams et al., 2023). These medium sandstone beds are massive at the base and grade to horizontal laminations in the uppermost beds (0.3–0.8 cm thick; Figure 4.12C). The track-bearing palaeosurface is ~30 m long and preserves large-scale ripple marks and desiccation cracks (Figure 4.12D). Over 30 tridactyl tracks, with anatomical fidelity ranging between 1–2, are preserved at the ichnosite. Tracks with higher anatomical fidelity preserve features such as claw marks and digital pad impressions (Abrahams et al., 2023).

Petrography

The Mokhosi sandstone mainly comprises very fine sand (67%) with majority of the grains ranging between 0.09–0.12 mm (Figure 4.13A). The sandstone also has a significant fine sand component (33%) with grains averaging ~0.14 mm (Figure 4.13A). The sand grains are moderately to well sorted, subangular to subrounded, with low sphericity, moderate packing and concavo-convex grain contacts (Figure 4.13B; Appendix B). Based on the modal composition analysis, the sandstone comprises monocrystalline quartz (83.6%), lithic fragments (10.6%), plagioclase feldspar (5%) and a trace amount of alkali feldspar and mica (Figure 4.13B). The XRD analysis findings indicate the presence of quartz (66%), plagioclase feldspar (21%) and alkali feldspar (13%; Appendix C). Unlike the feldspar grains, the quartz grains have both high sphericity and low sphericity, and accessory minerals present in the sandstone are opaque minerals (Appendix B).

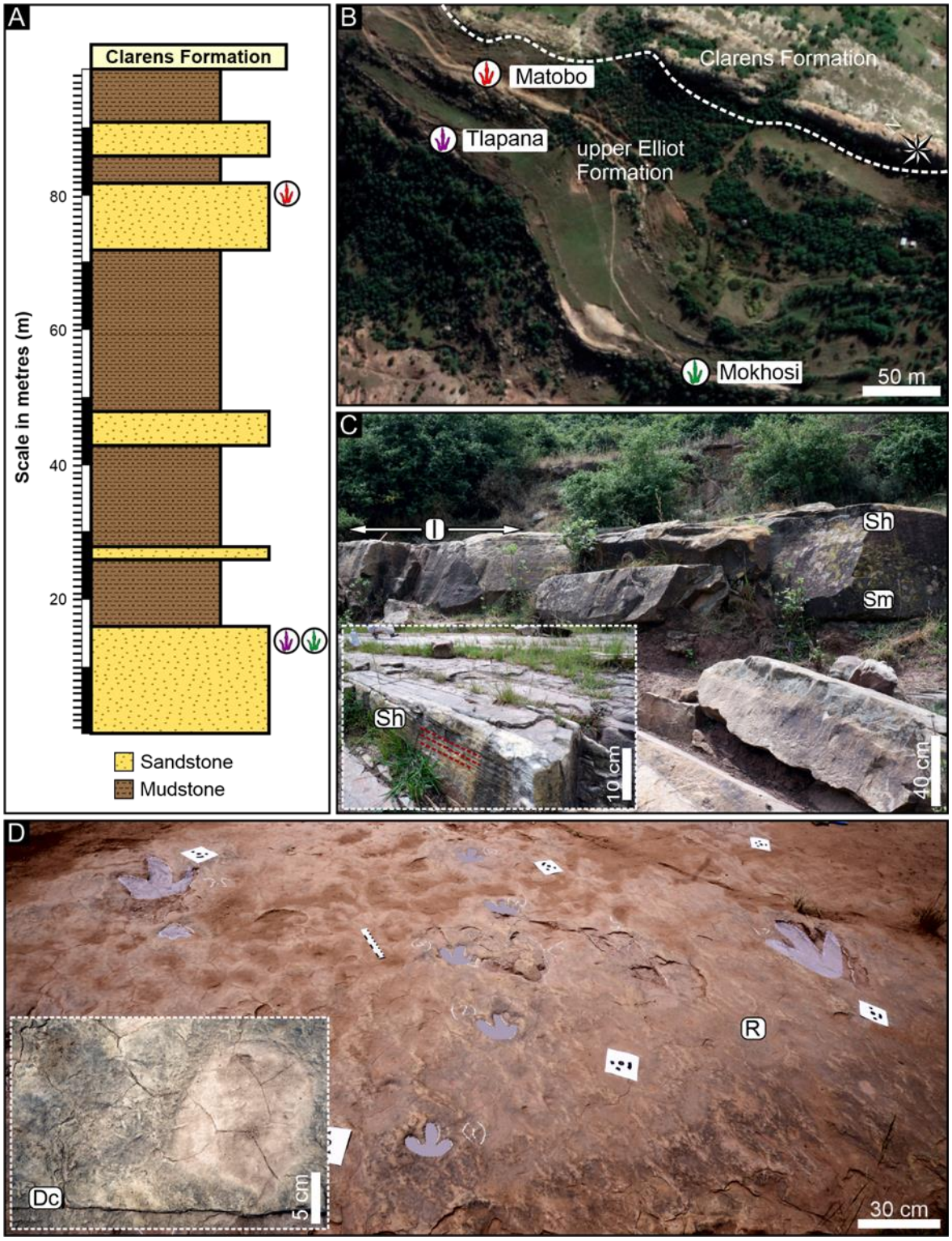

Figure 4.12. Sedimentological context of the Mokhosi ichnosite in the Roma Valley. **A)** Generalised sedimentary log highlighting the relative stratigraphic positions of the Roma ichnosites. **B)** Google Earth image marking the locations of the Roma ichnosites. **C)** Track-bearing host rocks forming laterally continuous, tabular, multistorey, medium sandstone beds. An inset of the sandstone beds grading from massive sandstone (Sm) to horizontal laminations (Sh) in the uppermost beds. **D)** Palaeosurface preserving tridactyl tracks, large scale interference ripple marks and desiccation cracks. (Abbreviations:- Dc: desiccation cracks, I: ichnosite, Sh: horizontal lamination, Sm: massive sandstone, R: interference ripple marks).

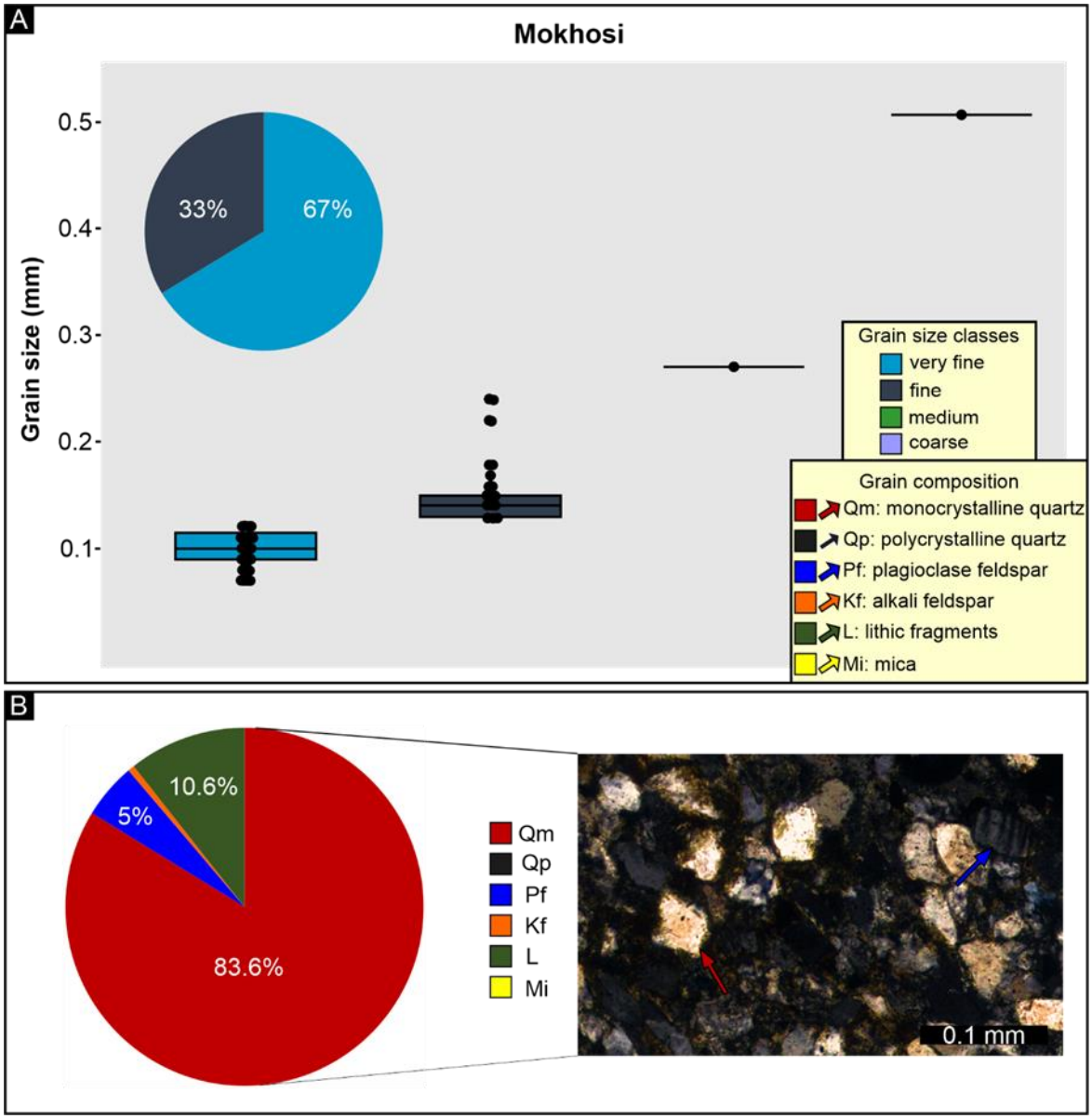

Figure 4.13. Petrographic properties of Mokhosi ichnosite sandstone. **A)** Grain size distribution. **B)** Modal composition and photomicrograph of the sandstone under cross-polarized light showing sub-angular to subrounded grains of monocrystalline quartz and plagioclase feldspar.

Tlapana

The Tlapana palaeosurface consists of discontinuous slabs of sandstone and is located on the same stratigraphic level as Mokhosi, ~400 m apart, with no tracks identified between the two ichnosites thus far. At Tlapana, the surface preserves ripple marks, desiccation cracks, wavy laminations, localised soft sediment deformation structures and invertebrate traces (Abrahams, 2020). The tracks preserved occur sporadically across multiple slabs, predominantly as isolated tracks with anatomical fidelity grades between 0 and 3. Two

samples were collected from the ichnosite about 8 m apart from each other (Tlapana A and Tlapana B, respectively).

Petrography: Tlapana A

The Tlapana A sandstone comprises very fine sand (55%) with majority of the grains ranging between 0.1–0.12 mm (Figure 4.14A). The sandstone also has a significant fine sand component (45%) with grains averaging ~0.15 mm (Figure 4.14A). The sand grains are moderately to well sorted, subangular to subrounded, with low sphericity, moderate packing and concavo-convex grain contacts (Figure 4.14B; Appendix B). Based on the modal composition analysis, the sandstone consists of monocrystalline quartz (76.6%), lithic fragments (12%), plagioclase feldspar (10%) and trace amount of mica (Figure 4.14B). These findings are comparable with the XRD analysis, which indicated the presence of quartz (66%), plagioclase feldspar (25%) and alkali feldspar (9%; Appendix C). The quartz grains have both high sphericity and low sphericity, unlike the other types of grains present in the sandstone. Accessory minerals present in the sandstone are opaque minerals (Appendix B).

Petrography: Tlapana B

The Tlapana B sandstone mainly comprises very fine sand (63%) with majority of the grains ranging between 0.08–0.12 mm (Figure 4.15A). The sandstone also has a significant fine sand component (37%) with grains averaging about ~0.15 mm (Figure 4.15A). The sand grains are moderately to well sorted, subangular to subrounded, with low sphericity, moderate packing and concavo-convex grain contacts (Figure 4.15B; Appendix B). Based on the modal composition analysis, the sandstone comprises monocrystalline quartz (76.6%), lithic fragments (16.3%), plagioclase feldspar (6.3%) and trace amounts of mica (Figure 4.15B). In comparison, the XRD analysis findings indicate the presence of quartz (62%), plagioclase feldspar (22%), alkali feldspar (9%) and mica (7%; Appendix C) The quartz grains have both high sphericity and low sphericity, unlike the other types of grains present. Accessory minerals present in the sandstone are opaque minerals (Appendix B).

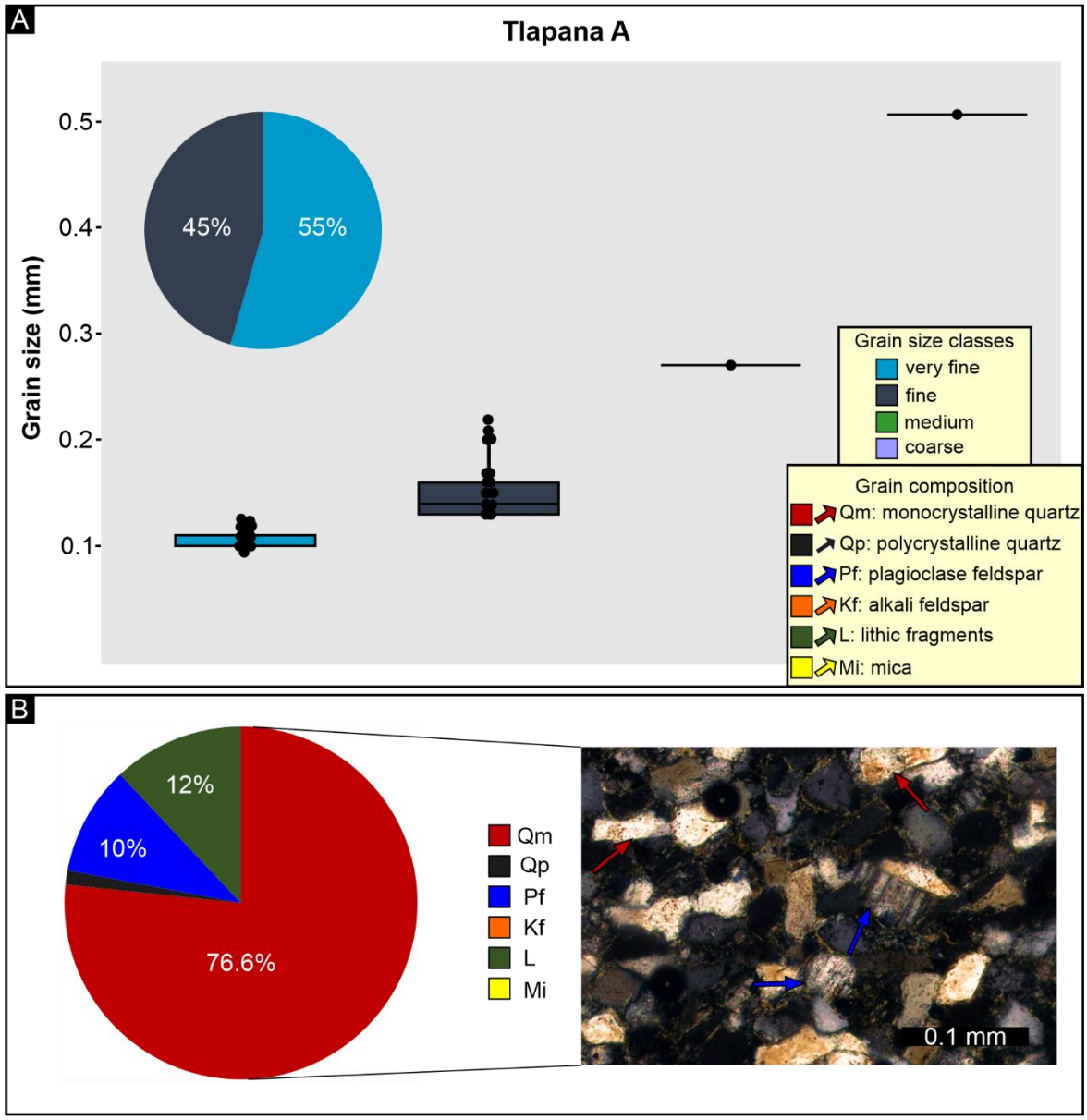

Figure 4.14. Petrographic properties of Tlapana A sandstone. **A)** Grain size distribution. **B)** Modal composition and photomicrograph of the sandstone under cross-polarized light showing sub-angular to subrounded grains of monocrystalline quartz and plagioclase feldspar.

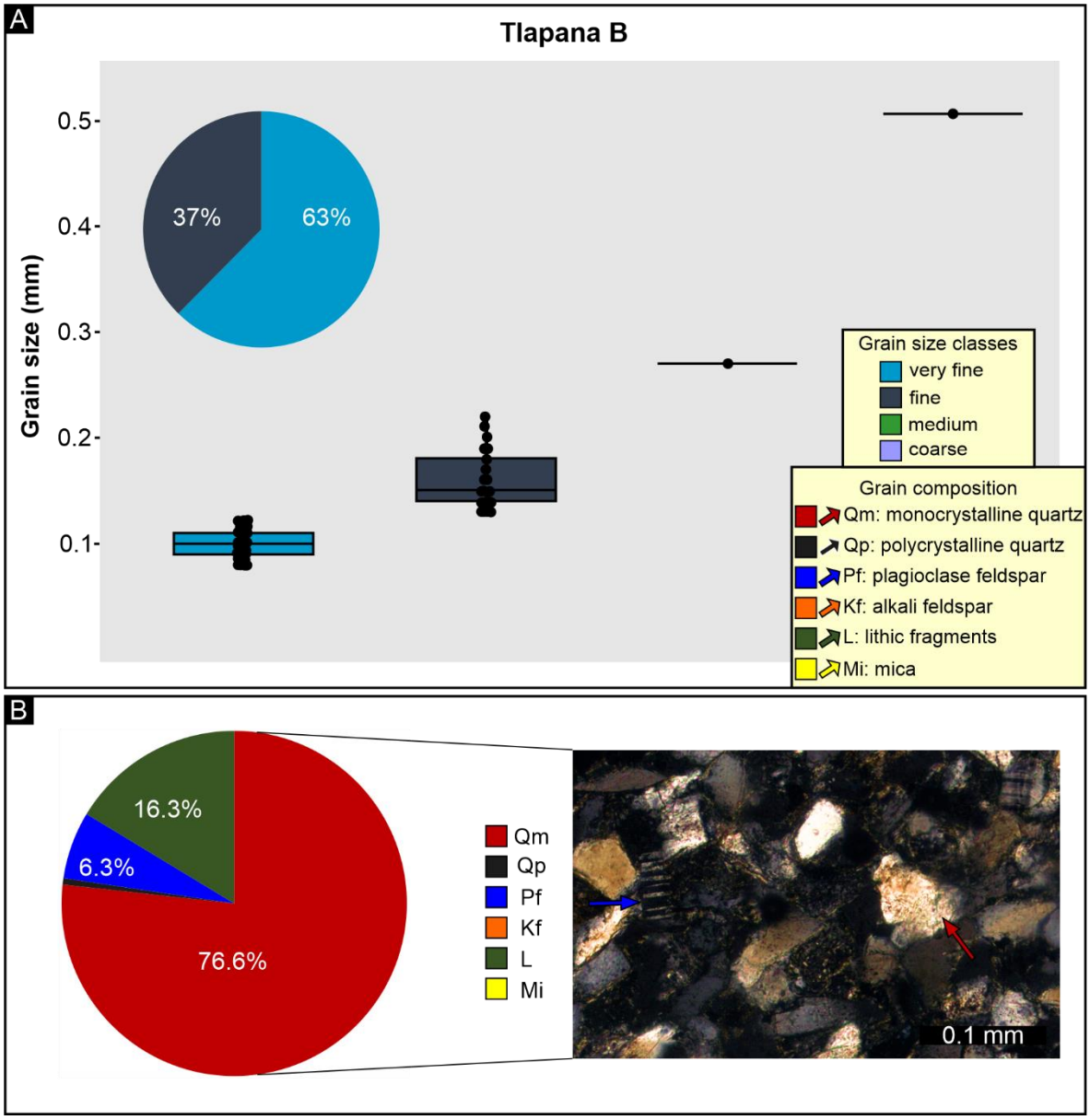

Figure 4.15. Petrographic properties of Tlapana B sandstone. **A)** Grain size distribution. **B)** Modal composition and photomicrograph of the sandstone under cross-polarized light showing sub-angular to sub-rounded grains of monocrystalline quartz and plagioclase feldspar.

Synthesis of the Tlapana track-bearing sandstone

The two track-bearing sandstones at Tlapana have very similar petrographic properties. Both sandstones predominantly comprise very fine sand, with Tlapana B having a slightly higher proportion of very fine sand than Tlapana A (63% vs 55%, respectively). Unlike Tlapana B, Tlapana A has a smaller grain size distribution (0.08–0.12 mm vs 0.1–0.12 mm). The sandstones have similarities in terms of sorting, roundness, sphericity, packing and grain contacts. Overall, the composition of the sandstones is comparable.

4.1.2.4 Synthesis of the uEF ichnosites

The track-bearing sandstones from the uEF ichnosites are mainly characterized by very fine and fine sands, accounting ~57% of the grains (Figure 4.8–4.15). The sand grains range from 0.08–0.2 mm, with very fine sand class being the most prevalent (0.08–0.12 mm). However, the Lower Moyeni ichnosite stands out within the uEF as it mainly comprises fine sands (0.14–0.12 mm). The sandstones generally exhibit moderate to well sorting, with low sphericity, subangular-subrounded grains, and similar packing and grain contacts. The Roma sites, unlike the other uEF ichnosites, contain some high sphericity grains. There are no significant differences in the sandstone composition among the ichnosites.

Within the uEF ichnosites, there is generally high track abundance and anatomical fidelity. The preserved tracks have constrained anatomical fidelity, for example, Mokhosi and Matobo with grades 1–2, and Mafube with grades 1–3. Despite having relative coarser sands, the Lower Moyeni preserves tracks with the highest anatomical fidelity grades and abundance with ~250 tracks graded 2–3. The subordinate component of high sphericity grains observed in the Roma ichnosites does not appear to affect track anatomical fidelity or track abundance.

A strong correlation is observed between MISS, anatomical fidelity, and track abundance. Sites that preserve MISS tend to have higher track anatomical fidelity grades and/or greater track abundances. At Mafube, MISS is associated with higher track abundance but lower anatomical fidelity compared to other areas of the site (i.e., >80 tracks with grades 1–3, see Sciscio et al., 2016 for details). However, at Lower Moyeni, MISS is linked to higher track abundances and a high-level anatomical fidelity, with ~200 tracks with grades 2–3. Notably, there is a difference in the timing of microbial activity between the two sites: it occurred before track registration at Lower Moyeni, while at Mafube, it occurred after track registration. Given MISS binds sediments, its presence at Lower Moyeni may have contributed to the high track abundances and anatomical fidelity (e.g., Carvalho et al., 2013). Additionally, since MISS can cover and protect tracks, it might have played a role in preserving the high track abundance with lower anatomical fidelity at Mafube (Sciscio et al., 2016).

4.1.3 Clarens Formation ichnosites

4.1.3.1 Matsieng

The Matsieng ichnosite was first described by Ellenberger (1970, 1972) and later reported on by Ambrose (2016) and Rampersadh and Bordy (2019). The ichnosite preserves over 40 tridactyl tracks on at least three fallen sandstone blocks, as well as *in-situ* natural casts beneath a low overhang (Rampersadh and Bordy, 2019). The anatomical fidelity of the tracks varies from 1–3, with the majority of tracks ranging between 2 and 3. The fallen sandstone blocks are ripple-marked, desiccated and preserve some pervasive MISS expressed as diverse wavy wrinkle structures. The timing of the microbial activity in relation to the registration of tracks is unclear since the preserved MISS and tracks are not in contact. In addition to the vertebrate tracks, the palaeosurface preserves numerous invertebrate traces. Two sandstone samples were collected: one from a fallen sandstone block and the other about 5 m from where the block had fallen (Matsieng A and Matsieng B, respectively).

Petrography: Matsieng A

The Matsieng A sandstone predominantly comprises very fine sand (75%) with the majority of the grains ranging between 0.08–0.12 mm (Figure 4.16A). The sandstone also has a subordinate fine sand component (25%) with grains averaging ~0.13 mm (Figure 4.16A). The sand grains are mostly subrounded and well sorted, with low sphericity, moderate to close packing and concavo-convex grain contacts (Figure 4.16B; Appendix B). Based on the modal composition analysis, the sandstone comprises monocrystalline quartz (89.3%), polycrystalline quartz (2%), plagioclase feldspar (7%) and mica (1%; Figure 4.16B). The XRD analysis findings indicate the presence of quartz (55%), plagioclase feldspar (13%), alkali feldspar (6%), mica (7%), kaolinite (8%), smectite (7%) and calcite (4%; Appendix C). Some sections of the sand grains are bound together by calcite cement (Figure 4.16B). Accessory minerals in the sandstone include opaque minerals and zircon inclusions in quartz grains (Appendix B).

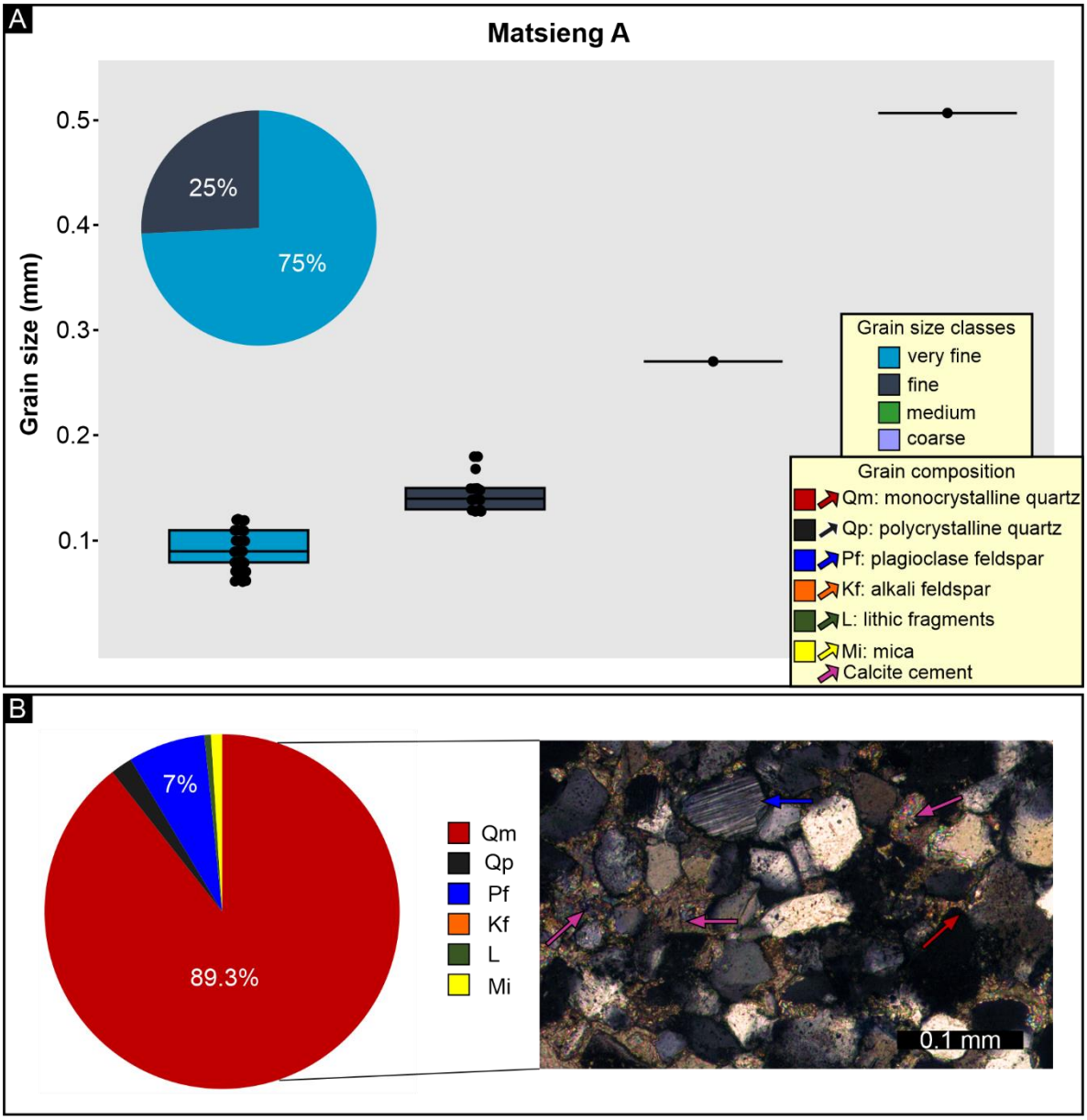

Figure 4.16. Petrographic properties of Matsieng A sandstone. **A)** Grain size distribution. **B)** Modal composition and photomicrograph of the sandstone under cross-polarized light showing calcite cement bounding subrounded grains of monocrystalline quartz and plagioclase feldspar.

Petrography: Matsieng B

The Matsieng B sandstone mainly comprises very fine sand (71%), with the majority of the grains ranging between 0.08–0.12 mm (Figure 4.17A). The sandstone also has a subordinate fine sand component (29%) with grains averaging ~0.14 mm (Figure 4.17A). The sand grains are mostly subrounded, well sorted, with low sphericity, moderate to close packing and concavo-convex grain contacts (Figure 4.17B; Appendix B). Based on the modal composition analysis, the sandstone comprises monocrystalline quartz (85%), polycrystalline quartz (1.6%), plagioclase feldspar (11.6%), lithic fragments (1.3%) and trace amount of mica (Figure

4.17B). The XRD analysis results indicate the presence of quartz (54%), plagioclase feldspar (24%), mica (10%), kaolinite (8%) and calcite (4%; Appendix C). Some sections of the sand grains are bound together by calcite cement in some parts, and accessory minerals in the sandstone include opaque minerals and zircon inclusions in quartz grains (Figure 4.17B; Appendix B).

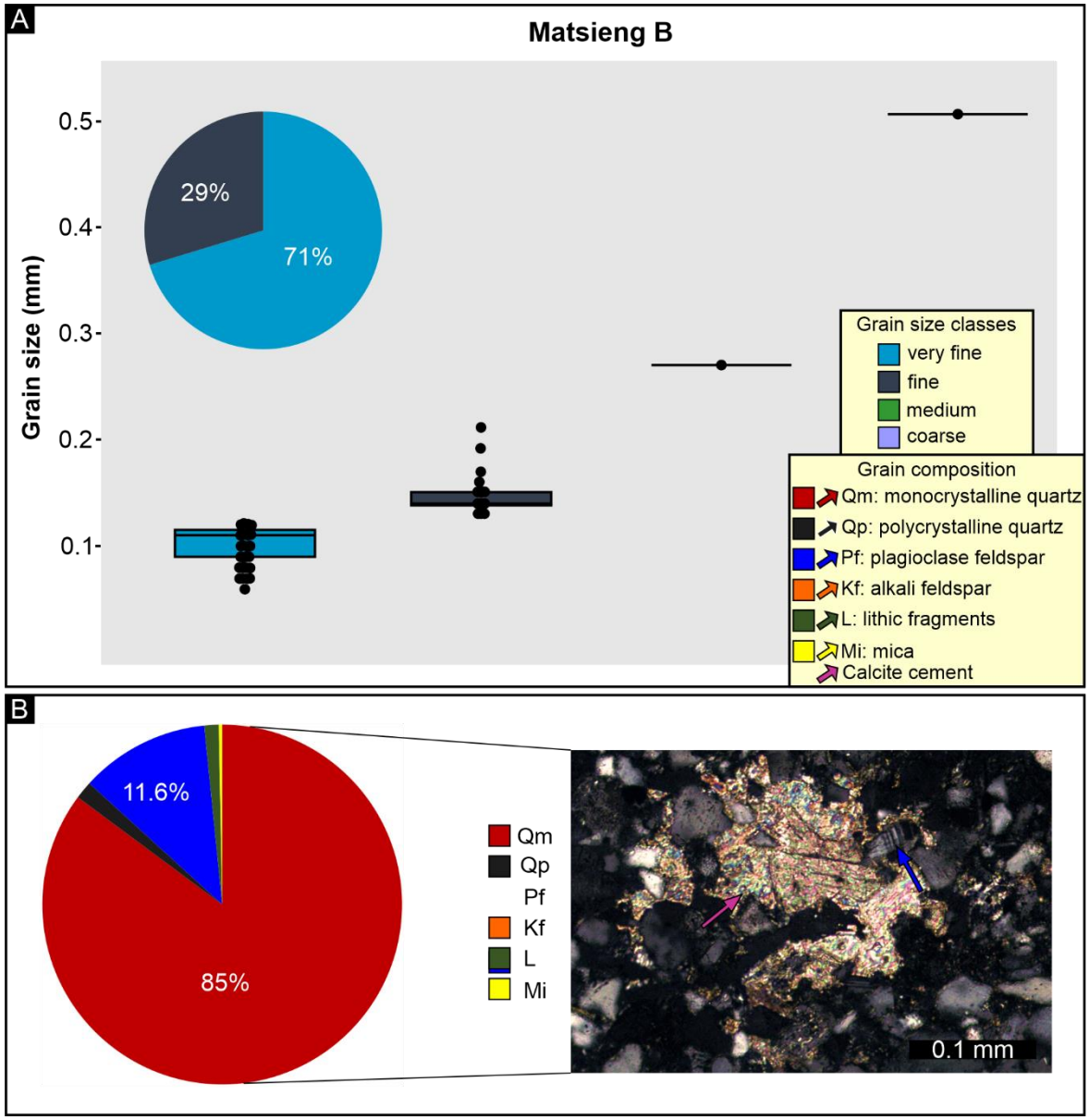

Figure 4.17. Petrographic properties of Matsieng B sandstone. **A)** Grain size distribution. **B)** Modal composition and photomicrograph of the sample under cross-polarized light showing calcite cement bounding the very fine sand grains.

Synthesis of the Matsieng track-bearing sandstones

The two track-bearing sandstones at Matsieng have very similar petrographic properties. Both sandstones primarily comprise very fine sand, with Matsieng A having a slightly higher proportion of very fine sand than Matsieng B (75% vs 71%, respectively). Both sandstones have a similar dominant grain size distribution (0.08–0.12 mm) and are mostly subrounded and well sorted, with low sphericity and similar grain packing and contacts. The two sandstones have calcite cement, and their composition is generally indistinguishable. The presence of calcite cement may potentially be linked to the calcification of microbes during their decomposition, which can induce early track lithification by cementing the substrate (e.g., Schieber, 2007; Carvalho et al., 2013). This could explain the high track abundance observed within a relatively small area of the ichnosite, with over 40 tracks preserved on three sandstone blocks.

4.1.3.2 Morija

The Morija ichnosite was first documented by Dornan (1908), and later described by Ellenberger (1970, 1972); Ambrose (2016); Rampersadh and Bordy (2019). The ichnosite preserves tridactyl tracks as natural casts on a ceiling overhang, as well as hyporeliefs on a large fallen sandstone block. The ceiling overhang and fallen sandstone block are both ripple-marked and desiccated, but unlike the fallen block, the ceiling overhang preserves MISS expressed as wavy wrinkle structures. At Morija the tracks have anatomical fidelity from 1–3, with most tracks ranging between 2 and 3.

Petrography

The fallen block Morija sandstone predominantly comprises very fine sand (68%) with the majority of the grains ranging between 0.08–0.12 mm (Figure 4.18A). The sandstone also has a significant fine sand component (32%) with grains averaging ~0.13 mm (Figure 4.18A). The grains are mostly subrounded, well sorted, with low sphericity, moderate to close packing and concavo-convex grain contacts (Figure 4.18B; Appendix B). Based on the modal composition analysis, the sandstone comprises monocrystalline quartz (90%), polycrystalline quartz (2%), plagioclase feldspar (6.6%) and trace amount of mica (Figure 4.18B). The XRD analysis findings indicate the presence of quartz (50%), plagioclase feldspar (23%), alkali feldspar (8%), mica

(8%), kaolinite (5%) and smectite (6%; Appendix C). Accessory minerals in the sandstone include zircon inclusions in quartz grains and opaque minerals (Appendix B).

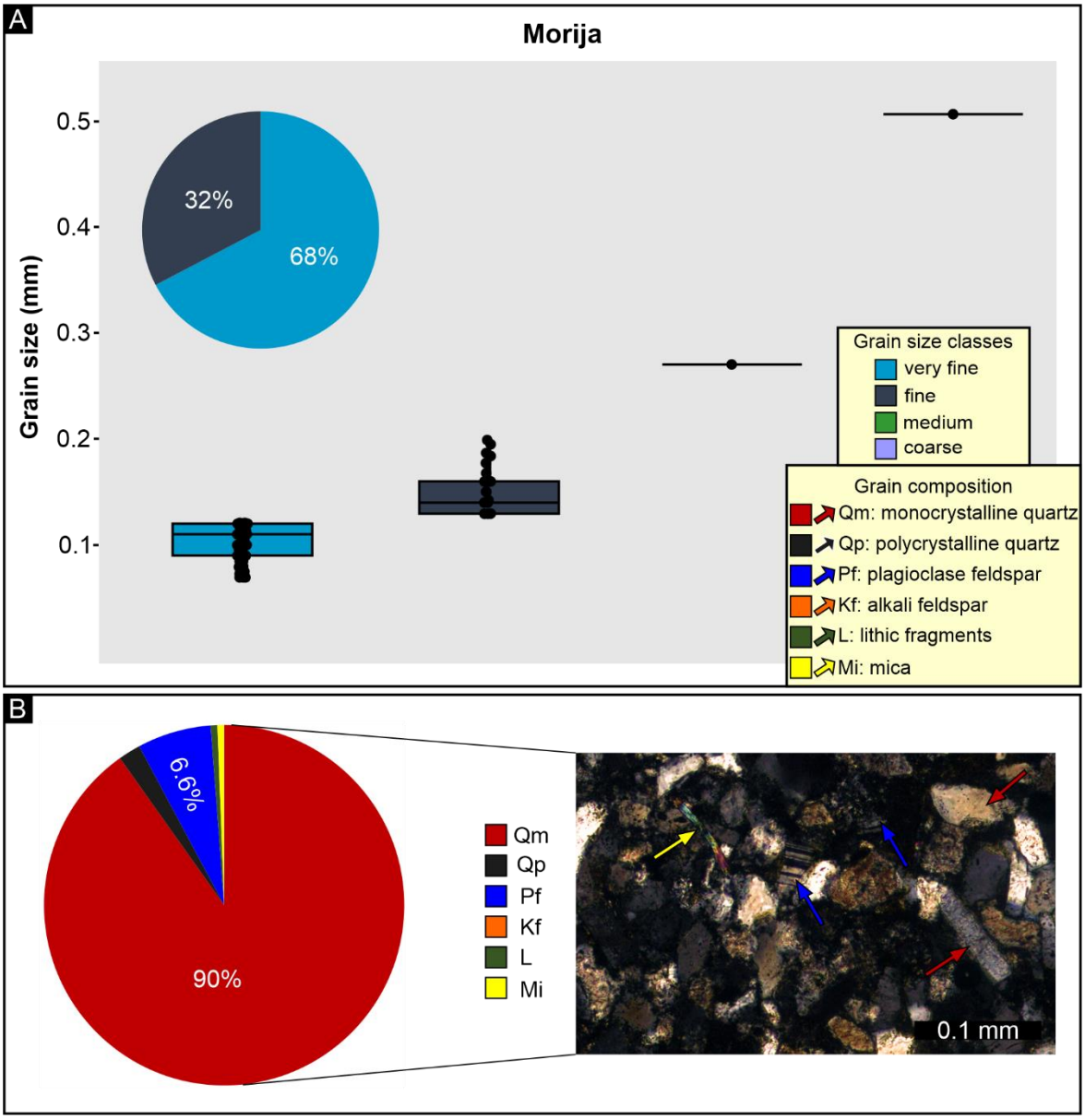

Figure 4.18. Petrographic properties of Morija ichnosite sandstone. **A)** Grain size distribution. **B)** Modal composition and photomicrograph of the sandstone under cross-polarized light showing subrounded grains of monocrystalline quartz, plagioclase feldspar and mica.

4.1.3.3 Qalo

The Qalo ichnosite was first recorded by Dornan (1908) and was subsequently described by Ellenberger (1970, 1972), Ambrose (2016), and Rampersadh and Bordy (2019). The ichnosite preserves over 70 tridactyl tracks as natural casts beneath a cave ceiling overhang (Rampersadh and Bordy, 2019). The cave ceiling is ripple-marked, desiccated and preserves

diverse MISS expressed as long, wavy and bun-shaped microbial structures with positive relief. MISS covers the ceiling, including the tracks, indicating that microbial activity occurred after the tracks were registered. The anatomical fidelity of tracks varies from 1–3, with majority of tracks ranging between 2 and 3. These tracks preserve anatomical features such as claw marks, digital pad impressions, and even, remarkably, skin impressions.

Petrography

The Qalo sandstone predominantly comprises very fine sand (79%) with majority of the grains ranging from 0.09–0.11 mm and a dominant grain size of ~0.1 mm (Figure 4.19A). The sandstone also has a subordinate fine sand component (21%) with grains averaging ~0.13 mm (Figure 4.19A). The grains are mostly subrounded and well sorted, with low sphericity, moderate to close packing and concavo-convex grain contacts (Figure 4.19B; Appendix B). Based on the modal composition analysis, the sandstone comprises monocrystalline quartz (89%), plagioclase feldspar (7%), lithic fragments (3.3%) and trace amount of mica (Figure 4.19B). The XRD analysis results indicate the presence of quartz (72%), plagioclase feldspar (15%), alkali feldspar (8%), mica (5%; Appendix C). Accessory minerals in the sandstone include opaque minerals and zircon inclusions in quartz grains (Appendix B).

4.1.3.4 Synthesis of the CLAR ichnosites

The track-bearing sandstones from the CLAR ichnosites are predominantly composed of very fine sands, accounting for ~73% of the grains (Figure 4.16–4.19). The majority of the sand grains fall within the range between 0.08–0.15 mm, with the most prevalent sand class being very fine sand class (0.08–0.12 mm). These sand grains are mostly subrounded, well sorted, with low sphericity, moderate to close packing and concavo-convex grain contacts. While the composition of CLAR sandstones is generally similar, the Matsieng sandstones differ from the Qalo and Morija sandstones in that they contain calcite cement.

There is a strong association between the grain size, MISS, track anatomical fidelity, and track abundance at the CLAR sites. MISS is preserved in all the very fine-grained CLAR track-bearing sandstones, and the majority of tracks have high grades of anatomical fidelity, with exceptional anatomical details. For example, the Qalo tracks with grades 2–3 and preserving skin traces. Additionally, the track abundance is relatively high across all CLAR ichnosites (e.g.,

Qalo with >70 tracks). The presence of calcite cement in Matsieng sandstones (Figures 4.16, 4.17) suggests a potential association with microbial calcification within the substrates. The timing of the microbial activity at Qalo is be inferred to have occurred after track registration, while the timing at Matsieng and Morija remains unclear.

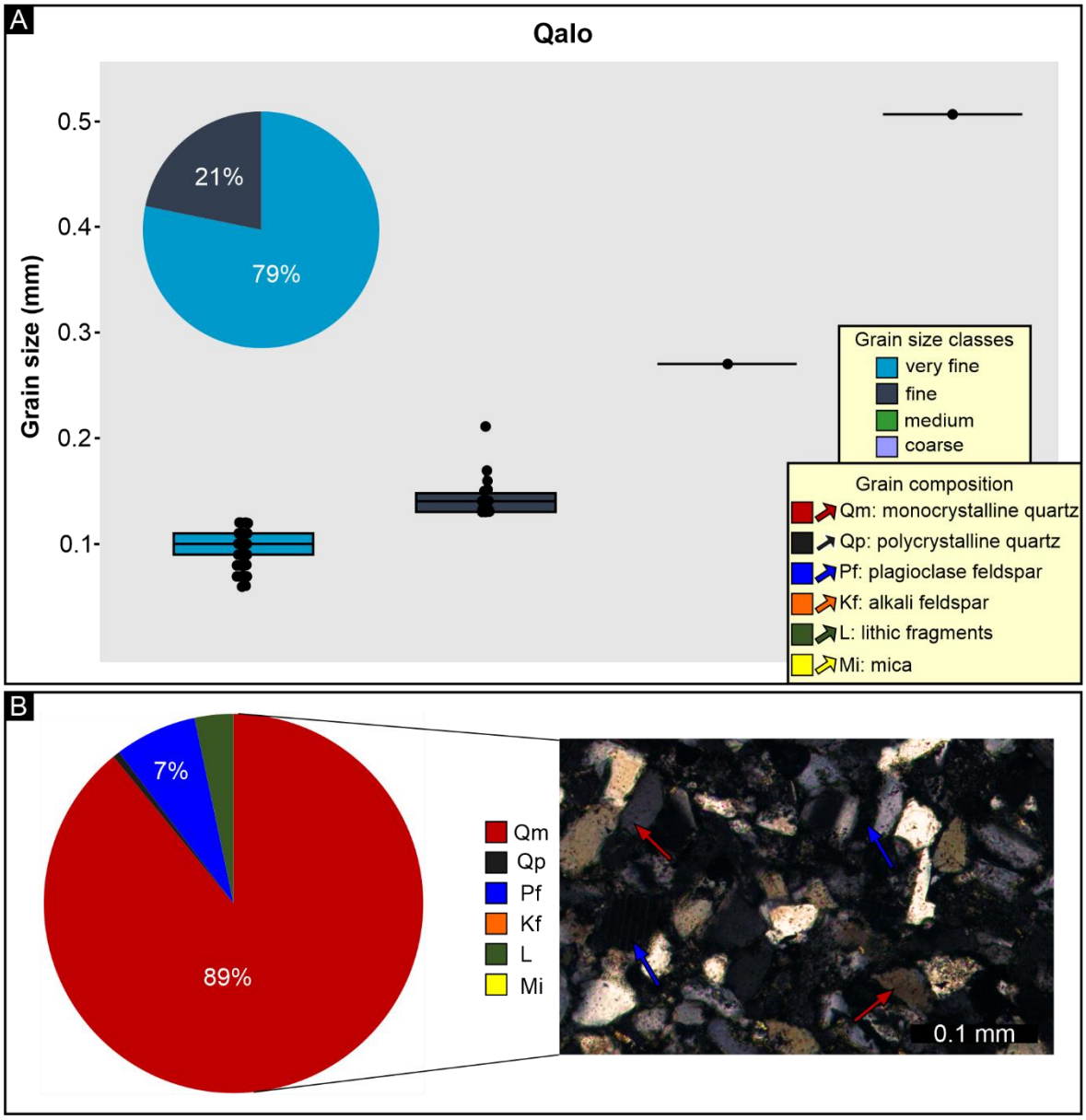

Figure 4.19. Petrographic properties of Qalo ichnosite sandstone. **A)** Grain size distribution. **B)** Modal composition and photomicrograph of the sandstone under cross-polarized light showing subrounded grains of monocrystalline quartz and plagioclase feldspar.

4.2 Petrographic analysis synthesis

The semi-quantitative assessment of track-bearing sandstones in the upper Stormberg Group shows notable changes and associations between grain size, MISS, track abundance and anatomical fidelity up-stratigraphy (Figure 4.20). The track-bearing sandstones in the lEF ichnosites contain a wide range of sand grains from very fine to coarse, with the majority of grains falling within the medium to fine sand class (~74%; Figure 4.20). In contrast, the uEF and CLAR track-bearing sandstones consist exclusively of fine and very fine sand, with the CLAR having a higher proportion of very fine sand compared to the uEF (73% vs 57%; Figure 4.20). The very fine sands in the uEF and CLAR track-bearing sandstones preserve tracks with relatively higher anatomical fidelity compared to the coarser sands of the lEF (grades 1–3, 2–3 vs grades 0–3, respectively; Figure 4.20). Moreover, the very fine sands also preserve higher track abundances than the coarser sands (e.g., on average, >60 tracks in the CLAR vs >30 tracks in the lEF). However, the Lower Moyeni ichnosite stands out as it primarily consists of fine sands but preserves tracks with high abundance and anatomical fidelity (~200 tracks with grades 2–3).

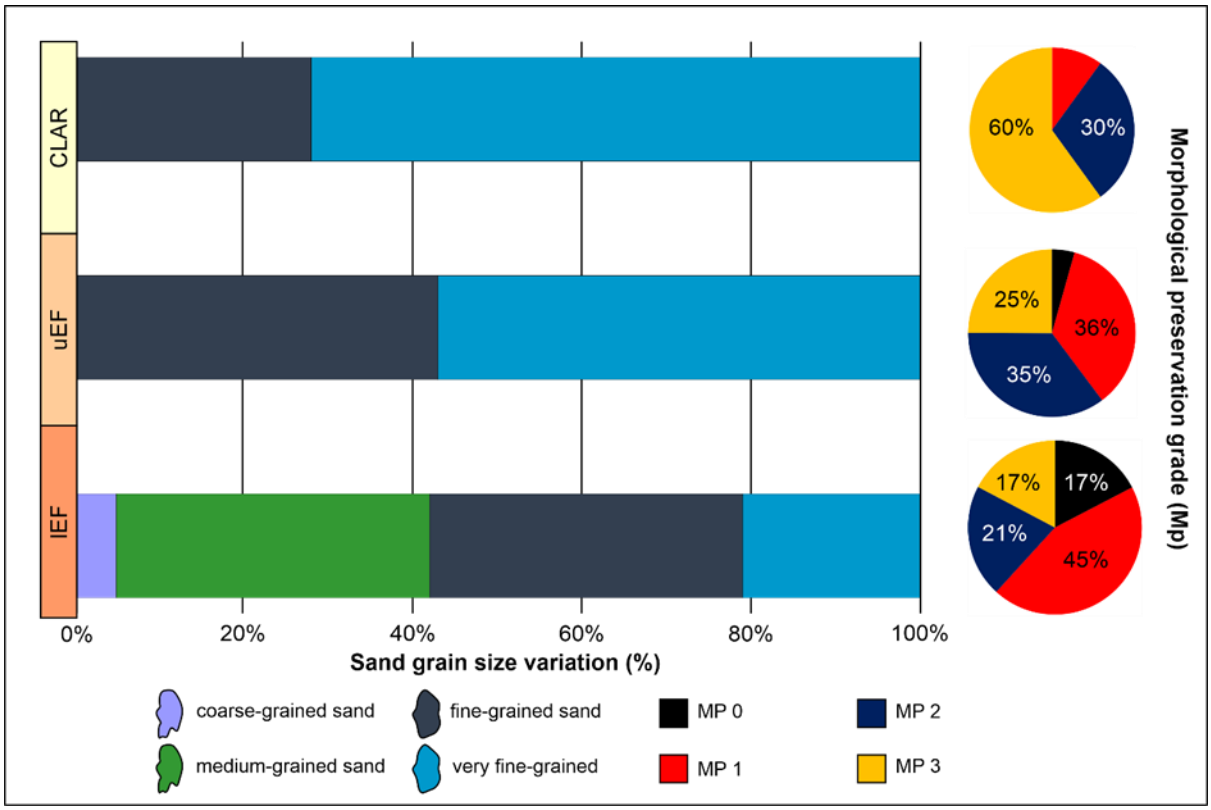

Figure 4.20. Up-stratigraphic variation of the dominant grain size and the average morphological preservation grade (Mp) of the preserved tracks in the upper Stormberg Group (*sensu* anatomical fidelity; Gatesy and Falkingham, 2017).

Ichnosites that preserve MISS, such as Mafube, Lower Moyeni, Qalo, Matsieng, Morija, preserve tracks with consistently higher anatomical fidelity and/or track abundance. In Mafube, MISS is associated with a higher track abundance, but lower anatomical fidelity compared to other areas of the site (i.e., >80 tracks with grades 1–3). Lower Moyeni preserves tracks with high abundances and high anatomical fidelity (i.e., ~200 tracks with grades 2–3). At Qalo, the majority of tracks have high grades of anatomical fidelity (2–3) and exceptional preservation of anatomical details, such as skin traces. The timing of microbial activity plays a significant role in track anatomical fidelity. At Qalo and Lower Moyeni, microbial activity is inferred to have occurred before track registration, resulting in both a high track abundance and anatomical fidelity. Conversely, at Mafube, microbial activity occurred after track registration, resulting in a high track abundance but low grades of anatomical fidelity. The timing of microbial activity at Matsieng and Morija remains unclear as the MISS and tracks are not in direct contact.

The composition of sandstones remains uniform across ichnosites and stratigraphy (Figure 4.21), suggesting that it likely does not have a significant impact on track registration and anatomical fidelity. Modal composition analysis showed that the detrital grains are primarily composed of quartz (70–90%), with smaller amounts of lithic fragments (9–12%), feldspar (6–9%), and mica (1–2%; Figure 4.21A). XRD analysis findings indicated presence of quartz (~71%), plagioclase feldspar (~15%), alkali feldspar (~5%), mica (~5%) and kaolinite (~3). However, the presence of calcite cement on Matsieng sandstones (4.21B) could potentially be associated with the calcification of microbes during their decomposition, which may have played a role in enhancing the track preservation potential at the site (e.g., Schieber, 2007; Carvalho et al., 2013).

In summary, the observed pattern of increase in track abundance and anatomical fidelity up-stratigraphy corresponds to: 1) A pronounced decrease in the dominant grain size from medium and fine sands to predominantly very fine sands (0.15–0.4 mm vs 0.08–0.12 mm) from the lEF to CLAR, 2) More constrained grain size ranges from the lEF to CLAR (0.08–0.6 mm to 0.08–0.12 mm), 3) Increase in roundness and sorting from the lEF to CLAR, and 4) A greater prevalence of MISS in the CLAR than lEF.

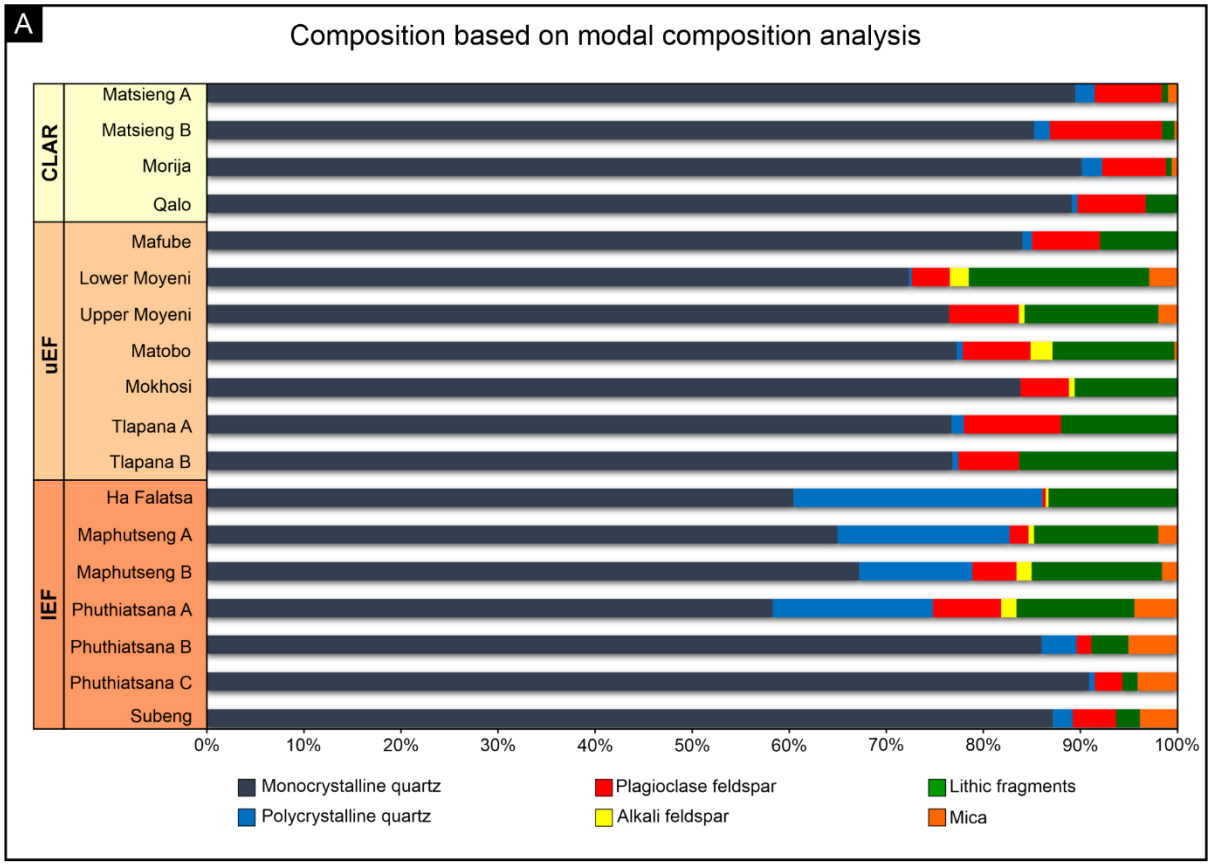

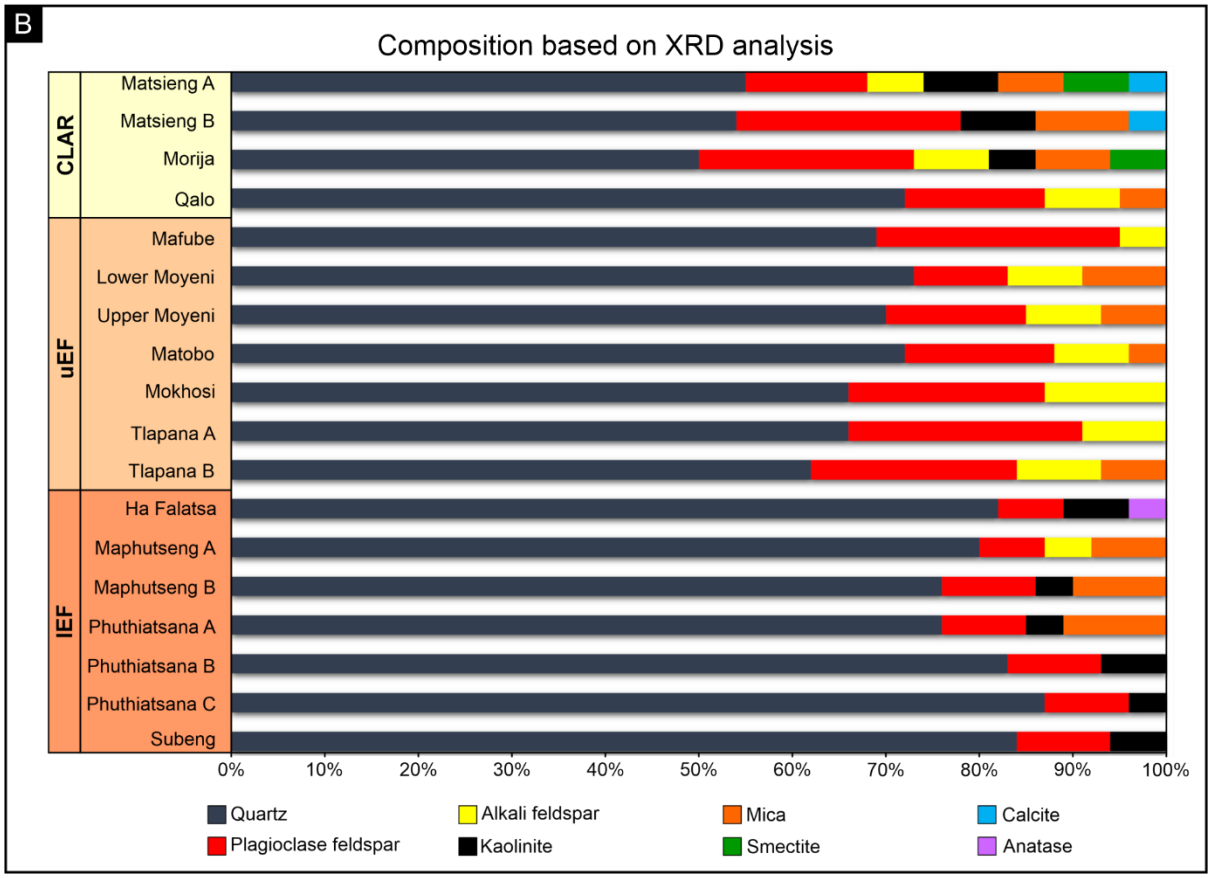

Figure 4.21. Composition of the track-bearing sandstones in the upper Stormberg ichnosites based on **A)** Modal composition analysis and **B)** XRD analysis.

5. Discussion

5.1 The role of substrate

The influence of grain size and moisture content on track registration and preservation has been demonstrated experimentally (see section 2.2.1), with the results showing that the optimal conditions for track registration, resulting in high anatomical fidelity, are found in muddy, silty and fine-grained sand sediments containing low- to moderate-moisture levels (e.g., Gatesy et al., 1999; Milan and Bromley, 2006, 2008; Jackson et al., 2010; Mancuso et al., 2022). Consequently, it is crucial to understand the grain size and moisture content when assessing fossil tracks.

The upper Stormberg track-bearing sandstones preserve ripple marks and desiccation cracks, suggesting that track registration and preservation likely occurred in gentle currents or stagnant ponds, and subsequently dried under subaerial conditions (e.g., Sciscio et al., 2016; Abrahams et al., 2020, 2021). Within the upper Stormberg Group, the tracksites comprising predominantly very fine sands have a relatively higher track abundance (e.g., Matsieng, Morija, Qalo with >65 tracks) compared to tracksites with medium to fine sands (e.g., Ha Falatsa, Maphutseng, Subeng with >30 tracks). Moreover, individual tracks associated with very fine sands tend to preserve higher anatomical fidelity grades and overall, the track anatomical fidelity grades are less variable. A notable exception is the Lower Moyeni ichnosite, which comprises fine sand (0.14–0.2 mm; Figure 4.9) and preserves over 200 tracks with anatomical fidelity between 2 and 3, and unique traces like stomach drag marks of a temnospondyl. This correlation between fine-grained sediments and higher track abundances with greater anatomical fidelity is consistent in globally distributed dinosaur tracksites. (e.g., Currie et al., 1990; Paik et al., 2001, 2007; Xing et al., 2019). However, similar to Lower Moyeni, there are a few exceptions to this trend, with high abundances of fossil tracks preserved in coarse-grained sandstones (e.g., Shapiro et al., 2009; Moreau et al., 2021).

In the upper Stormberg Group, as we move up-stratigraphy, there is a decrease in the mean grain size of the track-bearing sandstones (see section 4.2). The lEF track-bearing sandstones have the largest variation in grain size (ranging from 0.08–0.6 mm) but are primarily medium- to fine-grained (0.15–0.4 mm). The uEF track-bearing sandstones have a narrower range

(0.08–0.2 mm) and are predominantly very fine-grained (~57%; 0.08–0.12 mm). Lastly, the CLAR track-bearing sandstones have the smallest range in grain size (0.08–0.15 mm) and are predominantly very fine-grained (~73%; 0.08–0.12 mm). Coupled with this decrease in grain size up-stratigraphy, there is an observed increase in the average track anatomical fidelity grades. The majority of tracks preserved in the CLAR sandstones range between 2 and 3, and preserving exquisite detail like skin impressions.

Extensive studies have been conducted on the tracksites of the upper Stormberg Group since the early 1900s (e.g., Dornan, 1908), with a surge in reports during the 1970s (e.g., Ellenberger, 1970, 1972, 1974) and more recently in the 2010s (e.g., Sciscio et al., 2016, 2017; Abrahams et al., 2017, 2020, 2021; Bordy et al., 2017, 2023; Rampersadh et al., 2018; Bordy, 2021). Building upon these works, a recent study by Abrahams et al. (2022) noted a consistent trend in the upper Stormberg Group, where the number of preserved tracksites, track abundance at individual sites, and average anatomical fidelity grade increase up-stratigraphy from the Upper Triassic (lEF) to Lower Jurassic (uEF and CLAR). Our findings suggest that these trends can be attributed, at least partially, to a decrease in grain size within the upper Stormberg Group. This decrease in grain size, particularly towards very fine sands, favours track registration and preservation with greater detail (e.g., Milan and Bromley, 2006). The uEF and CLAR exhibit finer grain sizes (ranging from 0.08 – 0.12 mm), providing more favourable conditions for the registration and preservation of tracks compared to the coarser sands of the lEF (ranging from 0.15 – 0.4 mm). Consequently, there is an increase in the abundance of tracksites, track abundance and average anatomical fidelity grades in the younger strata of the upper Stormberg Group strata.

While conducting detailed grain size analysis on ancient track-bearing sandstones is feasible, assessing past moisture content remains challenging. However, certain sites, such as Mafube, Phuthiatsana and Upper Moyeni, exhibit distinctive features associated with fossil tracks, such as sediment collapse features and expulsion rims, which can provide insights into the ancient moisture content (e.g., Gatesy et al., 1999). These track-bearing surfaces, preserving evidence of a saturated palaeosubstrate, constitute a minor component of the overall track record in the upper Stormberg Group (3/10 of tracksites considered in this study). These inferred saturated track-bearing surfaces are characterised by high track abundances but with low

anatomical fidelity (i.e., the track morphology is obscured by extra-morphological features). The abundance of tracks at these sites is more likely attributed to the very fine grain size of the track-bearing sandstones than the moisture content. Similar effects of increasing moisture on track morphologies have been observed at other global dinosaur fossil tracksites (e.g., Razzolini et al., 2014, 2016; Xing et al., 2019).

5.2 The role of MISS

MISS form from the interaction between microbes and sediment (Noffke et al., 2001, 2022) and have been linked to aiding track registration, lithification and preservation (e.g., Carmona et al., 2011; Carvalho et al., 2013; Dai et al., 2015; see section 2.2.2). Neoichnological studies have demonstrated that microbially-stabilised substrates are more cohesive, resulting in track impressions with higher anatomical fidelity due to the elastic nature of the substrate (e.g., Marty et al., 2009; Carmona et al., 2011; Dai et al., 2015). Furthermore, microbial activity on substrate surfaces can act as a protective layer, reducing the erodibility of the underlying tracks and enhancing track preservation potential (e.g., Marty et al., 2009; Carmona et al., 2011; Carvalho et al., 2013; Dai et al., 2015; Figure 2.4). Decomposition of microbes can also lead to carbonate precipitation, inducing early lithification and cementation of the substrate, further enhancing the track preservation potential (e.g., Schieber, 2007; Carvalho et al., 2013).

Within the upper Stormberg Group, various ichnosites considered in this study, preserve MISS expressed as diverse surface textures, such as wrinkle structures, pitted and pustular textures (see section 4.1). It is observed that ichnosites preserving MISS are associated with higher track densities (e.g., Mafube > 80 tracks; Lower Moyeni > 200 tracks) and/or with higher track anatomical fidelity (e.g., Matsieng, Morija and Qalo with the majority of tracks ranging 2–3). The preserved MISS can cover extensive areas (e.g., Mafube) or be more localised (e.g., Lower Moyeni). At Mafube, MISS is associated with higher track abundance but lower anatomical fidelity compared to other areas of the site (see Sciscio et al, 2016). The localised MISS, which formed after track registration, likely played a crucial role in track consolidation and subsequent preservation (e.g., Carvalho et al., 2013; Dai et al., 2015). Conversely, at Lower Moyeni, where high track abundances are preserved, the MISS pre-dates track registration, and the preserved tracks have high anatomical fidelity, suggesting that the MISS may have contributed to the cohesiveness of the substrate, allowing for more pedal detail to be

captured (e.g., Kvale et al., 2001; Xing et al., 2007; Carvalho et al., 2013; Dai et al., 2015). At Qalo, some tracks are preserved with exceptional anatomical fidelity, exhibiting striations and grooves interpreted as skin impressions (Dornan, 1908). In Matsieng, the track bearing sandstones are bounded by calcite cement (Figures 4.16, 4.17), where carbonate precipitation, possibly associated with microbial activity, may have aided track consolidation (e.g., Carvalho et al., 2013).

Overall, within the upper Stormberg Group, two notable trends are observed: an increase in the presence of MISS at tracksites and an increase in the diversity of MISS up-stratigraphy. Given that microbial activity influences track registration and preservation potential, these factors likely contributed to the observed patterns of track abundance and anatomical fidelity in the younger upper Stormberg Group strata. In other words, the greater presence of microbes in these strata may partially explain the higher track abundance and anatomical fidelity. Consequently, the observed track trends across the Triassic-Jurassic boundary in the MKB, may be attributed to favourable substrate conditions for track registration and preservation, specifically the presence of very fine sands with microbial films, which become more prevalent in the younger stratigraphic units.

5.3 Palaeoenvironmental changes

The registration and preservation of tracks in the geological record is influenced by a variety of environmental factors, including the substrate grain size, water content, cohesiveness and sedimentation processes (e.g., Carvalho et al., 2013; Razzolini et al., 2014; Carvalho and Leonardi, 2021; see section 2.2). Generally, fine-grained sediments coupled with MISS provide a more optimal environment for track registration (e.g., Carvalho et al., 2013; Dai et al., 2015; Paik et al., 2017; Xing et al., 2019; sections 5.1, 5.2), and track preservation potential is greater in environments with low and cyclic sedimentation rates (e.g., Razzolini et al., 2014; Carvalho and Leonardi, 2021). Globally, the majority of fossil tracks occurrences in the geological record are associated with semi-arid palaeoenvironments characterized by episodic sedimentation with subsequent exposure (e.g., Carvalho, 2000; Carvalho et al., 2013; Paik et al., 2017; Xing et al., 2019; Carvalho and Leonardi, 2021). This is also the case for the upper Stormberg Group.

The upper Stormberg Group was deposited under increasingly semi-arid climatic conditions (see Bordy et al., 2020a, 2021; Table 2.1; Figure 5.1), with the changing environments likely having a significant impact on the abundance and distribution of tracks (e.g., Carvalho, 2000; Xing et al., 2019). The lEF was deposited in perennial, moderately meandering fluvial channels, whereas the uEF was deposited in ephemeral, flash flood-dominated fluvial channels and lakes (Bordy et al., 2004b, 2020a). Unlike the lEF, the uEF deposits were subjected to extended repeated periods of sedimentation and exposure, as evidenced by the extensive pedogenic alteration features preserved (e.g., prevalent pedogenic carbonate nodules, rootlets; Bordy et al., 2004b, 2020a, Table 2.1). The repeated flooding (i.e., sedimentation) and exposure events may have created more favourable conditions for track registration and preservation, resulting in the observed greater track abundance in the uEF than in the lEF (see Abrahams et al., 2022). The CLAR is subdivided into three zones: the lower and upper zones reflect wet aeolian conditions with ephemeral lakes, whereas the middle zone reflects the predominance of drier aeolian conditions (Beukes, 1970; Bordy and Head, 2018; Bordy et al., 2021; Head and Bordy, 2022). Unlike the middle zone, which is dominated by large-scale cross-bedded fine- to medium-grained sandstones, the lower and upper zones consist of loess-like siltstones interbedded with silty, very fine-grained sandstones and thinly laminated, dark grey to green mudstones (Bordy and Head, 2018; Head and Bordy, 2022), which are more suitable for track registration and preservation (e.g., Xing et al., 2019; Carvalho and Leonardi, 2021). In the CLAR, tracks are concentrated in the basal most strata (e.g., Dornan, 1908; Ellenberger, 1970; Abrahams et al., 2021; Mukaddam et al., 2021), with only a few reported from the middle zone (e.g., Ellenberger, 1970; Haupt, 2018). While this distribution is most likely the result of palaeoenvironmental changes, it is plausible that track resolution in the CLAR become poorer up-stratigraphy due to its limited accessibility (i.e., the CLAR is exposed as high cliffs).

Given these environmental considerations, the changes in grain size properties reported herein reflect the changes in the palaeoenvironment, which transitioned from high-energy meandering rivers to lower energy shallow ephemeral rivers/streams and aeolian systems with lakes (Figure 5.1). Furthermore, these environmental changes also played a role in the prevalence of microbial activity. Therefore, the observed increase in track abundance and anatomical fidelity observed up stratigraphy, which we have linked to fine and very-fine sandy

substrates with microbes (Section 5.1), was ultimately controlled by the dominant palaeoenvironment.

5.4 The end-Triassic mass extinction events

The end-Triassic mass extinction events are among the five major extinction events of the Phanerozoic that are widely acknowledged to have had a significant impact on terrestrial and marine life (e.g., Raup and Sepkoksi, 1982; McElwain et al., 1999; Pálfy et al., 2007). The Triassic–Jurassic boundary represents a crucial period in the evolution and radiation of dinosaurs, as evidenced by increases in their population sizes, diversity and body size during the Early Jurassic (e.g., Olsen et al., 2002; Brusatte et al., 2008, 2010; Benson et al., 2014; Bordy et al., 2020a; Abrahams et al., 2022). In southern Africa, the Triassic–Jurassic boundary is contained within the Elliot Formation, likely near or at the lEF–uEF boundary, although its exact stratigraphic position is still unknown (Bordy et al., 2020a).

The observed increase in dinosaur track abundance up-stratigraphy within the upper Stromberg Group has been attributed to the boom in trackmaker populations (Abrahams et al., 2022). However, as demonstrated herein, the locally observed track trends are not solely a reflection of the increase in dinosaur populations but also of an increase in the prevalence of ideal substrate conditions that resulted from palaeoenvironmental changes. It is plausible that changes in dinosaur populations and palaeoenvironment were interlinked: factors such as the migration of Gondwana towards the equator, eruption of flood basalts of the Central Atlantic Magmatic Province, and significant warming and acidification of the atmosphere following the end-Triassic mass extinction events (e.g., McElwain et al., 1999; Blackburn et al., 2013; Lucas and Tanner, 2015), may have contributed to the increasing abundance of semi-arid environments, which, in turn, provided more favourable conditions for the continued existence and flourishing of certain vertebrates, particularly dinosaurs (Bordy et al., 2020b, 2022).

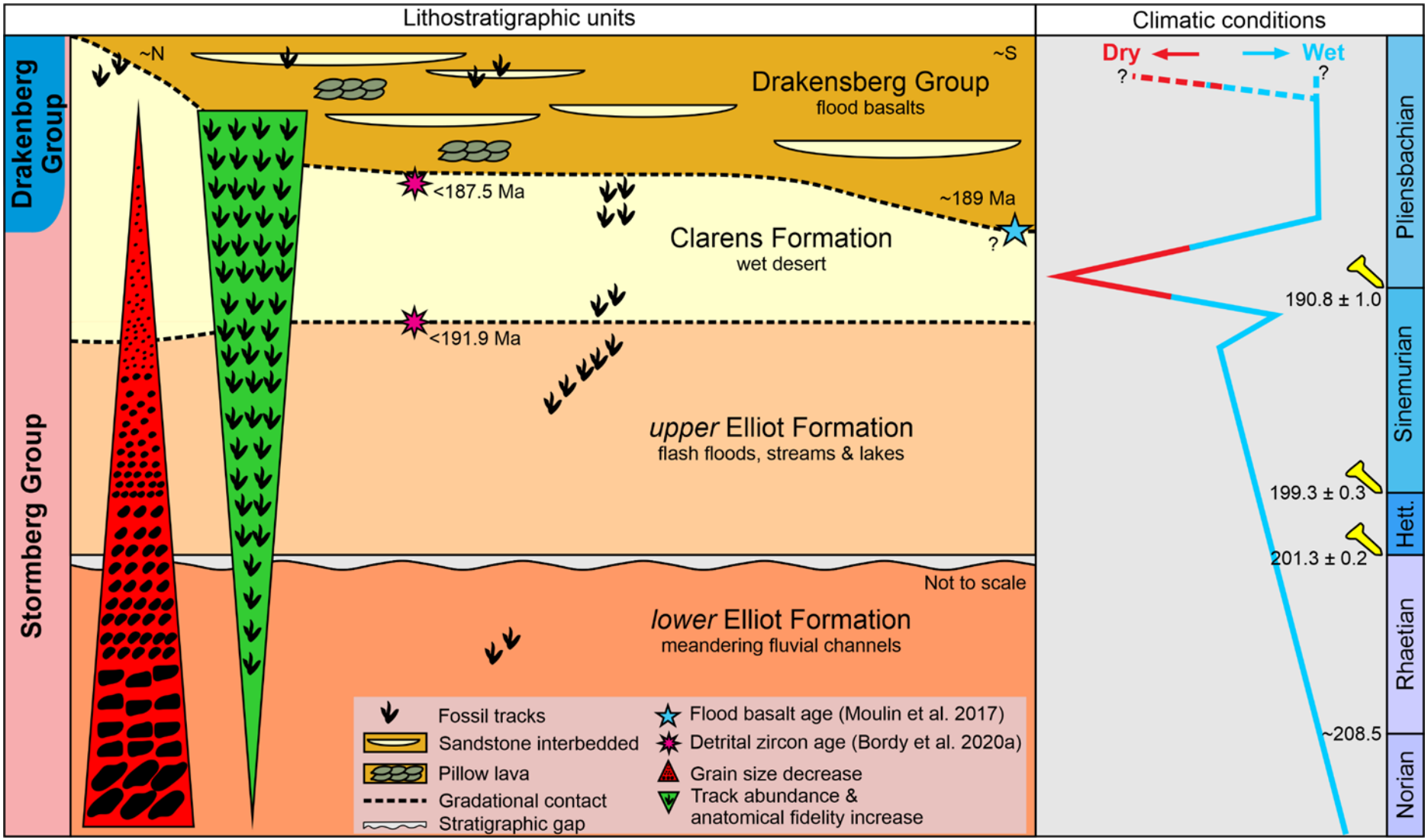

Figure 5.1. Summary of the upper Stormberg Group palaeoenvironment and climatic changes and how they are reflected in the grain size distribution and track abundance and anatomical fidelity. Modified from Bordy et al. 2021.

6. Conclusion

The morphology of fossil tracks provides important information about the pedal anatomy of the trackmaker, its behaviour and the substrate conditions at the time of track registration. Consequently, they are valuable for understanding the palaeodiversity, palaeoecology, and palaeoethology of ancient animals, especially in deposits where complete body fossils are scarce or absent. This study aimed to examine the micro-sedimentary features of track-bearing units in the upper Stormberg Group to add new insights on the palaeosubstrate conditions and its influence on fossil track registration and preservation from the Late Triassic to the Early Jurassic. Based on this semi-quantitative analysis, the following deductions can be made:

1. Finer grained sandstones preserve tracks in higher abundance and better anatomical fidelity compared to the coarser sands.
2. Substrates modified by microbial activity preserve tracks in higher abundance and better anatomical fidelity.
3. Grain size decreases and roundness increases up-stratigraphy from the lower Elliot to the Clarens Formation.

By integrating clastic sedimentary properties, the influence of microbial activity, and the fossil tracks, we have demonstrated the associations between grain size, MISS, track abundance and anatomical fidelity. We have observed an increasing prevalence of very fine-grained and microbially modified strata in the younger stratigraphic units, which is reflected in the local track trends of increasing track abundance and better anatomical fidelity up-stratigraphy. These findings have implications for the Triassic–Jurassic boundary, a period when dinosaur populations proliferated, and the end-Triassic mass extinction events was globally credited for the track abundance increase. However, our results suggest that the observed increase in track abundance (and improved anatomical fidelity) from the Upper Triassic to Lower Jurassic may be partially attributed, to the decrease in dominant grain size and increase in roundness reported herein and also documented in Bordy et al. (2005). These grain size properties were controlled by large-scale changes in the palaeoenvironment, transitioning from high-energy

meandering fluvial to lower-energy aeolian-lacustrine settings, which affected substrate conditions. Ultimately, these environmental changes resulted in the prevalence of very fine sands and MISS up-stratigraphy, significantly influencing the observed local track trends in the Lower Jurassic tracksites.

Consequently, our findings complement the existing macro-sedimentary observations, providing a deeper understanding of the palaeosubstrate conditions and refining our knowledge of the palaeoenvironmental context within the upper Stormberg Group. This knowledge contributes to a better understanding of the local tracks trends in the southern African region.

7. References

Abdala, F., Damiani, R., Yates, A., and Neveling, J., 2007. A non-mammaliaform cynodont from the Upper Triassic of South Africa: a therapsid Lazarus taxon? Paleontologia africana, 42, 17–23.

Abrahams, M., 2020. Evaluation of tridactyl theropod tracks in southern Africa: quantitative morphometric analysis across the Triassic-Jurassic boundary. PhD Thesis, University of Cape Town, 208p.

Abrahams, M., Bordy, E.M., Sciscio, L., and Knoll, F., 2017. Scampering, trotting, walking tridactyl bipedal dinosaurs in southern Africa: ichnological account of a Lower Jurassic palaeosurface (upper Elliot Formation, Roma Valley) in Lesotho. Historical Biology, 29(7), 958–975. DOI: http://dx.doi.org/10.1080/08912963.2016.1267164

Abrahams, M., Sciscio, L., Reid, M., Haupt, T., and Bordy E.M., 2020. Large tridactyl dinosaur tracks from the early Jurassic of southern Gondwana – uppermost Elliot Formation, Upper Moyeni, Lesotho. Annales Societatis Geologorum Poloniae, 90, 1–26. DOI: http://doi.org/10.14241/asgp.2020.07

Abrahams, M., Bordy, E.M., and Knoll, F., 2021. Hidden for one hundred years: a diverse theropod ichnoassemblage and cross-sectional tracks from the historic Early Jurassic Tsikoane ichnosite (Clarens Formation, northern Lesotho, southern Africa). Historical Biology, 33(10), 2504-2519. DOI: https://doi.org/10.1080/08912963.2020.1810681

Abrahams, M., Bordy, E.M., Knoll, F., and Farlow, J.O., 2022. Theropod Tridactyl Tracks Across the Triassic–Jurassic Boundary in Southern Africa: Implications for Pedal Morphology Evolution. Frontiers in Ecology and Evolution, 10. DOI: https://doi.org/10.3389/fevo.2022.925313

Abrahams, M., Rampersadh, A., and Mpangala, L., 2023. Riches of the Roma Valley: theropod and ornithischian tracks from the Early Jurassic southern Africa. Historical Biology. DOI: https://doi.org/10.1080/08912963.2023.2221306

Ambrose, D., 2003. A note on fossil trackways at Roma, Lesotho. Lesotho miscellaneous documents. No 4, House 9 publications Roma, 14p.

Ambrose, D., 2016. A Note on Ellenberger and a Checklist of Lesotho Fossil Footprint Sites. House 9 Publications & Mohokare Trust, Roma, Maseru, 50p.

Avanzini, M., 1998. Anatomy of a footprint: Bioturbation as a key to understanding dinosaur walk dynamics. Ichnos, 6, 129–139.

Avanzini, M., Piñeula, L., and Garcia-Ramos, J.C., 2012. Late Jurassic footprints reveal walking kinematics of theropod dinosaurs. Lethaia, 45, 238–252.

Belvedere, M., and Farlow, J.O., 2016. A Numerical Scale for Quantifying the Quality of Preservation of Vertebrate Tracks. In: Falkingham, P.L., Marty, D., Richter, A. (Eds): Dinosaur tracks: the next steps, 93–98.

Benson, R.B.J., Campione, N.E., Carrano, M.T., Mannion, P.G., Sullivan, C., Upchurch, P., and Evans, D.C., 2014. Rates of dinosaur body mass evolution indicate 170 million years of sustained ecological innovation on the avian stem lineage. PLOS Biology, 12(6). DOI: http://doi.org/10.1371/journal.pbio.1001853

Beukes, N.J., 1970. Stratigraphy and sedimentology of the Cave Sandstone stage, Karoo System. In: Proceedings 2nd IUGS Symposium on Gondwana Stratigraphy and Palaeontology, Pretoria, CSIR, 321–341.

Blackburn, T.J., Olsen, P.E., Bowring, S.A., McLean, N.M., Kent, D.V., Puffer, J., McHone, G., Rasbury, E.T., and Et-Touhami, M., 2013. Zircon U-Pb geochronology links the end-Triassic extinction with the Central Atlantic Magmatic Province. Science, 340(6135), 941–945.

Boggs Jr, S., 2009. Petrology of sedimentary rocks: Second Edition. Cambridge University Press.

Bordy, E.M., 2021. Darting towards Storm Shelter: a minute dinosaur trackway from southern Africa. South African Journal of Science, 117 (5/6). DOI: https://doi.org/10.17159/sajs.2021/9145

Bordy, E.M. and Eriksson, P., 2015. Lithostratigraphy of the Elliot Formation (Karoo Supergroup), South Africa. Geological Society of South Africa, 118, 311–316.

Bordy, E.M., Hancox, P.J., and Rubidge, B.S., 2004a. Basin development during the deposition of the Elliot Formation (Late Triassic - Early Jurassic), Karoo Supergroup, South Africa. South African Journal of Geology, 107, 397–412.

Bordy, E.M., Hancox, P.J., and Rubidge, B.S., 2004b. Fluvial style variations in the Late Triassic-Early Jurassic Elliot formation, main Karoo Basin, South Africa. Journal of African Earth Sciences, 38, 383–400.

Bordy, E.M., Hancox, P.J., Rubidge, B.S., 2004c. Provenance Study of the Late Triassic – Early Jurassic Elliot Formation, main Karoo Basin, South Africa. South African Journal of Geology, 107, 587–602.

Bordy, E.M., Hancox, P.J., Rubidge, B.S., 2005. The contact of the Molteno and Elliot formations through the main Karoo Basin, South Africa: A second-order sequence boundary. South African Journal of Geology, 108, 351–364.

Bordy, E.M., Gend, J., Mcphee, B., and Tucker, R., 2015. Stratigraphic context of the dinosaur trackways and bone bed in the Upper Triassic – Lower Jurassic Elliot Formation (Lesotho). 1st International Congress on Continental Ichnology.

Bordy, E.M., Sciscio, L., Abdala, F., McPhee, B., and Choniere, J. 2016. First Lower Jurassic vertebrate burrow from southern Africa (upper Elliot Formation, Karoo Basin, South Africa). Palaeogeography, Palaeoclimatology, Palaeoecology, 468, 362–372. DOI: https://doi.org/10.1016/j.palaeo.2016.12.024

Bordy, E.M., Abrahams, M., and Sciscio, L. 2017. The Subeng vertebrate tracks: stratigraphy, sedimentology and a digital archive of a historic Upper Triassic palaeosurface (lower Elliot Formation), Leribe, Lesotho (southern Africa). Bollettino della Società Paleontologica Italiana, 56(2), 181–198.

Bordy, E.M and Head, H.V., 2018. Lithostratigraphy of the Clarens Formation (Stormberg Group, Karoo Supergroup), South Africa. Geological Society of South Africa, 121, 119–130.

Bordy, E.M., Abrahams, M., Sharman G., Viglietti, P., Benson, R., McPhee, B., Barrett, P., Sciscio, L., Condon, D., Mundil, R., Rademan, Z., Jinnah, Z., Clark, J., Suarez, C., Chapelle, K., and Choiniere, J., 2020a. A chronostratigraphic framework for the upper Stormberg Group: Implications for the Triassic-Jurassic boundary in southern Africa. Earth-Science Reviews. 203. DOI: http://dx.doi.org/10.1016/j.earscirev.2020.103120

Bordy, E.M., Rampersadh, A., Abrahams., M., Lockley, M.G., and Head, H., 2020b. Tracking the Pliensbachian–Toarcian Karoo firewalkers: Trackways of quadruped and biped dinosaurs and mammaliaforms. PLoS ONE 15(1). DOI: https://doi.org/10.1371/journal.pone.0226847

Bordy, E.M., Haupt, T., and Head, H.V., 2021. Karoo lava-fed deltas and a petrified forest from the Lower Jurassic of southern Gondwana. Palaeogeography, Palaeoclimatology, Palaeoecology, 575. DOI: https://doi.org/10.1016/j.palaeo.2021.110484

Bordy, E.M., Lockley, M.G., Rampersadh, A., Mukaddam, R., and Head, H., 2022. Life and land engulfed in the late Early Jurassic Karoo lavas of southern Gondwana. Geological Magazine, 160(4), 645–666. DOI: https://doi.org/10.1017/S0016756822001169

Brusatte, S.L., Benton, M.J., Ruta, M. and Lloyd, G.T., 2008. The first 50 Myr of dinosaur evolution: macroevolutionary pattern and morphological disparity. Biology letters, 4, 711–736. DOI: http://doi.org/10.1098/rsbl.2008.0441

Brusatte, S.L., Nesbitt, C.J., Irmis, R.B., Butler, R.J., Benton, M.J. and Norrel, M.A., 2010. The origin and early radiation of dinosaurs. Earth Science Reviews, 101, 68–100. DOI: https://doi.org/10.1016/j.earscirev.2010.04.001

Carmona, N.B., Bournod, C.N., Ponce, J.J., and Cuadrado, D.G., 2011. The role of microbial mats in the preservation of bird fooptrints: a case study from the mesotidal Bahia Blanca estuary (Argentina). Society for Sedimentary Geology Special Publication, 101, 37–45.

Carvalho, I.S., 2000. Geological environments of dinosaur footprints in the intracratonic basins of north east Brazil during the Early Cretaceous opening of the South Atlantic. Cretaceous Research, 21, 255–267.

Carvalho, I.S., Borghi, L., and Leonardi, G., 2013. Preservation of dinosaur tracks induced by microbial mats in the Sousa Basin (Lower Cretaceous), Brazil. Cretaceous Research, 1–10. DOI: http://dx.doi.org/10.1016/j.cretres.2013.04.004

Carvalho, I.S., and Leonardi., G, 2021. Fossil footprints as biosedimentary structures for palaeoenvironmental interpretation: Examples from Gondwana. Journal of South American Earth Sciences, 106. DOI: https://doi.org/10.1016/j.jsames.2020.102936

Catuneanu, O., Hancox, P.J., and Rubidge, B.S., 1998. Reciprocal flexural behavior and contrasting stratigraphies: a new basin development model for the Karoo retroarc foreland system, South Africa. Basin Research, 10, 417–439.

Catuneanu, O., and Elango, H.N., 2001. Tectonic control on fluvial styles: The Balfour Formation of the Karoo Basin, South Africa. Sedimentary Geology, 140, 291–313.

Catuneanu, O., Wopfner, H., Eriksson, P.G., Cairncross, B., Rubidge, B.S., Smith, R.M.H., and Hancox, P.J., 2005. The Karoo basins of south-central Africa. Journal of African Earth Sciences, 43, 211–253.

Cole, D.I., 1992. Evolution and development of the Karoo Basin. In: De Wit, M.J., Ransome, I.G.D. (Eds). Inversion Tectonics of the Cape Fold Belt, Karoo and Cretaceous Basins of Southern Africa. Rotterdam: Balkem, 87–99.

Currie, P.J., Nadon, G.C., and Lockley,M.G., 1990. Dinosaur footprints with skin impressions from the Cretaceous of Alberta and Colorado. Canadian Journal of Earth Sciences, 28, 102–115. DOI: https://doi.org/10.1139/e91-009

Dai, H., Xing, L., Marty, D., Zhang, J., Persons IV, W.S., Hu, H., and Wang, F. 2015. Microbially-induced sedimentary wrinkle structures and possible dinosaur impact of microbial mats for the enhances preservation of dinosaur tracks from the Lower Cretaceous Jiaguan Formation near Qijiang (Chongqing, China). Cretaceous Research, 53, 98–109.

Dickinson, W.R., 1979. Plate Tectonics and Sandstone Compositions. AAPG Bull, 63, 2164–2194.

Dickinson, W.R., 1985. Interpreting Provenance Relations from Detrital Modes of Sandstones. In Provenance of Arenites; Springer Science and Business Media LLC: Berlin/Heidelberg, Germany, 333–361.

Dornan, S.S., 1908. Notes on the geology of Basutoland. Geological Magazine, 5(2), 57–63. DOI: https://doi.org/10.1017/S0016756800112877

Duncan, R.A, Hooper, P.R., Rehacek, J., Marsh, J.S., and Duncan, A.R., 1997. The timing and duration of the Karoo igneous event, southern Gondwana. Journal of Geophysical Research: Solid Earth, 102, 18127–18138.

Folk, R. L., 1968. Bimodal supermature sandstones. Product of the desert floor. 23rd Proceedings International Gondwana Congress, 8, 9–32.

Gatesy, S.M., Middleton, K.M., Jenkins, F.A., and Shubin N.H., 1999. Three-dimensional preservation of foot movements in Triassic theropod dinosaurs. Nature, 399, 141–144.

Gatesy, S.M., and Falkingham, P.L., 2017. Neither bones nor feet: track morphological variation and 'preservation quality'. Journal of Vertebrate Paleontology, 37(3). DOI: https://doi.org/10.1080/02724634.2017.1314298

Hansma, J., Tohver, E., Schrank, C., Jourdan, F. and Adams, D., 2016. The timing of the Cape Orogeny: New40Ar/39Ar age constraints on deformation and cooling of the Cape Fold Belt, South Africa. Gondwana Research, 32, 122–137.

Haupt, T., 2018. Palaeoenvironmental change from the Hettangian to Toarcian in Moyeni (Quthing District), southwestern Lesotho. Master Thesis (unpublished), University of Cape Town, 119p.

Head, H.V., and Bordy, E.M., 2022. Lake dynamics in an Early Jurassic desert: Evidence from the Clarens Formation in southern Africa. Sedimentology, 70, 865–894. DOI: https://doi.org/10.1111/sed.13066

Hitchcock, E., 1836. Ornithichnology: Description of the Footmarks of birds (Ornithichnites) on new Red Sandstone in Massachusetts. American Journal of Science, Series 1 (29), 307–340.

Hitchcock, E., 1856. Description of a new and remarkable species of fossil footmark, from the sandstone of Turner's Falls, in the Connecticut Valley. American Journal of Science, Series 2 (21), 97– 100.

Ingersoll, R.V., Bullard, T.F., Ford, R.L., Grimm, J.P., Pickle, J.D. and Sares, S.W., 1984. The effect of grain size on detrital modes: a test of the Gazzi-Dickinson point-counting method. Journal of Sedimentary Research, 54, 103–116.

Jackson, S.J., Whyte, M.A., and Romano M., 2010. Range of experimental dinosaur (hypsilophodon foxii) footprints due to variation in sand consistency: how wet was the track? Ichnos, 17, 197–214.

Jerram, D. A., 2001. Visual comparators for degree of grain-size sorting in two and three dimensions. Computers and Geosciences, 27, 485–492.

Johnson, M.R., 1994. Thin section grain size analysis revisited. Sedimentology, 41, 985–999. DOI: https://doi.org/10.1111/j.1365-3091.1994.tb01436.x

Johnson, M.R., Van Vuuren, C.J., Hegenberger, W.F., Key, R., and Shoko, U., 1996. Stratigraphy of the Karoo Supergroup in southern Africa: An overview. Journal of African Earth Sciences, 23, 3–15.

Johnson, M.R., Van Vuuren, C.J., Visser, J.N.J., Cole, D.I., de Wickens, H.V., Christie, A.D.M., and Roberts, D.L., 1997. The Foreland Karoo Basin, South Africa. In: R.C. Selly (ed.): African Basins. Sedimentary Basins of the World, 3. Amsterdam: Elsevier Science B.V, 269–317.

Kitching, J. W., and Raath, M. A., 1984. Fossils from the Elliot and Clarens formations (Karoo Sequence) of the north-eastern Cape, Orange Free State and Lesotho, and a suggested biozonation based on tetrapods. Palaeontologia Africana, 25, 111–125.

Knoll, F., 2004. Review of the tetrapod fauna of the "Lower Stormberg Group" of the main Karoo Basin (southern Africa): implication for the age of the Lower Elliot Formation. Bulletin de la Societe géologiquede France, 175(1), 73–83.

Knoll, F., 2005. The tetrapod fauna of the Upper Elliot and Clarens formations in the main Karoo Basin (South Africa and Lesotho). Bulletin de la Société géologique de France, 176(1), 81–91.

Li, D., Azuma, Y., Fujita, M., Lee, Y., and Arakawa, Y., 2006. A preliminary report on two new vertebrate track sites including dinosaurs from the Early Cretaceous Hekou Group, Gansu province China. Journal of the Paleontological society of Korea, 22, 29–49.

Lockley, M.G., Gierlinski, G.D., and Lucas, S.G., 2011. *Kayentapus* revisited: Notes on the type material and the importance of this theropod footprint ichnogenus. New Mexico Museum of Natural History and Science Bulletin, 53, 330–336.

Lucas., S.G., and Tanner, L.H, 2015. End-Triassic nonmarine biotic events. Journal of Palaeogeography, 4(4), 331–348. DOI: http://doi.org/10.1016/j.jop.2015.08.010

Lull, R.S., 1904. Fossil footprints of the Jurassic-Triassic of North America. Memoirs of the Boston Society of Natural History, 5, 461–557.

Mancuso, A.C., Marsicano, C.A., and Krapovickas, V., 2022. Tetrapod-track taphonomic modes (TTTM) applied to Triassic lacustrine systems from southern South America. Journal of African Earth Sciences, 196. DOI: https://doi.org/10.1016/j.jafrearsci.2022.104735

Marchetti, L., Belvedere, M., Voigt, S., Klein, H., Castanera, D., Díaz-Martínez, I., Marty, D., Xing, L., Feola, S., Melchor, R.N., and Farlow, J.O., 2019. Defining the morphological quality of fossil footprints. Problems and principles of preservation in tetrapod ichnology with examples from the Paleozoic to the present. Earth-Science Reviews, 193, 109–145. DOI: https://doi.org/10.1016/j.earscirev.2019.04.008

Marty, D., Strasser, A., and Meyer, C.A., 2009. Formation and taphonomy of human footprints in microbial mats of present day tidal flat environments: Implication for the study of fossil footprints. Ichnos, 16, 127–142. DOI: https://doi.org/10.1080/10420940802471027

McElwain, J. C., Beerling, D. J., and Woodward, F. I., 1999. Fossil plants and global warming at the Triassic-Jurassic boundary. Science, 285(5432), 1386–1390.

McPhee, B.W., Bordy, E.M., Sciscio, L., and Choiniere, J.N., 2017. The sauropodomorph (Dinosauria) biostratigraphy of the Elliot Formation of southern Africa: tracking the evolution of Sauropodomorpha across the Triassic–Jurassic boundary. Acta Palaeontologica Polonica, 62, 441–465.

Miall, A.D., 1996. The Geology of Fluvial Deposits. Sedimentary Facies, Basin Analysis, and Petroleum Geology. Springer-Verlag Berlin Heidelberg, 565.
Mílan, J., and Bromley, R.G., 2006. True tracks, undertracks and eroded tracks, experimental work with tetrapod tracks in laboratory and field. Palaeogeography, Palaeoclimatology, Palaeoecology, 231, 231–264.

Mílan, J., and Bromley, R.G., 2008. The impact of sediment consistency on track and undertrack morphology: experiments with Emu tracks in layered cement. Ichnos, 15, 19–27. DOI: https://doi.org/10.1080/10420940600864712

Moreau, J.D., Sciau, J., Gand, G., and Fara, E., 2021. Uncommon preservation of dinosaur footprints in a tidal breccia: *Eubrontes giganteus* from the early Jurassoc Mongisty tracksite of Aveeyron, southern France. Geological Magazine, 158, 1403–1420. DOI: https://doi.org/10.1017/S0016756820001454

Muir, R.A., Bordy, E.M., Mundil, R., and Frei, D., 2020. Recalibrating the breakup history of SW Gondwana: U-Pb radioisotopic age constraints from the southern Cape of South Africa. Gondwana Research, 84, 177–193. DOI: http://dx.doi.org/10.1016/j.gr.2020.02.011

Mukaddam, R., Bordy, E.M., Lockley, M.G., and Chapelle, K.E.J., 2021. Reviving *Kalosauropus*, an Early Jurassic sauropodomorph track from southern Africa (Lesotho). Historical Biology, 33(11), 2908–2930. DOI: https://doi.org/10.1080/08912963.2020.1834542

Noffke, N., Gerdes, G., Klenke, T. and Krumbein, W. E., 2001. Microbially Induced Sedimentary Structures: A New Category within the Classification of Primary Sedimentary Structures. Journal of Sedimentary Research, 71(5), 649. DOI: 10.1306/2DC4095D-0E47-11D7-8643000102C1865D.

Noffke, N., Beraldi-Campesi, H., Callefo, F., Carmona, N., Cuadrado, D.G., Hickman-Lewis, K., Homann, M., Mitchell, R., Sheldon, N., Westall, F., and Xiao, S., 2022. Microbially Induced Sedimentary Structures (MISS), 2(5).

Olsen, P.E., 1980. Fossil great lakes of the Newark Supergroup in New Jersey. In: Manspeizer, W. (Ed): Field studies in New Jersey geology and Guide to field trips, 352–398.

Olsen, P.E., and Galton, P.M. 1984. A review of the reptile and amphibian assemblages from the Stormberg Group of southern Africa with special emphasis on the footprints and the age of the Stormberg. Palaeontologia africana, 25, 87–110.

Olsen, P.E., Smith, J.B., and McDonald, N.G., 1998. Type material of the type species of the classic theropod footprint genera *Eubrontes*, *Anchisauripus*, and *Grallator* (Early Jurassic,

Hartford and Deerfield basins, Connecticut and Massachusetts, USA). Journal of vertebrate Paleontology, 18, 586–601.

Olsen, P.E., Kent, D.V., Sues, H.D., Koeberl, C., Huber, H., Montanari, A., Rainforth, E.C., Fowell, S.G., Szajna, M.J., and Hartline, B.W., 2002. Ascent of dinosaurs linked to an Iridium anomaly at the Triassic–Jurassic Boundary. Science, 296, 1305–1307. DOI: http://doi.org/10.1126/science.1065522

Padian, K., and Olsen, P., 1984. The fossil trackway pteraichnus: not pterosaurian but crocodilian. Journal of Palaeontology, 58, 178–184.

Paik, I.S., Kim, H.J., and Lee, Y.I., 2001. Dinosaur track-bearing deposits in the Cretaceous Jindong Formation, Korea: occurrence, palaeoenvironments and preservation. Cretaceous Research, 22, 79–92. DOI: https://doi.org/10.1006/cres.2000.0241

Paik, I.S., Kim, H.J., Lee, H., and Kim, S., 2017. A large and distinct skin impression on the cast of a sauropod dinosaur footprint from Early Cretaceous floodplain deposits, Korea. Scientific Reports, 7(16339). DOI: https://doi.org/10.1038/s41598-017-16576-y

Pálfy, J., Demény, A., Haas, J., Carter, E. S., Görög, Á., Halász, D., Oravecz-Schefferg, A., Hetényih, A., Mártonf, E., Orchardi, M. J., Ozsvárta, P., Vetőj, I., and Zajzon, N., 2007. Triassic–Jurassic boundary events inferred from integrated stratigraphy of the Csővár section, Hungary. Palaeogeography, Palaeoclimatology, Palaeoecology, 244(1-4), 11–33.

Powers, M.C, 1953. A New Roundness Scale for Sedimentary Particles. Journal of Sedimentary Research, 23, 117–119.

Rampersadh, A., and Bordy, E.M., 2019. Early Jurassic dinosaur ecosystems in southwestern Gondwana: steps towards refining its palaeoecology. 3rd International Conference of Continental Ichnology (ICCI), Halle (Saale), Germany, 23rd – 29th September.

Rampersadh, A., Bordy, E.M., Sciscio, L., and Abrahams, M., 2018. Dinosaur behaviour in an early ecosystem – uppermost Elliot formation, Ha Nohana, Lesotho. Annales Societatis Geologorum Poloniae, 88. DOI: https://doi.org/10.14241/asgp.2018.010

Raup, D. M. and Sepkoski, J. J., 1982. Mass Extinctions in the Marine Fossil Record. Science, 215, 1501– 1503.

Razzolini, N.L., Vila, B., Castenera, D., Flakingham, P.L., Barco, J.L., Canuda, J.I., Manning, P.L., and Galobart, A., 2014. Intra-Trackway Morphological Variations Due to Substrate Consistency: The El Frontal Dinosaur Tracksite (Lower Cretaceous, Spain). PloS ONE, 9(4). DOI: https://doi.org/10.1371/journal.pone.0093708

Razzolini, N.L., Oms, O., Castanera, D., Vila, B., dos Santos, V.F., and Galobart, A., 2016. Ichnological evidence of Megalosaurid Dinosaurs Crossing Middle Jurassic Tidal Flats. Scientific Reports, 6(31494). DOI: https://doi.org/10.1038/srep31494

Rubidge, B.S., 2009. The Karoo, a geological and palaeontological superlative: economic potential of deep history.

Scheiber-Enslin, S.E., Ebbing, J. and Webb, S.J., 2015. New depth maps of the main Karoo Basin, used to explore the Cape Isostatic Anomaly, South Africa. South African Journal of Geology, 118(3), 225–248.

Schieber, J., 2007. Mat features in sandstones: diagenetic features related to mat metabolism and decay. In: Schieber, J., Bose, P., Eriksson, P.G., Banerjee, S., Altermann, W., Catuneanu, O. (Eds.), Atlas of microbial mats features preserved within the siliciclastic rock record. Elsevier, 72–75.

Sciscio, L., Bordy, E.M., Reid, M., and Abrahams, M., 2016. Sedimentology and ichnology of the Mafube dinosaur track site (Lower Jurassic, eastern Free State, South Africa): a report on footprint preservation and palaeoenvironment. PeerJ, 4. DOI: https://doi.org/10.7717/peerj.2285

Sciscio, L., Bordy, E.M., Abrahams, M., Knoll, F., and McPhee B.W., 2017. The first megatheropod tracks from the Lower Jurassic upper Elliot Formation, Karoo Basin, Lesotho. Plos ONE 12(10). DOI: https://doi.org/10.1371/journal.pone.0185941

Shapiro, R.S., Fricke,H.C., and Fox, K., 2009. Dinosaur-bearing oncoids from ephemeral lakes of the Lower Cretaceous Cedar Mountain Formation, Utah. Palaios 24, 51–58.

Smith, R.M.H., Eriksson, P.G., and Botha, W.J., 1993. A review of the stratigraphy and sedimentary environments of the Karoo-aged basins of Southern Africa. Journal of African Earth Sciences, 16, 143–169.

Smith, R.M.H., Marsicano, C.A., and Wilson, J.A., 2009. Sedimentology and paleoecology of a diverse Early Jurassic tetrapod tracksite in Lesotho, southern Africa. Palaios, 24, 672–684.

Soeder, D.J., and Borglum, S.J., 2019. The fossil fuel revolution: shale gas and tight oil.

Taylor, J. M., 1950. Pore-space reduction in sandstones. Bulletin of The American Association of Petroleum Geologists, 34, 701–716.

Wentworth, C.K., 1922. The canonical definition of sediment grain sizes. The Journal of Geology, 30, 377–392.

Wilson J.A., Marsicano C.A., and Smith R.M., 2009. Dynamic locomotor capabilities revealed by early dinosaur trackmakers from Southern Africa. PLoS ONE 4(10). DOI: http://doi.org/10.1371/journal.pone.0007331

Xing, L.D., Wang, F.P., Pan, S.G., Chen, W., 2007. The discovery of dinosaur footprints from the Middle Cretaceous Jiaguan Formation of Qijiang County, Chongqing city. Acta Geologica Sinica (Chinese edition), 81, 159–1602.

Xing, L., Lockley, M.G., Tang, D., Klein, H., Peng, G., Ye, Y., and Hao, B., 2019. Early Jurassic basal sauropodomorpha dominated tracks from Guizhou, China: Morphology, ethology, and paleoenvironment. Geoscience Frontiers, 10, 229–240.

8. Appendix

Appendix A

The raw and semi-processed clast count data mentioned as Appendix A in the text of this thesis can be downloaded from here:

https://docs.google.com/spreadsheets/d/1wBdcYA2WoI3zliw7c5tzxvvt5vgRUnpK/edit?usp=sharing&ouid=109723697021056296275&rtpof=true&sd=true

Appendix B

Table 8.1A. Petrographic descriptions of the lEF sandstones samples as well as a summary of the site overviews.

SAMPLE	Ha Falatsa	Maphutseng A	Maphutseng B	Phuthiatsana A	Phuthiatsana B	Phuthiatsana C	Subeng
FORMATION	lEF	lEF	lEF	lEF	lEF	lEF	lEF
TEXTURE							
Dominant grain size	medium-coarse	medium	medium	very fine-fine	very fine-fine	very fine-fine	fine-medium
Sorting	moderate	moderate	moderate	moderate	moderate	moderate	moderate
Sphericity	low	low	low	low	low	low	low
Roundness	subangular-subrounded	subangular-subrounded	subangular	subangular	subangular	subangular	subangular-subrounded
Fabric	homogeneous	homogeneous	homogeneous	homogeneous	homogeneous	homogeneous	homogeneous
Grain packing	mostly concavo-convex and long	mostly concavo-convex and long	mostly concavo-convex and long	mostly concavo-convex and long	mostly concavo-convex and long	mostly concavo-convex and long	mostly concavo-convex and long
Grain contacts	closely packed	closely packed	closely packed	moderately packed	moderately packed	moderately packed	closely packed
Matrix %	<5%	<5%	<5%	<5%	<5%	<5%	<5%
Maturity	submature	submature	submature	submature	submature	submature	submature
MINERAL COMPOSITION%							
Monocrystalline quartz	60.3	66.6	64.6	85.3	90.3	86.6	57.3
Polycrystalline quartz	25.6	11.6	17.6	3.6	0.6	2	16.3
Plagioclase feldspar	t	4.6	2	1.6	3	4.6	7.3
Alkali feldspar	t	1.6	0.6	-	-	-	1.6
Lithic fragments	13.3	13.6	13	4	1.6	2.6	12.6
Mica	t	1.6	2	5.3	4.3	4	4.6
Accessory minerals	zircon, rutile, opaque minerals	zircon, rutile, opaque minerals	zircon, rutile, opaque minerals	rutile, opaque minerals	rutile, opaque minerals	rutile, opaque minerals	zircon, rutile, opaque minerals
SITE OVERVIEW							
Track overview	tridactyl, tetradactyl, pentadactyl	tridactyl	tridactyl, tetradactyl	tridactyl, tetradactyl, pentadactyl	tridactyl, tetradactyl, pentadactyl	n/a	tridactyl, tetradactyl, pentadactyl
Morphological quality	0-2	0-3	0-3	1-3	1-3	n/a	0-2

Table 8.1B. Petrographic descriptions of the uEF sandstones samples as well as a summary of the site overviews.

SAMPLE	Matobo	Tlapana A	Tlapana B	Mokhosi	Lower Moyeni	Upper Moyeni	Mafube
FORMATION	uEF	uEF	uEF	uEF	uEF	uEF	uEF
TEXTURE							
Dominant grain size	very fine-fine	very fine-fine	very fine-fine	very fine-fine	fine	very fine-fine	very fine-fine
Sorting	moderate-well	moderate-well	moderate-well	moderate-well	moderate	moderate-well	moderate-well
Sphericity	low	low	low	low	low	low	low
Roundness	subangular-subrounded	subangular-subrounded	subangular-subrounded	subangular-subrounded	subangular-subrounded	subangular-subrounded	subangular-subrounded
Fabric	homogeneous	homogeneous	homogeneous	homogeneous	homogeneous	homogeneous	homogeneous
Grain contacts	mostly concavo-convex	mostly concavo-convex	mostly concavo-convex	mostly concavo-convex	mostly concavo-convex	mostly concavo-convex	mostly concavo-convex and long
Grain packing	moderately packed	moderately packed	moderately packed	moderately packed	moderately packed	moderately packed	moderately packed
Matrix %	<5%	<5%	<5%	<5%	<5%	<5%	<5%
Maturity	submature	submature	submature	submature	submature	submature	submature
MINERAL COMPOSITION%							
Monocrystalline quartz	77	76.6	76.6	83.6	71.6	76	84
Polycrystalline quartz	0.6	1.3	0.6	-	0.3	-	1
Plagioclase feldspar	7	10	6.3	5	4	7.3	7
Alkali feldspar	2.3	-	-	0.6	2	0.6	-
Lithic fragments	12.6	12	16.3	10.6	19	14	8
Mica	0.3	t	t	t	3	2	-
Accessory minerals	opaque minerals	opaque minerals	opaque minerals	opaque minerals	rutile, opaque minerals	zircon, rutile, opaque minerals	zircon, opaque minerals
SITE OVERVIEW							
Tracks overview	tridactyl	tridactyl	tridactyl	tridactyl	tridactyl, tetradactyl, pentadactyl	tridactyl	tridactyl
Morphological quality	1-2	0-3	0-3	1-2	2-3	1-3	1-3

Table 8.1C. Petrographic descriptions of the CLAR sandstones samples as well as a summary of the site overviews.

SAMPLE	Matsieng A	Matsieng B	Morija	Qalo
FORMATION	CLAR	CLAR	CLAR	CLAR
TEXTURE				
Dominant grain size	very fine	very fine	very fine	very fine
Sorting	well	well	well	well
Sphericity	low	low	low	low
Roundness	mostly subrounded	mostly subrounded	mostly subrounded	mostly subrounded
Fabric	homogeneous	homogeneous	homogeneous	homogeneous
Grain contacts	mostly concavo-convex	mostly concavo-convex	mostly concavo-convex	mostly concavo-convex
Grain packing	moderate-closely packed	moderate-closely packed	moderate-closely packed	moderate-closely packed
Matrix %	<5%	<5%	<5%	<5%
Maturity	submature	submature	submature	submature
MINERAL COMPOSITION%				
Monocrystalline quartz	89.3	85	90	89
Polycrystalline quartz	2	1.6	2	0.6
Plagioclase feldspar	7	11.6	6.6	7
Alkali feldspar	-	-	-	-
Lithic fragments	0.6	1.3	0.6	3.3
Mica	1	0.3	0.6	t
Accessory minerals	zircon, opaque minerals	zircon, opaque minerals	zircon, opaque minerals	zircon, opaque minerals
SITE OVERVIEW				
Track overview	tridactyl	tridactyl	tridactyl	tridactyl
Morphological quality	2-3	2-3	2-3	2-3

Appendix C

Figure 8.1. XRD diffractograms for individual ichnosites.

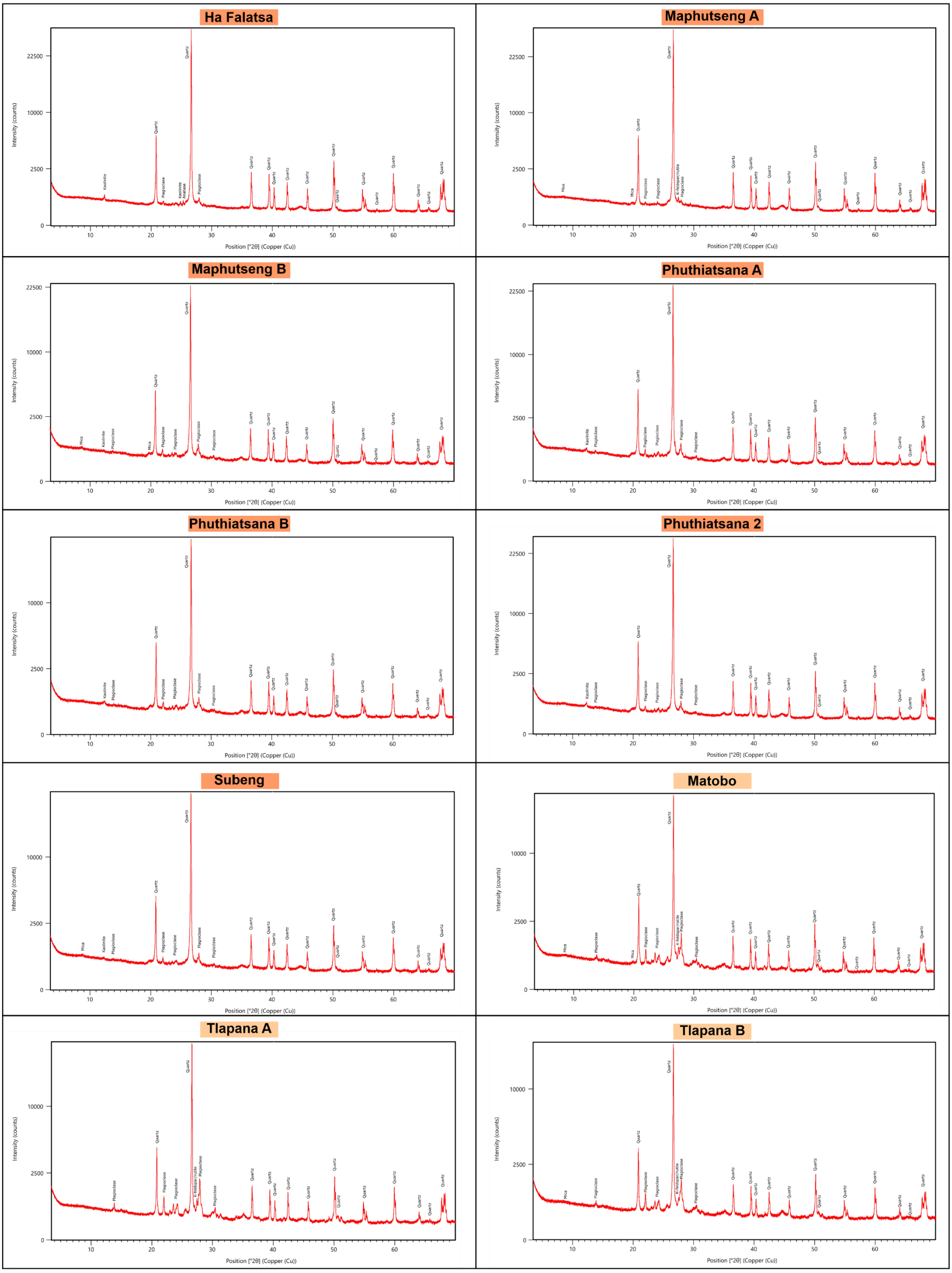

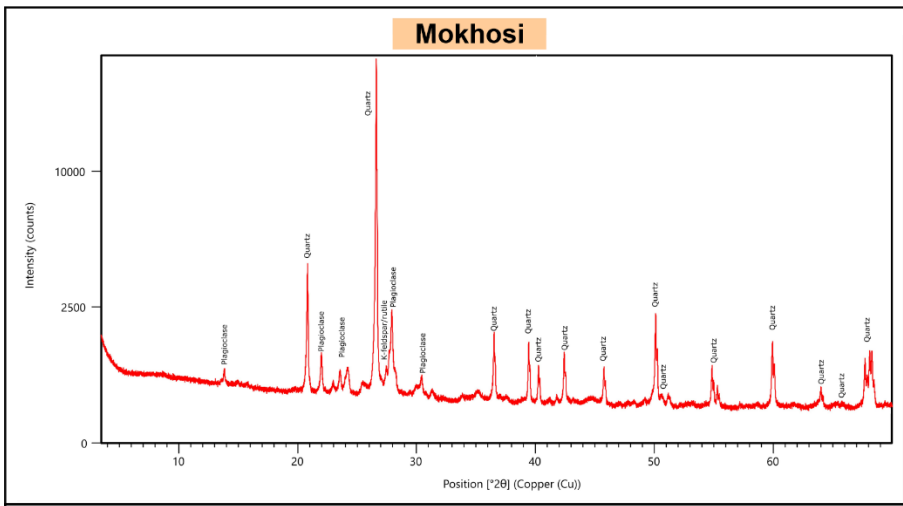
Mokhosi
Intensity (counts)
Position [°2θ] (Copper (Cu))
Quartz
Plagioclase
K-feldspar/rutile

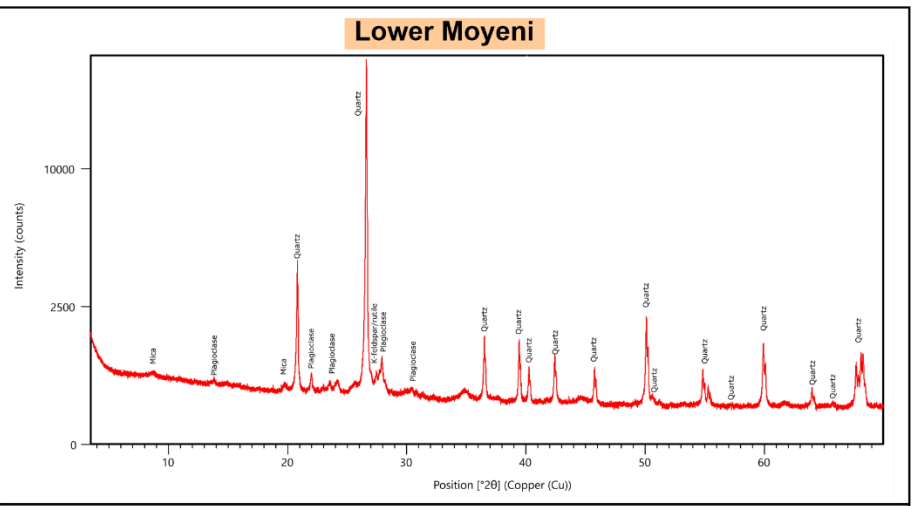
Lower Moyeni
Intensity (counts)
Position [°2θ] (Copper (Cu))
Mica
Quartz
Plagioclase
K-feldspar/rutile

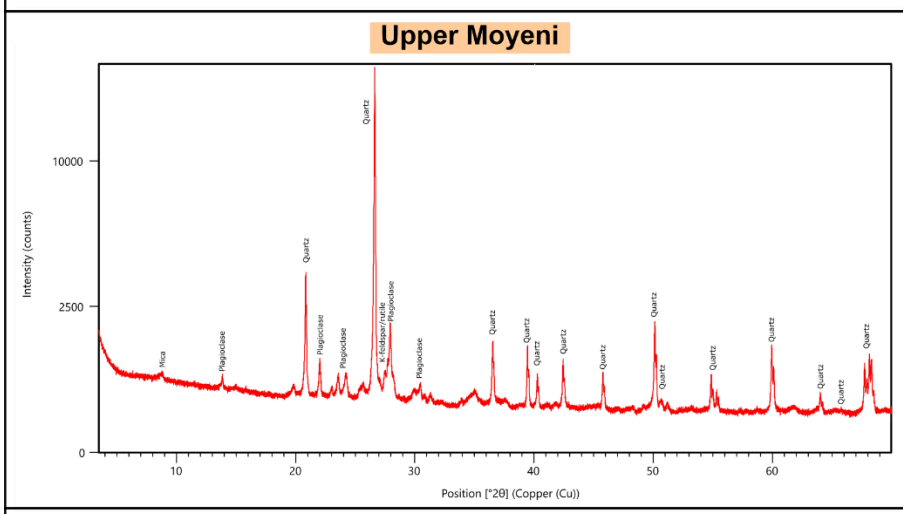
Upper Moyeni
Intensity (counts)
Position [°2θ] (Copper (Cu))
Mica
Quartz
Plagioclase
K-feldspar/rutile

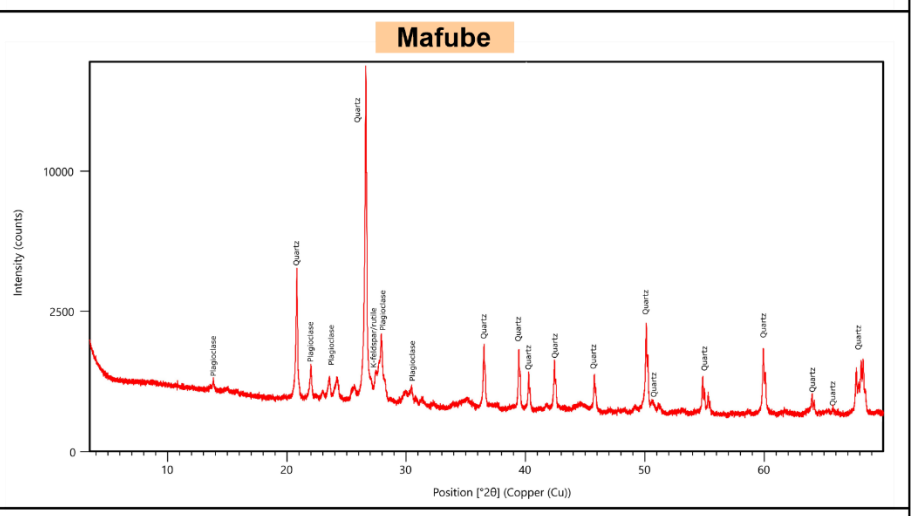
Mafube
Intensity (counts)
Position [°2θ] (Copper (Cu))
Plagioclase
Quartz
K-feldspar/rutile

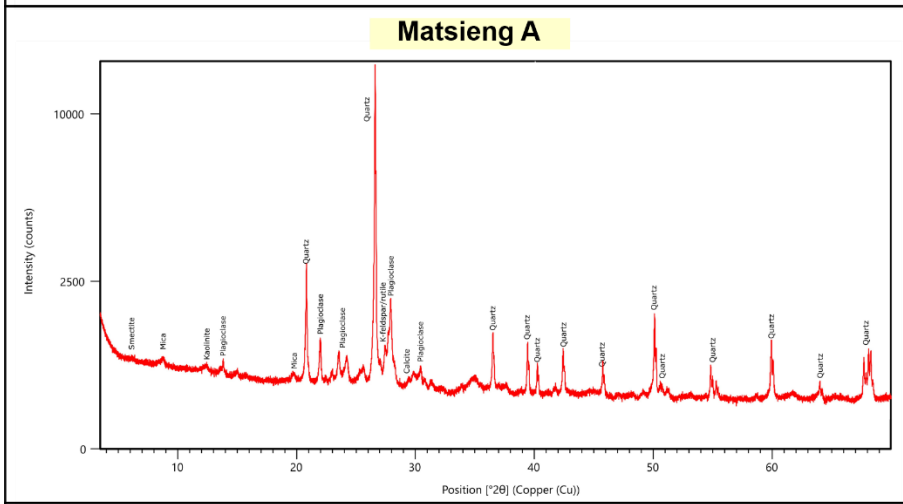
Matsieng A
Intensity (counts)
Position [°2θ] (Copper (Cu))
Smectite
Mica
Kaolinite
Plagioclase
Quartz
K-feldspar/rutile
Calcite

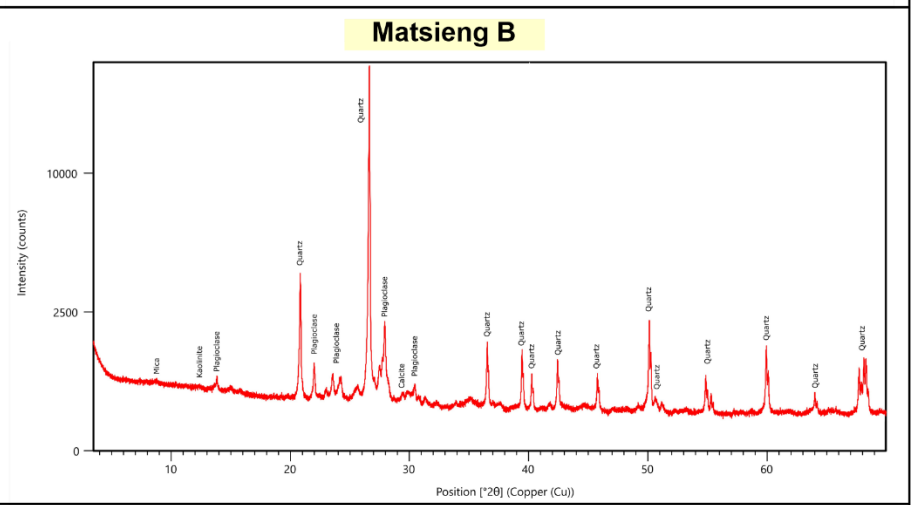
Matsieng B
Intensity (counts)
Position [°2θ] (Copper (Cu))
Mica
Kaolinite
Plagioclase
Quartz
Calcite

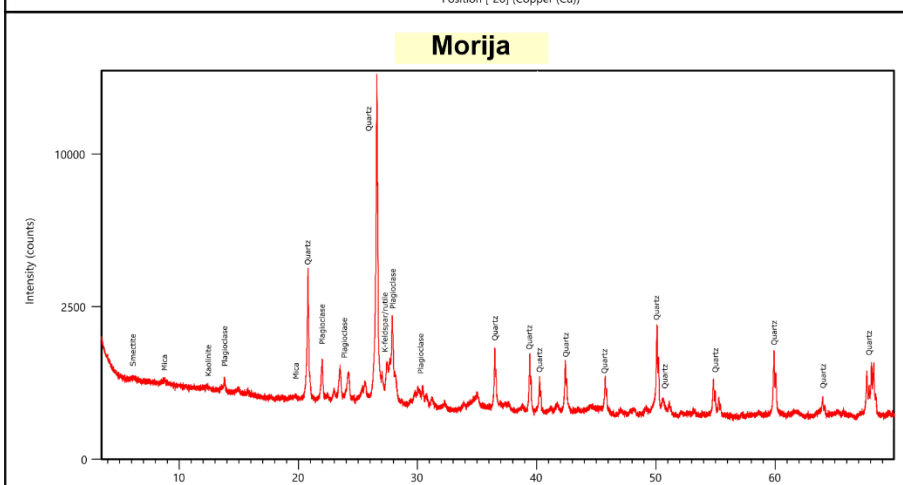
Morija
Intensity (counts)
Position [°2θ] (Copper (Cu))
Smectite
Mica
Kaolinite
Plagioclase
Quartz
K-feldspar/rutile

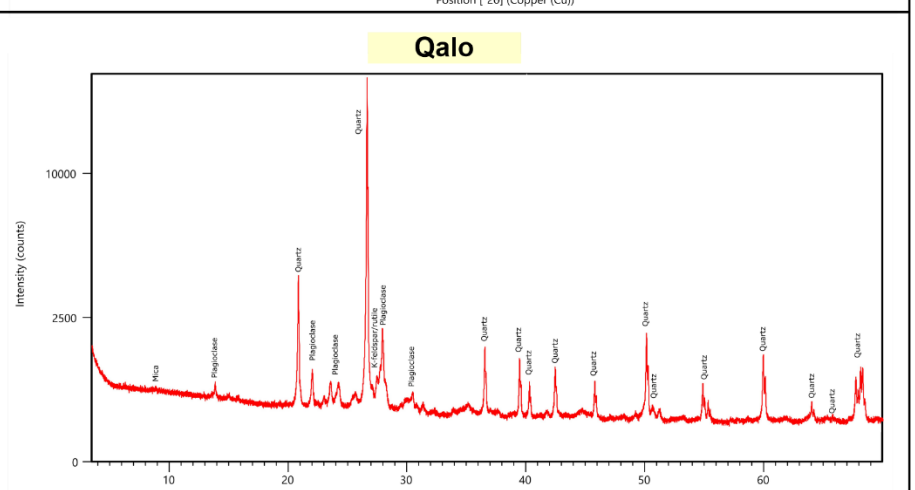
Qalo
Intensity (counts)
Position [°2θ] (Copper (Cu))
Mica
Plagioclase
Quartz
K-feldspar/rutile